SYNTHESIS AND CHARACTERIZATION OF TIN OXIDE AND COPPER DOPED TIN OXIDE THIN FILMS BY SPRAY PYROLYSIS

BY
SONJIT SEN ROY
ROLL NO. 100714022 F
SESSION: OCTOBER, 2007

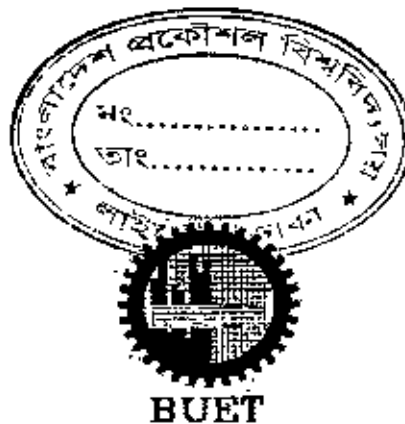**BUET**

DEPARTMENT OF PHYSICS
BANGLADESH UNIVERSITY OF ENGINEERING AND TECHNOLOGY
DHAKA-1000, BANGLADESH

SYNTHESIS AND CHARACTERIZATION OF TIN OXIDE AND COPPER DOPED TIN OXIDE THIN FILMS BY SPRAY PYROLYSIS

BY
SONJIT SEN ROY
ROLL NO. 100714022 F
SESSION: OCTOBER, 2007

DISSERTATION SUBMITTED TO THE DEPARTMENT OF PHYSICS, BANGLADESH UNIVERSITY OF ENGINEERING AND ECHNOLOGY (BUET), DHAKA-1000, BANGLADESH, IN PARTIAL FULFILLMENT FOR THE DEGREE OF MASTER OF PHILOSOPHY (M. Phil)

BUET

DEPARTMENT OF PHYSICS
BANGLADESH UNIVERSITY OF ENGINEERING AND TECHNOLOGY
DHAKA-1000, BANGLADESH

September, 2009

BUET

CANDIDATE'S DECLARATION

It is hereby declared that this thesis or any part of it has not been submitted elsewhere for the award of any degree or diploma.

_____

SONJIT SEN ROY

BANGLADESH UNIVERSITY OF ENGINEERING AND TECHNOLOGY
DHAKA
DEPARTMENT OF PHYSICS

BUET

Certification of Thesis Work

The thesis titled *"SYNTHESIS AND CHARACTERIZATION OF TIN OXIDE AND COPPER DOPED TIN OXIDE THIN FILMS BY SPRAY PYROLYSIS"*, submitted by **SONJIT SEN ROY**, Roll No: 100714022F, Registration No: 100714022, and Session: October'07, has been accepted satisfactory in partial fulfillment of the requirement for the degree of **Master of Philosophy (M. Phil) in Physics** on **15 September 2009**.

<u>BOARD OF EXAMINERS</u>

1. *Jiban Podder*

    Dr. Jiban Podder   Chairman
    Professor   (Supervisor)
    Department of Physics, BUET, Dhaka

2. _____

    Dr. Md. Feroz Alam Khan   Member
    Professor & Head   (Ex-Officio)
    Department of Physics, BUET, Dhaka

3. _____

    Dr. Md. Abu Hashan Bhuiyan   Member
    Professor
    Department of Physics, BUET, Dhaka

4. *Bikiran Barua 15/9/09*

    Dr. Bikiran Prasad Barua   Member (External)
    Professor
    Department of Physics
    Chittagong University, Chittagong

ACKNOWLEDGEMENTS

Abstract

Transparent conducting tin oxide (SnO_2) thin films are of great interest due to their variety of applications in devices as window layers, heat reflectors in solar cells, Light emitting diodes (LEDS), liquid crystal displays, various gas sensors etc. Pure SnO_2 and copper doped SnO_2 thin films have been deposited onto glass substrate by spray pyrolysis method. Deposition parameters: substrate temperature, deposition time and flow rate of solution, amount of base material, distance between the substrate and spray gun tip was kept constant Tin chloride and copper nitrate were used as source of tin (Sn) and copper (Cu). The doping concentration of Cu was varied from 1-8 wt. %. The surface morphological, structural, electrical and optical properties of the as-deposited tin oxide films have been investigated as a function of Cu-doping level. The as-deposited films are found homogeneous. The thickness of the films was estimated by Fizeau fringes interference method. The films thicknesses were varied from 190 to 210 nm.

The scanning electron microscopy (SEM) micrographs of as-deposited film show uniform surface and deposition covers the substrate well. Energy Dispersive Analysis of X-ray (EDAX) results clearly showed that the grains were typically comprised of both Sn and O for pure and Sn, oxygen (O) and Cu for Cu doped films. From EDAX (EDX) data it was found that atomic weight % of Cu is increased with the increase of Cu concentration in Cu doped SnO_2 films.

X-ray diffraction studies show the polycrystalline nature of the films with preferential orientation along the (110), (101), (200), (210), and (211) planes and an average grain size of 7.244579 Å. The peaks were found to shift from their standard positions in the presence of the Cu dopant. There is a deviation in the lattice parameters and it may be happened due to the positioning of dopant atoms into the interstitial lattice sites.

The transmittance and absorbance spectra for the as-deposited films were recorded in the wavelength range of 190 to 1100 nm. The optical transmission of the films was found to increase from 71 % to 79 % (at initial) with the addition of Cu up to 4% and then decreases for higher percentage of copper doping Optical constants such as band gap and refractive index were calculated from the ultra-violet transmittance and absorption graphs.

IV

The optical band gap for pure tin oxide film is found to be 3.75 eV. Due to Cu doping, the band gap is shifted to lower energies and then increases further with increasing concentration of the dopants. The refractive index of the films is found 1.63 and the variation of refractive index is observed due to Cu concentrations and the lowest value of refractive index is found to be 1.54 for 4% Cu doped SnO_2 thin films.

The high electrical conductivity has been found for 4 wt. % $CuNO_3$ + 96 wt % SnO_2. The films deposited at optimized depositions show electrical resistivity, ρ = 5.1065×10^{-4} Ω-m, conductivity, σ = 1.9582×10^3 $(\Omega\text{-m})^{-1}$ and sheet resistance of 2.5532×10^3 $\Omega/\square$ at room temperature 305 K obtained for 200 nm thick SnO_2 thin film. The resistivity of SnO_2 films is found to decrease from 4.5095×10^{-4} Ωm to 1.1395×10^{-4} Ωm as the Cu doping is varied from 1% to 4%, and above 4% Cu doping it is again increased. Activation energy of the samples varies from 0.022896 to 0.058889 eV. It is evident from the present study that the Cu doping promoted the film morphology and also its structural, optical and electrical properties of the films

CONTENTS

List of Figures

List of Tables

CHAPTER-I

GENERAL INTRODUCTION

CHAPTER-I

GENERAL INTRODUCTION

1.1 Introduction

'Thin Solid Film' is the new branch of science has become a great demand of microelectronics in science and technology has greatly stimulated due to the development of thin film and the expansion. Experimental work on thin films has been continued in different parts of the world for successful applications of their properties in scientific, engineering and industrial purposes. The increasing demands for microelectronics and micro structural components in different branches of science and technology have greatly expanded the sphere of thin film research [1-2]. Transparent and conducting oxides (TCOs) have attracted the researchers because of their wide applications in both industry and research. These oxides are extensively used for a variety of applications including architectural windows, flat-panel displays, thin film photovoltaic, smart windows, and polymer-based electronics. Among the available TCOs, pure and doped SnO_2 thin films on glass substrates are used extensively on glass windows for energy conservation and as electrodes in thin film photovoltaic solar cells. Due to their technological importance various researchers have reported the growth and properties of SnO_2 films.

The resources like oil and gas, which are at present the main sources of energy, will eventually exhaust after sometime, necessitating the search for newer energy resources. Nuclear energy is one option, but it induces acute rediative pollution and has some technical problems. Sun is a huge source of energy that can be converted into electrical energy using the solar cells and this is the best alternative option. In this work SnO_2 thin films have been studied as an antireflection coating which is an essential part of the solar cells. As an antireflection coating for heterojunction solar cells, it is an important device material for the detection, emission and modulation of visible and near ultra violet light. For blue light emitting laser diodes and thin film electroluminescent displays.

Thin films are thin material layers ranging from fractions of a nanometer to several micrometers in thickness. A thin layer of a substance deposited on an insulating base in a

vacuum by a microelectronic process. When a thin layer of solid material is formed on a solid substrate and if the layer thickness becomes comparable in magnitude with mean free path of the conduction electrons of solid material than this layer is terms as 'Thin Film'. Thin Film Technology is an important special branch of physics in which the characteristics of different materials, semiconductors and insulators are investigated in thin film form.

We have great interest to study and research on transparent conducting oxide thin films because of an important application of thin film technology from the point of view of global energy crunch is solar cell, which converts the energy of the solar radiation into useful electrical energy. The main requirement for thin film solar cells is the window material, which allows the visible region of solar spectrum to pass through but reflect the IR radiation. This can be achieved by the development of transparent and conducting oxide (TCO) coatings such as tin oxide (SnO_2), cadmium oxide (CdO), zinc oxide (ZnO), cadmium stannate (Cd_2SnO_4), cadmium indate ($CdIn_2O_4$), and indium oxide (In_2O_3). Studies on these highly conducting semiconductors have attracted the interest of many researchers because of their wide applications in both industry and research [3-8]. From these materials, tin oxide shows unique characteristics in chemical inertness, stability to heat treatment and mechanical hardness [9]. The present research work is aimed at the production of uniform, conductive pure and Cu doped tin oxide thin films by a low cost technique using precursor solution of $SnCl_2 2H_2O$. The advantages of the $SnCl_2$ are that it is cheaper than $SnCl_4$ and can be produced easily in a laboratory, and $SnCl_2$ leads to a higher rate of film formation with higher conductivity [10] There are many techniques, including sputtering, evaporation and chemical vapour or spray deposition, by which the SnO_2 films may be deposited on glass substrates In this study, tin oxide thin films were prepared by the spray pyrolysis technique which is particularly attractive because of its simplicity, fast, inexpensive, and suitable for mass production [11]

1.2 Properties of SnO$_2$

The standard values relating to the physical properties of SnO$_2$ are mentioned below:

(I) Other Names: Stannic Oxide, Tin (IV) Oxide, Stannic Anhydride, Flowers of Tin

(II) Molecular Formula: SnO$_2$, Inorganic

(III) Molar Mass: 150.708 g/mol

(IV) Appearance: white powder

(V) Melting point: 1127 °C

(VI) Crystal structure: tetragonal, n type Semiconductor

(VII) Band gap energy: 3.6 ~ 4 eV.
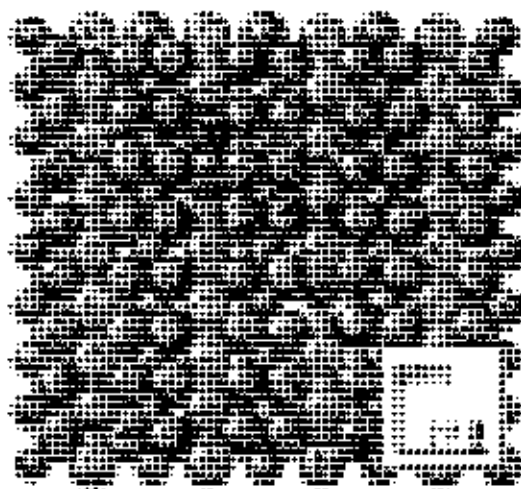
Fig. 1.1: The SnO$_2$ Surface

Figure shown here is a ball model illustration of a nearly perfect (ideal) SnO$_2$ (110) surface based on the ionic radii of the ions. The small balls (green) represent Sn^{4+} cations, while the larger balls (blue) represent O^{2-} anions. All the visible tin cations are in the second atomic layer. Increased shading of the oxygen anions represents increased depth away from the surface. Several "bridging" oxygen anions have been removed from the terminal layer to represent oxygen vacancies and to give a clearer view of the normally six fold-coordinated tin cations in the second layer.

1.3 Application Areas of Thin Films

Pure or doped tin oxide thin films have been wide studied because of their novel properties and wide range of applications. In fact thin films have superior electrical conductivity, high transparency, and chemically inert, mechanically hard, good uniform, stoichiometric and can resist high temperature so these films are to be uses in different type of fields. Infect thin films are broadly used in today's technology, and their applications are expected to be even more widespread in future. Thin films are most commonly used for antireflection, achromatic beam splitters, color filters, narrow pass band filters, semitransparent mirrors, heat control filters, high reflectivity mirrors, polarizer's and reflection filters. It is not possible to give an exhaustive survey over thin film applications, but a listing may, nevertheless, be of some interest.

Several kinds of materials, such as tin oxide, indium tin oxide (ITO), and zinc oxide, are known as Transparent Conductive Oxides (TCO) tin oxide (SnO_2) shows unique characteristics in chemical inertness, stability to heat treatment and mechanical hardness [13]. Transparent and semi-conducting SnO_2 thin films have various appealing features for technical applications in solar energy conversion, flat panel displays, electro-chromic devices, invisible security circuits, LEDs. SnO_2 thin films are currently being used in a wide range of applications, such as electrodes in electroluminescent displays, protective coating, gas and chemical sensors, touch-sensitive switches and many others mainly due to their outstanding properties [14, 15]. Hence large area SnO_2 films on cheap and easily available substrate are of considerable interest for the formation of most of the photonic structure.

It is not possible to give an exhaustive survey over thin film application, but a list of them is given bellow.

A. Optically Functional

1. Solar absorbing coatings

2. Automotive windows

3. Display devices (CD)

4. Mirrors

5. Anti- reflection layers on optical components

B. Electrically Functional:

1. Conductors, Insulators (resistors, capacitors)

3. Semiconductor, Super-conductors devices

4. Contacts

5. Micro electronic devices

6. Solar cells

C. Magnetically functional:

1. Computer memories, Computer logic elements

2. Radio-frequency and microwave

D. Mechanically functional:

1. Adhesion, lubrication, micromechanics

2. Hard coatings for cutting tolls

E. Chemically functional:

1. Barriers to diffusion or alloying

2. Batteries

3. Gas/liquid sensors

F. Decorative:

1. Eyeglass frames

2. Watch bezels and bands

3. Costume jewelry

1.4 Brief Review of Earlier Works of SnO_2 Thin Films

In recent years, thin film science has grown world-wide into a major research area. The importance of coatings and the synthesis of new materials for industry have resulted in a tremendous increase of innovative thin film processing technologies. Currently, this development goes hand-in-hand with the explosion of scientific and technological breakthroughs in microelectronics, optics and nanotechnology. A second major field comprises process technologies for films with thicknesses ranging from one to several microns. Presently, rapidly changing needs for thin film materials and devices are creating new opportunities for the development of new processes, materials and technologies.

Tin oxide is crystalline solid with a tetragonal crystal lattice. It is a wide band gap, non stoichiometric semiconductor and behaves more or less as a degenerate n-type semiconductor with a low n-type resistivity ~ 10^{-3} Ohm.cm, [16]. An important properties of tin oxide is that it is the most chemically stable in atmospheric ambient amongst the other metal oxides [17]. The SnO_2 films exhibit high transmission in the visible and UV ranges and high conductivity. SnO_2 can exists in two structures belonging to direct and indirect optical transitions, with different band gaps; a direct band gap that ranges from 3.6 to 4.6 eV and indirect band of about 2.6 eV at room temperature [18, 19]. For many years, transparent conductive oxide (TCO) layers have been studied extensively because of a wide range of technical applications, for instance as transparent electrodes in photovoltaic and display devices, gas sensors, and chemical sensors [20] and so on. Now may discuss in brief review of SnO_2 thin films prepared by many workers in a number of techniques bellow.

SnO_2:Nd thin films were prepared by vapour deposition technique under different deposition parameters: substrate temperature, time and flow rate of vapour deposition, amount of base material, distance between the substrate and spray gun tip, and dopant (Nd) concentration and studies on physical properties and carrier conversion [21]. X-ray diffraction studies shows the polycrystalline nature of the films with preferential orientation along the (101), (211) and (301) planes and an average grain size of 100 °A. The optical properties of these films were studied by measuring their optical transmission

spectra in the UV-VIS-NIR range. Optical transmission is found to increase with Nd doping. Band gap, refractive index and thickness of the films were calculated. On doping with Nd^{+3}, carrier conversion takes place from n-type to p-type; p-conductivity dominates. The resistivity of SnO_2 films changes from $91.9 \times 10^{-4} \Omega m$ to $1.073 \times 10^{-4} \Omega.m$ as the substrate temperature varied 400–575°C; and resistivity decreases initially on doping and increases as doping concentration increases. The minimum resistivity for the doped SnO_2 films was found to be $0.556 \times 10^{-4} \Omega m$ at the deposition temperature 575°C with 1 wt% concentration of the dopant. Photoconductivity and photovoltaic effects of doped SnO_2 films were also studied.

The results of structural characterization of SnO_2 films doped by impurities such as Fe, Cu, Ni, and Co during spray pyrolysis deposition [22] from 0.2 M $SnCl_4$–water solutions were presented. The change of parameters such as film morphology, the grain size, texture, and the intensity of X-ray diffraction peaks were controlled. It was shown that the doping promoted the change of the film morphology and the decrease of the SnO_2 grain size; however, these changes were not great. The doping influence becomes apparent more obviously for thin films and the films deposited at low temperatures (Tpyr =350°C). At higher pyrolysis temperatures (Tpyr= 450°C), the influence of the doping on both the grain size and the film morphology was weakened. We concluded that used additives had dominant influence on the structural properties of SnO_2 at the initial stages of the film growth, as well as at the stages of twinning and agglomeration of the SnO_2 crystallites. It was shown that the increase in the contents of the fine dispersion phase in as-deposited film is an important consequence of the SnO_2 doping.

Studies on Cu, Fe, and Mn doped SnO_2 semi-conducting transparent films prepared by a Vapour Deposition Technique [24] observed SnO_2 is a wide band gap n-type semi-conductor that has a wide range of applications. Cu, Fe, and Mn doped SnO_2 semi-conducting transparent thin films were prepared by a simple vapour deposition technique under different deposition parameters. The x-ray diffraction studies show the crystalline nature of the films having preferential orientation along the (101), (211), and (301) planes with an average grain size of 100 °A. Photoconductivity and photovoltaic effects of SnO_2

films were also studied. The optical properties of the films were studied by measuring their optical transmission as a function of wavelength. The optical transmission is found to be increased on doping, particularly with a remarkable increase on Mn doping. The band gap, refractive index, and thickness of the films were calculated from the ultra-violet transmittance and absorption graphs. The optical band gap of undoped film is found to be 4.08 eV. On doping it shifts to lower energies and then increases on increasing the concentration of the dopants. Its electrical properties were determined by the four probe, Vander Pauw, and Hall probe methods. Resistivity decreases on Cu and Fe doping but increases on Mn doping. The minimum resistivity for the doped SnO_2 films was found to be 0.381×10^{-4} ohm.m which is deposited at $575°$ C with 3 wt% of Fe doping.

The possibilities of successive ionic layer deposition (SILD) technology for deposition of nano-scalled SnO_2 films are discussed in structural and gas response characterization of nano-size SnO_2 films deposited by SILD method article [26]. SnO_2 thin films deposited using this technology contains porous agglomerated structures consisting of nano-size crystallites. Even after annealing at $T_{an}=800$ °C, the average size of crystallites does not exceed 6–7 nm. The average size of agglomerates depends on film thickness, and ranges from 20 to 80 nm. These SnO_2 films have good gas response especially to ozone and H_2. However, the rate of response to these gases is different. The response to ozone is fast, while the response to exposure to reducing gas, such as H_2, is slow. It is assumed that inter-crystallite gas diffusion in agglomerates limits the rate of response to reducing gases.

Effects of solution concentration on the properties of Cu_4SnS_4 thin films deposited by electro-deposition method [27]. Copper tin sulfide thin films were electrodeposited on the indium tin oxide substrate from an aqueous solution containing $CuSO_4$, $SnCl_2$ and $Na_2S_2O_3$ at pH1. Deposition at various concentrations was attempted in order to study the effect of electrolytes concentration on the film properties. The thin films produced were polycrystalline in nature. The XRD data showed that the most intense peak is at 96 Å which belongs to (221) plane of Cu_4SnS_4. The AFM images indicated that the lower concentration leads to smaller crystal size, as well as higher optical absorption values. The optimum bath composition was found to be 0.01 M for $CuSO_4$, $Na_2S_2O_3$ and $SnCl_2$.

The films with smaller crystal size and show better photo response have been obtained from lower electrolytes concentration (0.01 M). The films exhibited n-type semiconductor behavior with band gap energy of 1.7eV with indirect transition.

Optical properties of pure and antimony (Sb) doped tin oxide (SnO_2) thin films, prepared from $SnCl_2$ precursor [28], have been studied as a function of antimony doping concentration. This paper investigates the variation of optical and electrical properties of the as-deposited films with Sb doping. The doping concentration was varied from 0-4 wt. % of Sb. All the films were deposited on microscope glass slides at the optimized substrate temperature of 400° C. The films are polycrystalline in nature with tetragonal crystal structure. The details on the optical properties along with the sheet resistance values are investigated. The sheet resistance of the undoped films is decreased with initial doping of antimony to attain a minimum value and increased for higher level of doping. The sheet resistance achieved for the films doped with 2 wt. % Sb is the lowest among the earlier reports for these films from $SnCl_2$ precursor. The change in the sheet resistance is explained in terms of different oxidation states of antimony. The sheet resistance of tin oxide films was found to decrease from 38.22$\Omega/\square$ to 2.17$\Omega/\square$ for undoped and antimony doped films respectively. The transmittance increases initially with increase in doping concentration and then decreases for higher doping levels which is attributed to light absorption. The transmittance of the films was observed to increase from 42 % to 55 % (at 800 nm) on initial addition of Sb and then it is decreased for higher level of antimony doping. Hall measurement studies showed that the films are n-type and degenerate semiconductors. The effective mass of the conduction electrons was calculated using Drude theory and found to increase with Sb doping initially but then decrease for higher Sb doping.

SnO_2:F thin films for window materials in solar cells has been employed to prepare ~1.2 μm thick pure and fluorine doped tin oxide films [29]. The electrical and optical studies on the as prepared films were carried out. The obtained values of merit and reflectivity are discussed in the context of the suitability of this material for transparent and conducting window materials in heterojunction thin film solar cells. The sheet resistance was found to decrease with increasing doping concentration to a minimum for 15 wt. %

of NH$_4$F, but increased thereafter. The minimum sheet resistance observed in the present study is the lowest among the reported values for SnO$_2$:F films prepared from SnCl$_2$ precursor. The optical transmittance is found to increase with increase in the fluorine concentration to a maximum of 85 % at 800 nm (30 wt. % of NH4F). The calculated reflectivity in the infrared region is in the range of 94 - 98 % (for 5-30 wt% NH$_4$F).

Transparent, conducting and uniform SnO$_2$ thin films were developed by a low – cost CVD technique using a simple, home-made set up [30]. Two methods with different sources of oxygen were applied. The thin layers were deposited on glass substrates. All films were polycrystalline with cassiterite structure. The films were found to be polycrystalline, presenting a preferred orientation along the (110) plane. Temperature influences crystallinity more powerfully than deposition duration. Films exhibited higher crystallinity when air rather than pure oxygen was used as the oxidizer. Annealing in air improves the crystallinity, inducing the films higher conductivity, since the grain boundaries occupy a smaller part of the film volume. Especially, when pure oxygen is used as the oxidizer annealing is of major importance. Thickness of films varied from 150 nm to 400 nm. Extended study of the mechanism of diffusion of sodium ions out of the glass as well as its effects on film's quality was carried. Crystals of NaCl formed on the matrix of films, which had been grown with air functioning as the oxidizer. Measurements of the mean surface's roughness were conducted by a profilometer. When pure oxygen was used, the produced films presented a smoother surface without any pinholes or undesirable crystal formation. Electrical resistivity at room temperature and in the range from 25 to 250°C was also measured. Films of high conductivity were obtained for both methods at deposition temperatures between 515 and 545°C.

The low – cost spray pyrolysis technique, described in this study, was used to obtain uniform conductive layers of SnO$_2$, with good repeatability [31]. Glass surface was prepared by etching in HF and acetic acid solutions. The influence of the glass surface preparation on optical properties of SnO$_2$ was studied using reflectance spectroscopy. The results were shown that the titanium containing coating has the best sodium diffusion barrier property. The conductivity of SnO$_2$ film strongly depends on the glass surface.

In studies development of a spray pyrolysis coating process for tin oxide film heat mirrors preparation [32], at a lab scale, on 2.5 x7.5 cm glass substrates in a horizontal

reactor designed and constructed for research under the following conditions : substrate temperature (400°C, 450°, 500°C), initial solution concentration ($SnCl_4$:H_2O ratio:3:1), pneumatic force of spray nozzles (pneumatic transducer, pressure 5 bar), fluorine concentration in the initial solution (F:Sn atom ratios= 1;4, 1:2, 1:1, 2:1 and 4: 1) and spray time (120 s). The film spectral transmission was 82, 74 and 58 % in the wavelength regions of 300 - 760 nm and 70, 68 and 56 % in infrared wavelength regions of 760 - 3200 nm. The average transmittance of film of F:Sn atom ratio 1:1 and undoped films were 81 and 74% in the wavelength regions of 300 - 760 nm. In the infrared wavelength regions of 760 - 3200 nm, it was 59 and 68 % respectively. For the F:Sn atom ratio of 1:4, 1:2, 1:1, 2:1 and 4:1, the average transmittance of films were 69,78, 81, 76 and 68 % respectively in the wavelength regions of 300-760 nm and 65,60, 59, 54 and 52 % respectively in infrared wavelength regions of 760 - 3200 nm. The X-ray diffraction of F-doping SnO_2 films can not provide conclusive results of the effect of fluorine atoms in the film. It could be either that there are no F atoms incorporated in the SnO_2 films or they are present in a very small and undetectable amount. This is not too surprising as the calculated efficiency of stannic mass transfer is less than 0.1% whereas F and F-compounds are quite volatile and could readily evaporate and not deposit on the substrates.

Transparent conducting fluorine-doped tin oxide SnO_2-F films was deposited on glass substrates by pulsed laser deposition [36].The structural, electrical and optical properties of the SnO_2-F films have been investigated as a function of F-doping level and substrate deposition temperature. The optimum target composition for high conductivity was found to be 10 wt % SnF_2 + 90 wt % SnO_2. Under optimized deposition conditions (T_s = 300 °C, and 7.33 Pa of O_2), electrical resistivity of 5×10^{-4} Ω-cm, sheet resistance of 12.5 Ω/□, average optical transmittance of 87% in the visible range, and optical band-gap of 4.25 eV were obtained for 400 nm thick SnO_2-F films. Atomic force microscopy measurements for these SnO_2-F films indicated that their root-mean-square surface roughness ($\sim$ 6 Å) was superior to that of commercially available chemical vapor deposited SnO_2:F films ($\sim$ 85 Å).

1.5 Aim of the Present Work

The aim of the present work is nanostructure tin oxide thin films develop to be being carried out to decrease the band gap of tin oxide thin film, increase transmission of light, type of carrier can be change and resistivity decrease. The study of tin oxide is motivated by its applications as a solid state gas sensor material, oxidation catalyst, and transparent conductor. This review describes the physical and chemical properties that make tin oxide a suitable material for these purposes. Thin film process techniques and research are strongly related to the basic research activities in technology. Achieving high optical transparency and electrical conductivity simultaneously in thin film is governed by the deposition parameters, the dopants, and controlled non-stoichiometry.

On account of the numerous applications of tin oxide thin film, an attempt has been made to prepare Sn:Cu:O alloy film using the spray pyrolysis method. From technological point of interest, IV-VI group compound semiconductor thin films such as SnO_2 will be deposited on glass substrate by spray pyrolysis method. The objectives of this study is to synthesis, and characterize undoped and Cu doped SnO_2 films by locally fabricated spray pyrolysis system, so as to reduce the preparation cost and make it economically feasible. It is expected that various contents of Cu in SnO_2 will affect the structural, optical and electrical properties of the film and it will be optically transparent and uniform homogeneous thin film. Recent researches have shown that simple (binary) metal oxides in many cases did not have a combination of properties, necessary for the fabrication of the gas sensors, satisfying the requirements such as high sensitivity and good selectivity at high temporal stability of operating characteristics [70–72]. It was established that those problems could be resolved by an optimization of the metal oxide matrix composition through doping by various additives [73–76]. The same approach was also widely used during a design of the metal oxide varistors with high nonlinearity of the current–voltage (I–V) characteristics [77]. As a result of a special additive embedding, the magnetic properties of the metal oxides can be appreciably changed as well. It makes them very attractive for the spintronics and magnetic memory devices design [78]. The additives means Cu doped can change parameters of the metal oxides such as a

concentration of charge carriers, chemical and physical properties of the metal oxide matrix, electronic and physical– chemical properties of the surface (energetic spectra of the surface states, energy of adsorption and desorption of surface species, the sticking coefficients, etc.), a catalytic activity, the surface potential, the height of inter-crystallite barriers, the phase composition, the size of crystallites, and so on [79–82].

Good controllability of the thin films from aqueous solutions has great advantages of economy, convenience and capacity of large area deposition for production design. In the best decade, there has been a great deal of interest in the production of inexpensive thin films of tin oxide. Because a wide band gap of semiconductor, such as tin SnO_2, can be made highly conducting, when sufficiently doped, it has the desirable property of being transparent through most of the visible spectrum. Therefore, it is optimized that optically transparent and low resistivity, homogeneous and stoichiometric Cu doped thin films with high efficiency to be grown by using this low cost technique. Aqueous solutions will be prepared by mixing 0.1-0.3 M of tin chloride dihydrate $(SnCl_2.2H_2O)$ and ethanol (CH_3CH_2OH) for pure tin oxide and addition of (1wt%-10wt %) copper nitrate Cu $(NO_3)_2$ at different concentrations for copper doped tin oxide thin films. To enhance the solubility of prepared solution, a few drops of HCl is to be added. The thin films are to be prepared by spraying the precursor solution onto a heated glass and indium tin oxide coated (ITO) glass substrate kept at (300- 400°C). So the experimental investigations will be completed through appropriate and suitable way i.e.

   i.   The thickness of the films will be measured by interferometer method (Fizeau fringes)

   ii. By SEM, EDX and XRD the surface morphology, structures and phase of the deposited films will be analyzed.

   iii. The optical transmission and absorption, optical band gap (E_g), refractive index, etc. will be determined by UV visible spectrophotometer.

   iv. The electrical conductivity measurement will be carried out by four probe method.

CHAPTER-II

THEORETICAL BACKGROUND

2.1. Formation of Thin Films
2.1.1 Introduction
2.1.2 Different stages of film formation
2.1.3 Condensation
2.1.4 Nucleation
2.1.5 Growth
2.1.6 Polycrystalline and Amorphous Thin Films
2.1.7 The Incorporation of Defects during Growth

2.2. Band Gap of Semiconductor
2.2.1 Direct Band Gap of Semiconductor
2.2.2 Indirect Band Gap of Semiconductor

CHAPTER-II

THEORETICAL BACKGROUND

2.1 Formation of Thin Films

2.1.1 Introduction

Thin film science has grown world-wide into a major research area. The importance of coatings and the synthesis of new materials for industry have resulted in a tremendous increase of innovative thin film processing technologies. The properties of thin film strongly depend on their structure. So it is important to know the factors that govern the structure of the film. In thin film preparation, there are involved three steps:

a) Creation of atomic or molecular species
b) Transport of these species through a medium
c) Condensation of the species on a substrate.

Thin film is prepared by deposition of the film materials (metals, semiconductors, insulators, dielectric etc.) atom by atom on a substrate through a phase transformation. Sufficient time interval between the two successive deposition of atoms and also layers are required so that these can occupy the minimum potential energy configuration. In thermodynamically stable films, all atoms (or molecules) will take up positions and orientations energetically compatible with the neighboring atoms of the substrate or to the previously deposited layers, and then the effect substrate or the initial layers will diminish gradually [37].

2.1.2 Different stages of film formation

In thin film formation there are three mechanisms of thin film condensations which can be distinguished, depending on the strength of interaction between the atoms of the growing film and between the atoms of the film and substrate. These are:

a) The layer by layer growth

b) A three dimensional nucleation, forming, growth and coalescence of islands

c) Absorption of monolayer and subsequent nucleation on the top of this layer.

In most cases, mechanism (b) takes place and we shall focus our attention on this mechanism in brief.

2.1.3 Condensation

Much research on the mechanism of thin film growth has been done with evaporated films; extensive information on initial growth has been published by D. W. Pashley and his co-workers [38]. The structural behavior and properties of films depend on the growth process. Thin film is most commonly prepared by the condensation of atoms from the vapor phase of a material means, the transformation of a gas into a liquid or solid. The condensation of vapor atom is determined by its interaction with the impinged surface in the following manner. The impinging atom is attracted to the surface by the instantaneous dipole and quadruple moments of the surface atoms. As a result, the atoms losses its velocity component normal to the surface in a short time, provided the incident kinetic energy is not too high. The vapor atoms is then physically absorbed (called adatom), but it may or may not be completely thermally equilibrium. It may move over the surface and its own kinetic energy parallel to the surface. The adatom has a finite stay or residence time on the surface during which it may interact with other adatoms to form a stable cluster and be chemically absorbed, with the release of the heat of condensation. If not absorbed, the adatom evaporates or desorbs into the vapor phase. Therefore, thermodynamically, the only requirement for condensation to occur is that partial pressure of the film material in the gas phase be equal or larger than its vapor pressure in the condensed phase at that temperature [39].

The probability that an impinging atom will be incorporated into the substrate is called the "condensation" or "striking" coefficient. It is measured by the ratio of the amount material condensed on a surface to the total amount impinged. In fact, often the striking coefficient is so small that condensation is not observable by ordinary techniques. On the other hand, the striking coefficient is found to be strongly dependent on the total time during which the substrate was subjected to the impingement, and also on the substrate temperature. A non-unity striking coefficient is usually explained in terms of monomer re-evaporation form the areas on the substrate which are outside, the capture zones around each stable nucleus.

2.1.4 Nucleation

The stable clusters are called nuclei and the process of formation nuclei is called nucleation i.e. nucleation is the birth stage of a film. Condensation is initiated by the formation of small cluster through the combination of several absorbed atoms. These clusters are called nuclei and the process of formation is called nucleation.

There are two types of nucleation occur during the formation of a film;

I) Homogeneous nucleation: The total free energy is used in the formation of a cluster of adatoms.

II) Heterogeneous nucleation: Particular shapes of clusters are formed by collisions of atoms on the substrate surface, and in the vapor phase its super saturation is sufficiently high. [40].They initially developed with in increase in free energy until a critical size is reached above which growth continues with a decrease in free energy. In atomistic theory, in low substrate temperature or very high super saturations, the critical nucleus may be a single atom which will form a pair with another atom by random occurrence to become a stable cluster and grow spontaneously.

2.1.5 Growth

The growth sequence of a film was originally deduced by Andrade [ ] from the observed optical transmission behavior of silver films. This deduction is in remarkable agreement with the electron microscope observations. The process of enlargement of the nuclei to final form a coherent is termed as growth. There are four stages of the growth process based on the electron microscope observations are:

i) The island stage

ii) The coalescence stage

iii) The channel stage

iv)The continuous film stage

Nucleation   Nuclei grow   Coalescence

Channels   Holes   ⟶ Continuous Film
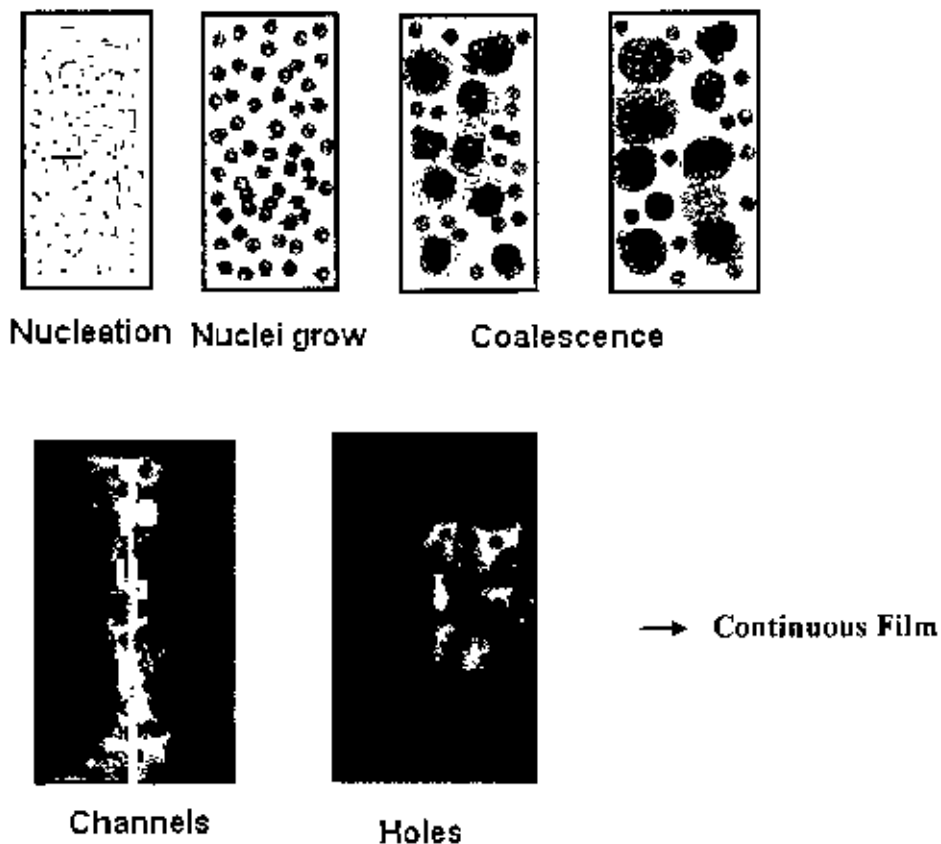
Figure 2.1: Different stages of film growth

2.1.5 (i) The Island Stage

When a substrate under impingement of condenses monomers is observed in the electron microscope, the first evidence of condensation is a sudden burst of nuclei of fairly uniform size. The smallest nuclei detected have a size of 2.0 to 3.0 nm. Growth of nuclei is three dimensional, but the growth parallel to the substrate is greater than that normal to it. This is probably because growth occurs largely by the surface diffusion of monomers on the substrate, rather by direct impingement from the vapor phase. The tendency to form an island structure is increased by

I) At high substrate temperature

II) At low boiling point of film material

III) At low deposition rate

IV) At weak binding energy between film material and substrate

V) At high surface energy of the film material and

VI) At low surface energy of the substrate.

2.1.5 (ii) The Coalescence Stage

As island increases their size by further deposition and come closer to each other, the larger ones appear to grow by coalescence of the smaller ones. The coalescence occurs in less than 0.1s for the small nuclei. After coalescence has taken place, the island assumes a more hexagonal profile is often faulted. A sequence of micrographs illustrating the effects as shown in Fig.2.1 where island which eventually becomes crystallographically shaped.

2.1.5 (iii) The Channel Stage

When larger islands grow together they have channels of interconnected holes of exposed substrate in the form of a network structure on the substrate. As deposition continues, secondary nucleation occurs in these channels and forms the last stage of nucleation.

2.1.5 (IV) Continuous Film Stage

This is the final stage of the film growth. This process is slow and filling the empty channels which requires a considerable amount of deposits. These empty channels are filled by secondary nucleation, growth and coalescence and in this way a continuous film are formed.

2.1.6 Polycrystalline and Amorphous Thin Films

The film deposited by spray pyrolysis are generally polycrystalline or amorphous in structure. Lower temperature and higher gas phase concentration are actually favorable in forming polycrystalline film. In this situation the rate of arrival of the aerosol at the surface is high, but the surface mobility of absorbed atoms is low. A large number of differently oriented nuclei are formed, after coalesce between them the films that are obtained possess grains of different orientation. Further decrease in temperature and increase in super saturation result in even more nuclei and consequently in finer grained films are deposited. When crystalline is completely stopped formation of amorphous film is favored [41].

2.1.7 The Incorporation of Defects During Growth

When the islands during the initial stages of thin film growth are still quite small, they are observed to be perfect single crystal. A large number of defects are incorporated in the film during their recrystallization process at the early stage of film formation [42]. The defects that are usually encountered in spray deposited films are lattice vacancies, stoichiometric excess and grain boundary. Another type of defect namely surface roughness which stems from the quality of the sprayer is especially important in the use of spray deposited films. The properties of the film are strongly affected due to surface roughness if the film thickness is low. The most frequently encountered defects in evaporated films are dislocations, which are less important in chemical spray deposited films.

2.2. Band Gap of Semiconductor

In semiconductor physics, the band gap of a semiconductor is always one of two types, a direct band gap or an indirect band gap. The minimal-energy state in the conduction band, and the maximal-energy state in the valence band, are each characterized by a certain k-vector in the Brillouin zone. If the k-vectors are the same, it is called a "direct gap". If they are different, it is called an "indirect gap".

2.2.1 Direct Band Gap of Semiconductor

The band gap represents the minimum energy difference between the top of the valence band and the bottom of the conduction band, however, the top of the valence band and the bottom of the conduction band are not generally at the same value of the electron momentum. In a direct band gap semiconductor, the top of the valence band and the bottom of the conduction band occur at the same value of momentum, as in the schematic below.
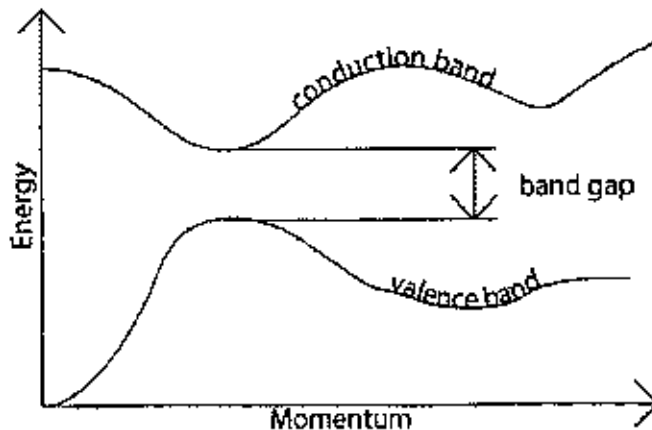
Figure 2.2 Energy-crystal momentum diagram of a direct band gap of semiconductor.

Energy vs. crystal momentum for a semiconductor with a direct band gap, showing that an electron can shift from the lowest-energy state in the conduction band (green) to the highest-energy state in the valence band (red) without a change in crystal momentum. Depicted is a transition in which a photon excites an electron from the valence band to the conduction band.

The momentum of photons is small compared to the crystal momentum; the latter essentially is conserved in the transition. The energy difference between the initial and final state is equal to the energy of the original photon, i.e.

$$E_f - E_e = h\nu \quad \text{.................................... (2.1)}$$

In terms of parabolic band

$$E_f - E_c = \frac{p^2}{2m_e^*} \quad \text{.............................. (2.2)}$$

$$E_v - E_i = \frac{p^2}{2m_h^*} \quad \text{.............................. (2.3)}$$

Therefore, the specific value of crystal momentum at which the transition occurs is given by

$$\left(E_f - E_i\right) - \left(E_c - E_v\right) = \frac{p^2}{2}\left[\frac{1}{m_e^*} + \frac{1}{m_h^*}\right]$$

$$\text{Or, } h\nu - E_g = \frac{p^2}{2}\left[\frac{1}{m_e^*} + \frac{1}{m_h^*}\right] \quad \text{.............. (2.4)}$$

Where, $E_f - E_i = h\nu =$ Photon Energy

And, $E_c - E_v =$ Energy gap

As the photon energy hv increases, so does the value of the crystal momentum at which the transition occurs. The energy from the band edge of both the initial and find states also increases. The probability of absorption depends on the density of the electron at the energy corresponding to the initial state as well as the density of empty states at the final energy. Since both these quantities increases with energy away from the band edge, the absorption co-efficient increases rapidly with increasing photon energy above E_g. A simple theoretical treatment gives the result as,

$$\alpha h\nu \approx A\left(h\nu - E_g\right)^{1/2} \quad \text{........................ (2.5)}$$

Where A is a constant having the numerical value of 2×10^4 when α is expressed in cm^{-1} and E_g and hv are in eV.

2.2.2 Indirect Band Gap of Semiconductor

In an indirect band gap semiconductor, the maximum energy of the valence band occurs at a different value of momentum to the minimum in the conduction band energy:
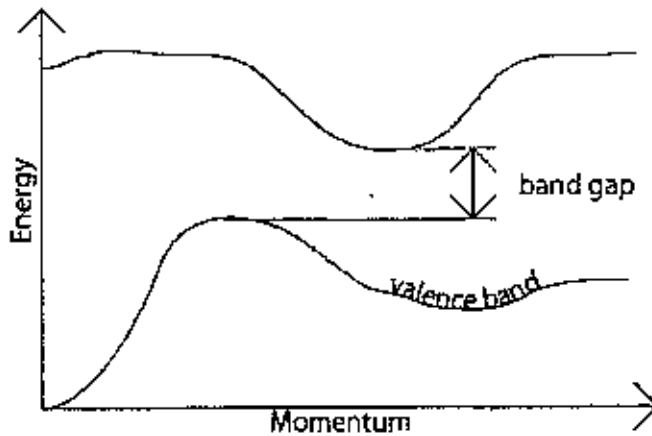
Fig. 2.3: Energy-crystal momentum diagram of an indirect band gap of Semiconductor.

Figure shows energy vs. crystal momentum for a semiconductor with an indirect band gap, showing that an electron cannot shift from the lowest-energy state in the conduction band to the highest-energy state in the valence band without a change in momentum. Here, almost all of the energy comes from a photon, while almost all of the momentum comes from a phonon.

The minimum photon energy required to exit an electron from the valance band to conduction band is

$$hv = E_g - E_p \qquad \dots\dots\dots\dots\dots\dots (2.6)$$

Where, E_p is the energy of an absorbed photon with the required momentum. An analysis of the theoretical value of the absorption co-efficient for the transition involving photon absorption gives the result

$$\alpha_a(hv) = \frac{A(hv - E_g + E_p)^2}{\exp(E_p/kT)^{-1}} \qquad \dots\dots\dots\dots (2.7)$$

For the transition involving photon emission

$$\alpha_e(hv) = \frac{A(hv - E_g + E_p)^2}{\exp(E_p/kT)^{-1}}$$

Since both photon emission and absorption are possible for $hv > (E_g + E_p)$, the absorption co-efficient is then

$$\alpha(hv) = \alpha_a(hv) + \alpha_e(hv) \qquad \dots\dots\dots\dots\dots (2.8)$$

CHAPTER-III

THIN FILM DEPOSITION TECHNIQUES

3.1. Introduction

3.2. Pulsed ion-beam Evaporation (IBE) Method

3.3. Molecular Beam Epitexy

3.4. Thermal or Vacuum Evaporation Method

3.5. Plasma-enhanced Chemical Vapor Deposition

3.6. Sputtering Method

3.7. Sol-gel Process

3.8. Spin Coating Process

3.9. Spray Pyrolysis Method

CHAPTER-III

THIN FILM DEPOSITION TECHNIQUES

3.1 Introduction

Pure and doped thin films can be prepared by many methods. Different types of deposition are used for the preparation of thin films such as,

1. Chemical Vapour Deposition
2. Physical Vapour Deposition
3. Chemical Bath Deposition

3.1.1. Chemical Vapour Deposition (CVD)

Precursor gases (often diluted in carrier gases) are delivered into the reaction chamber at approximately ambient temperatures. As they pass over or come into contact with a heated substrate, they react or decompose forming a solid phase and which are deposited onto the substrate. The substrate temperature is critical and can influence what reactions will take place. CVD covers processes such as:

1. Atmospheric Pressure Chemical Vapour Deposition (APCVD)
2. Metal-Organic Chemical Vapour Deposition (MOCVD)
3. Plasma Enhanced Chemical Vapour Deposition (PECVD)
4. Photochemical Vapour Deposition (PCVD)
5. Chemical Beam Epitaxy (CBE)

CVD coatings are usually only a few microns thick and are generally deposited at fairly slow rates, usually of the order of a few hundred microns per hour. CVD is an extremely versatile process that can be used to process almost any metallic or ceramic compound. Some of these include: Elements, Metals and alloys, Nitrides Carbides, Borides, Oxides, intermetallic compounds.

3.1.2. Physical Vapour Deposition (PVD):

Physical vapour deposition (PVD) is fundamentally a vaporization coating technique, involving transfer of material on an atomic level. It is an alternative process to electroplating. The process is similar to chemical vapour deposition (CVD) except that the raw materials/precursors, i.e. the material that is going to be deposited starts out in solid form, whereas in CVD, the precursors are introduced to the reaction chamber in the gaseous state. Consequently Physical Vapor Deposition (PVD) is a process by which a thin film of material is deposited on a substrate according to the following sequence of steps:

1) The material to be deposited is converted into vapor by physical means;
2) The vapor is transported across a region of low pressure from its source to the substrate;
3) The vapor undergoes condensation on the substrate to form the thin film. In VLSI fabrication, the most widely-used method of accomplishing PVD of thin films is by sputtering. PVD covers processes such as:

1. Sputter coating
2. Pulsed laser deposition (PLD)
3. Cathode arc deposition

Advantages of the Physical vapour deposition process as materials can be deposited with improved properties compared to the substrate material, almost any type of inorganic material can be used as well as some kinds of organic materials, the process is more environmentally friendly than processes such as electroplating etc. and some disadvantages of the physical vapour deposition process as it is a line of sight technique meaning that it is extremely difficult to coat undercuts and similar surface features, high capital cost, some processes operate at high vacuums and temperatures requiring skilled operators, the rate of coating deposition is usually quite slow.

3.1.3 Chemical Bath Deposition (CBD):

The technique of CBD involves the controlled precipitation from solution of a compound on a suitable substrate. The technique offers many advantages over the more established vapor phase synthetic routes to semiconductor materials, such as CVD, MBE and spray pyrolysis. Typical CBD processes for sulfides employ an alkaline media containing the chalcogenide source, the metal ion and added base. A chelating agent is used to limit the hydrolysis of the metal ion and impart some stability to the bath, which would otherwise undergo rapid hydrolysis and precipitation. The extent of the heterogeneous reaction on the substrate surface is limited by two major factors, the competing homogeneous reaction in solution (which results in massive precipitation in solution) and deposition of material on the CBD reactor walls. We are developing continuous flow-recyclable CBD processes for the fabrication of CdS thin films for use as window materials in solar cells. The large scale exploitation of these devices is partly dependent on a reduction of the potential environmental impact of the technology, as cadmium-containing compounds and waste are highly regulated in the EU and elsewhere.

We have more deposition processes as

1. Molecular beam epitaxy (MBE)

2. Reactive sputtering

Generally each method has its advantages and limitations. In this chapter some of the commonly used techniques are described briefly. In principle physical methods such as sputtering and thermal evaporation lead to weakly non-stoichiometric tin oxide with co-existence of other insulating phases like SnO, resulting into relatively high resistive films. On the other hand, chemical methods lead to strongly non-stoichiometric tin oxide, resulting into comparatively low resistive films.

The details of the literature for various deposition techniques and review articles can be found in [49-53], here shortly brief about these techniques. Among these techniques, the spray pyrolysis is well suited for the preparation of pure and doped tin oxide thin films. This technique has the advantage of simple and inexpensive experimental arrangement. In this case though, intrinsic advantages of **SPRAY PYROLYSIS TECHNIQUE** have been used to deposit SnO_2 thin films.

3.2 Pulsed ion-beam Evaporation (IBE) Method

A schematic of the experimental setup for thin film preparation by Pulsed ion-beam evaporation (IBE) method [49] is shown in Fig. 3.1. The Left-hand side represents an ion beam diode chamber, which produces a pulsed light ion beam (LIB), while the right-hand side represents the chamber to prepare thin films. The intense pulsed ion beam was extracted from the magnetically-insulated diode (MID) with a geometrically focused configuration. The MID consists of an aluminum anode, on which the flashboard (1.5 mm polyethylene) was attached as the ion source, and the cathode with slits to extracting the ion beam. The gap distance between the anode and the cathode is 10 mm. To achieve geometric focusing of the beam, the anode and the cathode were shaped as concave structures with curvature of 160 mm. The current supplied by the external slow capacitor bank produced a transverse magnetic field (~1 T) between the anode and the cathode, by which the electrons were magnetically insulated. The beams were mainly composed of protons (>75%) and some carbon ions.
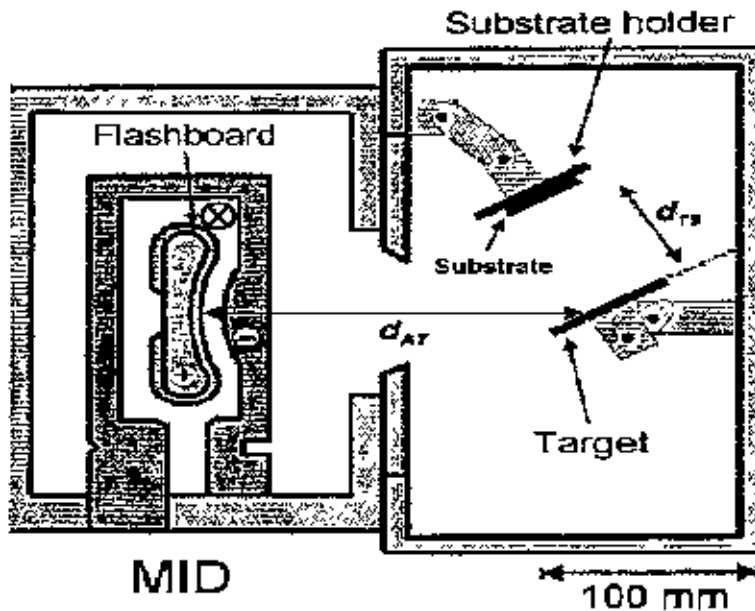
Figure 3.1: A schematic of the pulsed ion-beam evaporation (IBE) method

3.3. Molecular Beam Epitexy

Epitaxy means growth of film with a crystallographic relationship between film and substrate. Molecular beam epitaxy is a technique for epitaxial growth via the interaction of one or several molecular or atomic beams that occurs on a surface of a heated crystalline substrate [50]. In Fig.3.2 a scheme of a typical MBE system is shown. The solid sources materials are placed in evaporation cells to provide an angular distribution of atoms or molecules in a beam. The substrate is heated to the necessary temperature and, when needed, continuously rotated to improve the growth homogeneity. Ultra high vacuum (UHV) is the essential environment for MBE. Therefore, the rate of gas evolution from the materials in the chamber has to be as low as possible. Focusing on the possibility that, despite the fact that MBE processes occur under strong nonequilibrium conditions, for the III/V elements, a thermodynamic approach can be used on the basis of equations for mass action in combination with the equations describing the conservation of the mass of the interacting elements.
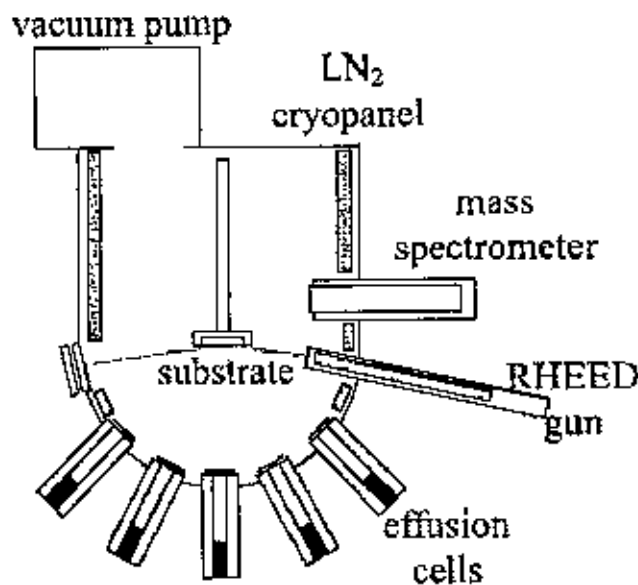
Figure 3.2: Diagram of a molecular beam epitaxy

3.4. Thermal or Vacuum Evaporation Method

Among physical vapor deposition techniques thermal evaporation (TE) is the one with the longest standing tradition. In intelligence, the story of high temperature superconductor (HTS) film deposition can serve as an example how this technique, sometimes regarded as old – fashioned, still bears a high potential for innovation and surprising efficiency. This technique is the simple, convenient and most widly used method for the preparation of the films. TE is the classical technique applied for metal - plating of glass or plastic surfaces, like e.g. aluminum coatings widely used for capacitors, plastic wrappings, and as barrier against water diffusion. It is evident that the deposition of quaternary metal – oxide compounds imposes quite different requirements to the technique and will go far beyond the rudimentary concept of evaporating a single metal in a vacuum chamber. The necessary features of a conventional HTS deposition system are depicted in figure 3.3 The metal species the superconductor is composed of are evaporated in high vacuum ambient. In this method materials are vaporized by heating to a sufficient high temperature and then condensation of the vapor into a relatively cooler substrate yielding thin solid films.
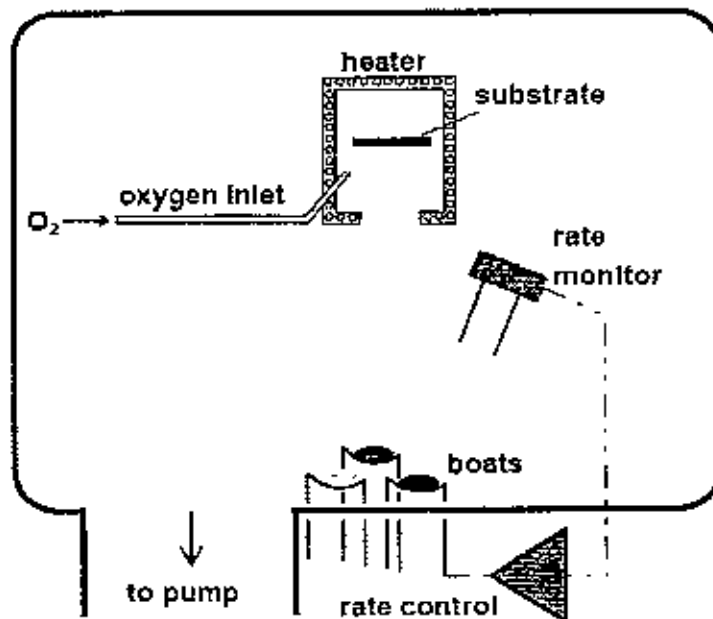
Figure 3.3: Thermal evaporation method

3.5 Plasma-enhanced Chemical Vapor Deposition (PECVD):

A novel manufacturing process using plasma-enhanced chemical vapor deposition (PECVD) for the synthesis of transparent conducting oxide (TCO) thin films like tin oxide [51]. In order to develop PECVD as a reliable manufacturing technology we plan to employ in-situ metrology coupled with nonlinear feedback control. Control designs will be developed through nonlinear system identification and semi global empirical modeling. PECVD offers several potential advantages over current processing technologies. Foremost is the opportunity to reduce deposition temperatures to below 250 °C. Achievement of this goal will create opportunities for device fabrication on lightweight, flexible polymer substrates. Second, reactant species may be introduced into the low-pressure PECVD reactor by direct liquid injection. PECVD is also compatible with current integrated circuit manufacturing processes. Along with the advantages of PECVD is the realization that it is a highly complex system. The reactor for this work is partially shown in Fig. 3.4. It is a custom-made, stainless steel thin film deposition system. Currently, the system is configured as a PECVD system. In addition to mechanical pumps, the system has a turbo molecular pump which attains a base pressure of 10^{-7} torr. The plasma is generated using a 300 Watt 13.6 MHz RF power supply and match network, with a 4" diameter deposition area.
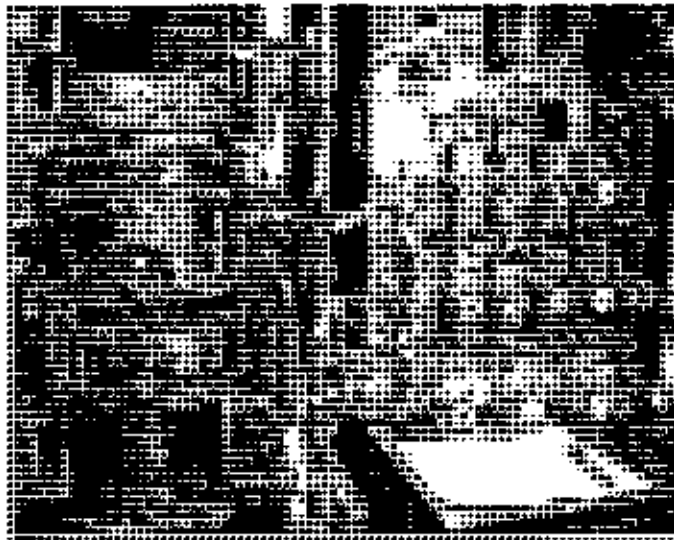
Figure 3.4: Schematic diagram of the PECVD reactor

3.6 Sputtering Method:

Sputtering is a mechanism by which atoms are dislodged from the surface of a material as a result of collision with high-energy particles. Thus, PVD by Sputtering is a term used to refer to a physical vapor deposition (PVD) technique wherein atoms or molecules are ejected from a target material by high-energy particle bombardment so that the ejected atoms or molecules can condense on a substrate as a thin film. Sputtering has become one of the most widely used techniques for depositing various metallic films on wafers, including aluminum, aluminum alloys, platinum, gold, TiW, and tungsten [52]. This method can possibly be used to synthesize thin films of other oxide materials as well. All the films were deposited in a chamber with a base pressure of 10¡7 Torr using rf-Plasma Products RF-10. Ar was used as the sputtering gas. Using a programmable rf power supply with an automatic tuner, the rf forward power could be varied between two different power levels. If an rf forward power as high as 250 W was dumped into the brittle ferrite target for a long time, the target cracked. Introducing the new method could save the target. The upper and lower rf forward power levels were varied between two values, with a pulse time of 30 seconds as shown in the example given in figure 1.
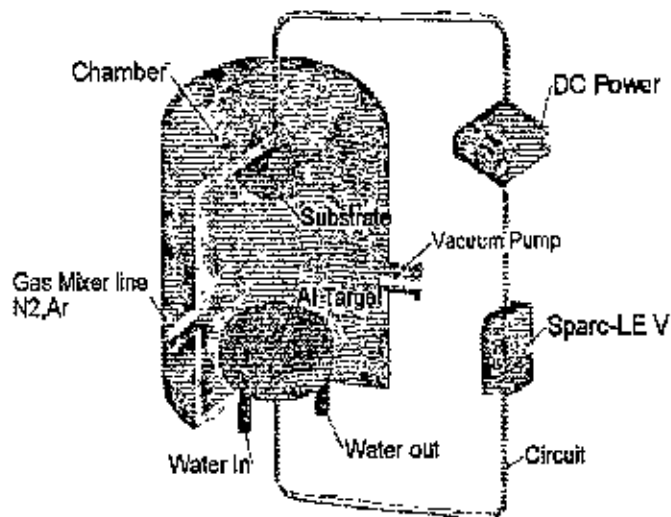
Figure 3.5: Schematic diagram of the magnetron sputtering system.

3.7 Sol-gel process:

Sol-gel method is a wet chemical route for the synthesis of colloidal dispersions of oxides which can be altered to powders, fibers, thin films and monoliths [53]. In general, sol-gel method consists of hydrolysis and condensation reactions. Sol-gel coating is a process of preparation of single or multicomponent oxide coating which may be glass, glass ceramic or crystalline ceramic depending on the process. Also, the nanomaterials used in modern ceramic and device technology require high purity and facilitate to control over composition and structure. The solgel coating is one of the interesting methods because it has many advantages. Examples are as the followings

1. The chemical reactants for sol-gel process can be conveniently purified by distillation and crystallization.

2. All starting materials are mixed at the molecular level in the solution so that a high degree of homogeneity of films can be expected.

3. Organic or inorganic salts can be added to adjust the microstructure or to improve the structural, optical and electrical properties of oxide films.

4. The sol-gel coating is almost exclusively applied for fabrication of transparent layers with a high degree of planarity and surface quality.
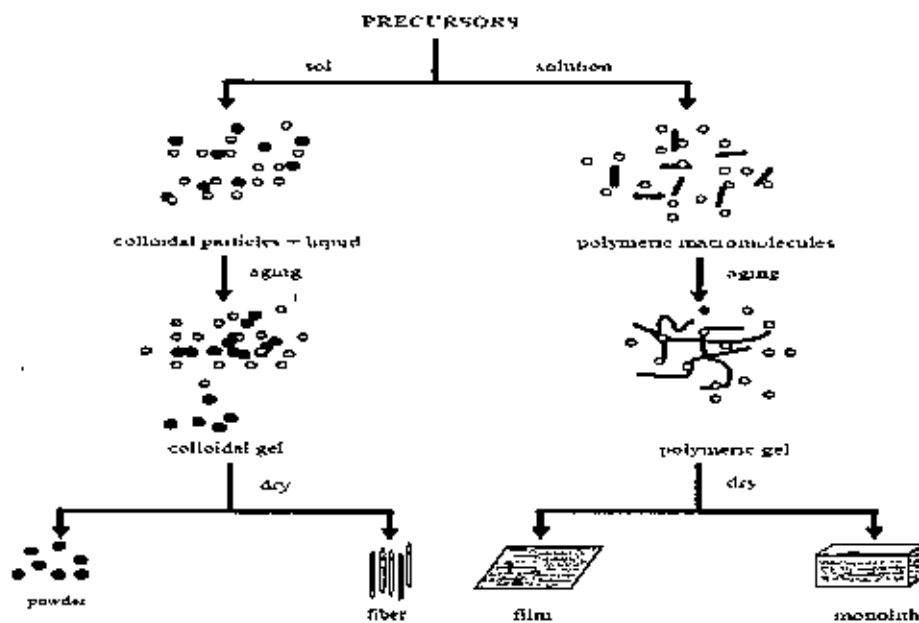
Figure 3.6: Generalized scheme of sol-gel synthesis

3.8 Spin Coating Process:

Spin coating has been used for several decades for the application of thin films. A typical process involves depositing a small puddle of a fluid resin onto the center of a substrate and then spinning the substrate at high speed (typically around 3000 rpm). Centripetal acceleration will cause the resin to spread to, and eventually off, the edge of the substrate leaving a thin film of resin on the surface. Final film thickness and other properties will depend on the nature of the resin (viscosity, drying rate, percent solids, surface tension, etc.) and the parameters chosen for the spin process. Factors such as final rotational speed, acceleration, and fume exhaust contribute to how the properties of coated film are defined. One of the most important factors in spin coating is repeatability. Subtle variations in the parameters that define the spin process can result in drastic variations in the coated film.
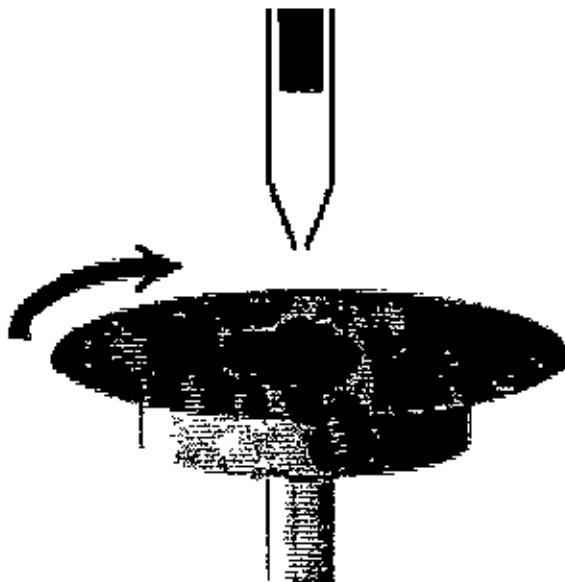
Figure 3.7: Schematic diagram of the spin coating process

3.9 Spray Pyrolysis Technique (SPD):

Spray pyrolysis is a convenient, low-cost, very simple and rapid method for the deposition of thin films, and is suitable for industrial applications and has been used for about 30 years for the manufacture of conductive glass. It is also an excellent method for preparing films of semiconductor alloys and complex compounds.

Spray Pyrolysis is a process in which a thin film is deposited by spraying a solution on a heated surface, where the constituents react to form a chemical compound. The chemical reactions are selected such that the products other than the desired compound are volatile at the temperature of deposition. The process is particularly useful for the deposition of oxides and has long been a production method for applying a transparent electrical conductor of SnO_x to glass. There have been studies in this area since the pioneering paper by Chamberlain and Skarmain on CdS films for solar cells in 1066, among then a review of transparent conductors and a bibliography Pamplin presented at a conference on spray pyrolysis. We discuss here the method and its control; the properties of the films that have been deposited (particularly in relation to the conditions), some specific films, particularly CdS; and device application.

Spray pyrolysis is a convenient, low-cost, and rapid method for the deposition of thin films, and has been used for about 30 years for the manufacture of conductive glass. Because individual droplets evaporate and react very quickly, grain sizes are very small, usually less than 0.1/~m. The small grains are a disadvantage for most semiconductor applications. The use of low concentration and slow spray rates to improve film quality tends to frustrate the low-cost processing objective, but post deposition heat treatment of small-grain. Films can improve stoichiometry and crystallinity. The process is sensitive to variables, particularly temperature, and the measurement at the surface is uncertain. Not only do the physical and electronic properties of the film vary with temperature, but the deposition efficiency decreases with increased temperature; stoichiometry is also affected, particularly for alloys. In spite of these difficulties, spray pyrolysis is an excellent method for the deposition of large-area thin films.

Viguie and Spitz classified chemical spray pyrolysis deposition process according to the type of reaction. In process

A) The droplet resides on the surface as the solvent evaporates, leaving behind a solid that may further react in the dry state.

B) The solvent evaporates before the droplet reaches the surface and the dry solid impinges on the surface, where decomposition occurs.

C) The solvent vaporizes and the vapor diffuses to the substrate, there to undergo a heterogeneous reaction. (They identify this process as true chemical vapor deposition.).

D) The enter reaction takes place in the vapor state.
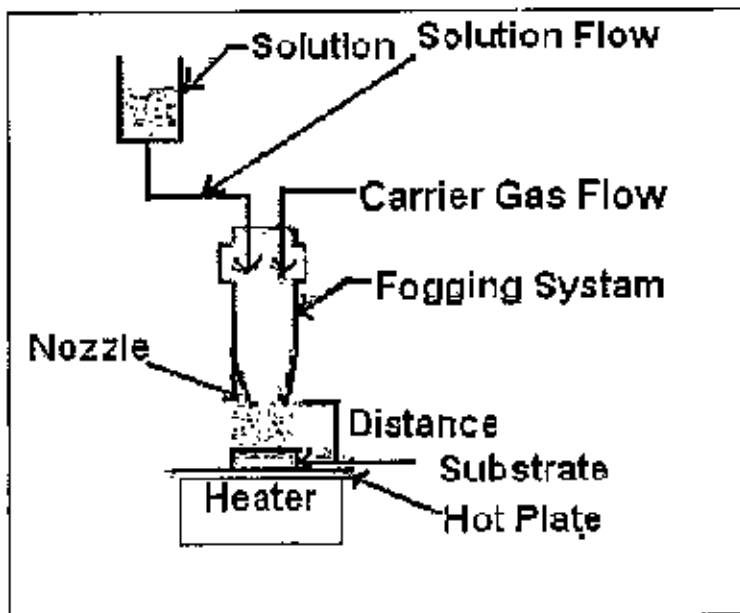
Figure 3.8: Schematic diagram of a spray pyrolysis technique

This technique involves spraying of an ionic solution, usually aqueous containing soluble salts of the constituent atoms of the desired compound onto heated substrates. Hydrolysis and pyrolysis are the main chemical reactions involved in the process. Spray pyrolysis is a process in which a thin film is deposited by spraying a solution on a heated surface, where the constituents react to form a chemical compound. The chemical reactants are selected such that the products other than the desired compound are volatile at the temperature of deposition. Here individual droplets evaporate and react very quickly, grain sizes are very small, usually less than 0.1/~m. The small grains are a disadvantage for most semiconductor applications. The process is sensitive to variables, particularly

temperature, and the measurement at the surface is uncertain. Not only do the physical and electronic properties of the film vary with temperature, but the deposition efficiency decreases with increased temperature; stoichiometry is also affected, particularly for alloys. The process is particularly useful for the deposition of oxides and has long been a production method for applying a transparent electrical conductor. In spite of these difficulties, spray pyrolysis is an excellent method for the deposition of large-area thin films.

Chemical spray deposition processes classified according to the type of reaction. In process A, the droplet resides on the surface as the solvent evaporates, leaving behind a solid that may further react in the dry state. In process B, the solvent evaporates before the droplet reaches the surface and the dry solid impinges on the surface, where decomposition occurs. In process C, the solvent vaporizes as the droplet approaches the substrate; the solid then melts and vaporizes, and the vapor diffuses to the substrate, there to undergo a heterogeneous reaction. (They identify this process as true chemical vapor deposition.) In process D, the entire reaction takes place in the vapor state. In all processes, the significant variables are the ambient temperature, carrier gas flow rate, nozzle-to-substrate distance, droplet radius, solution concentration, solution flow rate, and--for continuous processes--substrate motion. To this list one should add the chemical composition of the carrier gas and/or environment, and, most importantly, substrate temperature. Most spray pyrolysis depositions are type A or B. In our experiment we have used a modified spray pyrolysis technique and this will be discussed of the method and its control in some details later.

CHAPTER-IV

EXPERIMENTAL DETAILS

4.1. Film Deposition

4.1.1 Introduction

4.1.2 Experimental Equipments

4.1.3 Working Solution

4.1.4 Film Deposition Parameters

4.1.5 Optimization of the Deposition Process

4.1.6 Film Preparation

4.2. Measurement Details

4.2.1 Methods for the Film Thickness Measurement

4.2.2 Surface Morphology and Structural Analysis of Thin Films

4.2.3 Optical Property Analysis of Thin Films

4.2.4 Electrical Property Analysis of Thin Films

CHAPTER-IV

EXPERIMENTAL DETAILS

4.1 Film Deposition

4.1.1 Introduction

The spray pyrolysis method is particularly attractive because of its simplicity. It is fast, inexpensive, vacuum less and is suitable for thin film production. The spray pyrolysis method used is basically a chemical deposition method in which fine droplets of the desired material are sprayed onto a heated substrate. A continuous film is formed on the hot substrate by thermal decomposition of the material droplets.

We may prepare thin films from a variety of materials such as semiconductors, insulators, metals or dielectrics etc., and for this purpose various preparation techniques has also been developed. But spray pyrolysis is the most commonly used technique adopted for the deposition of metals, alloys and many compounds. Spray pyrolysis technique involves spraying of an ionic solution usually aqueous solution (0.2 M) of tin chloride ($SnCl_2.2H_2O$) and ethanol (CH_3CH_2OH) and copper nitrate [$Cu(NO_3)_2$] are taken as the precursor for Cu doped SnO_2 films containing soluble salts of the constituent atoms of the desired compound onto heated substrates around 300 ~ 400°C. Hydrolysis and pyrolysis are the main chemical reactions involved in the process. In this technique, the chemicals vaporized and react on the substrate surface after reaching on it. The flow rate of the solution during spraying is to be adjusted to be about 5 ml/min and kept constant through out the experiment. The distance between the spray nozzle and the substrate is to be maintained about 30 cm and the temperature of the substrate to be measured by Copper-Constantan thermocouple. The system is equipped with an electric heater and thermo couple. An air compressor pipe is attached within and an exhaust fan is fitted in order to remove the gas which is produced during the film deposition. This chapter deals various steps of the film deposition procedure of the spray pyrolysis method and discuss below.

4.1.2 Experimental Equipments

4.1.2.1 Preparation of Masks

In order to study the various properties of thin film, it is necessary that they must be properly patterned. The direct deposition of thin film pattern requires a suitably shaped aperture, commonly referred to as a mask. For the purpose of various experimental studies, film of specific size and shape are required. Mask was made from stainless steel plate with the desired pattern cut into it. The aperture was made in a bath machine.

The most commonly used method of patterning thin film is the physical masking, which is accomplished by placing the mask of desired shape on the substrate. In the present work, thin mica sheet was used for the preparation of masks as shown in figure 4.1.

Figure 4.1: Mask

Regardless of mask material and fabrication process all masks should be thoroughly cleaned and inspected before use. Surface contaminants, particularly oil, grease or other organic materials may become volatile when the mask is heated and then be absorbed by the substrate and this may be a cause of weak film adhesion. The mask is placed in proximity to the substrate, there by allowing condensation of evaporate only in the exposed substrate areas. The mask was prepared in such away that the edge of the mask is smooth so that it is helpful for determining the film thickness accurately.

4.1.2.2 Heater

The heater 'H' is an ordinary hot plate, 3 K watt nichrome wire heater which is put in spherical shape holder. An electronic power supply (voltage variance) unit is connected with the heater power line to supply proper heat to the substrate. A thick stainless steel plate 'G' is placed on heater. Substrate with mica sheet is placed on this suspected plate.

4.1.2.3 The Design of the Reactor

The design of the reactor is shown is Fig.4.2. It is a vertical batch type reactor composed of a galvanized iron enclosure 'E', heater 'H' and heat susceptor 'G', thermocouple 'T.C', lower tube "A", upper tube "P". For the rapid expulsion of the by product gases there are opening at the side and at the top of the reactor. It helps focusing the incoming sprayed solution towards the substrate 'S' and also provides a chimney action to the exhaust gas upwards.
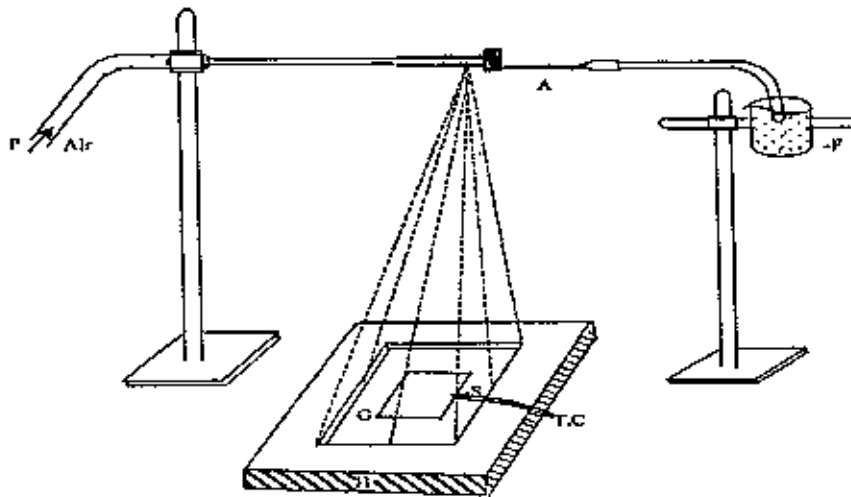
Figure 4.2: Experimental setup of spray pyrolysis technique.

Figure 4.3: Schematic diagram of spray pyrolysis system in laboratory.

4.1.2.4 The Fume Chamber

It is a large type chamber with a slanting top and is provided with a chimney. There is an exhaust fan fitted at the mouth of the chimney to remove the unused gases from the chamber. The slanting top and the sidewalls are made of glass and wood. There air tight doors in the front side. The chamber has purging facilities. The whole spray system and the reactor are kept inside this fume chamber at the time of film deposition because of the safety grounds and to check air current disturbances at the deposition site. These two points just stated are very important for the spray process when deposition is carried out in open-air atmosphere. The single spray nozzle consists of capillary tubes (stainless steel) fitted perpendicular to the other tube as shown in figure 4.2. A very fine needle shaped capillary tube was used for the spray nozzle and it may vary from nozzle to nozzle.

4.1.2.5 Air Compressor

It is reservoir type electrical air compressor. A rotary pump in this section mode draws atmospheric air and keeps it reserved in a large capacity air tank. At the outlet of the tank a pressure gauge is attached which records the pressure of the air at the time of supplying it from the tank. There is a by pass control valve which can keep the output pressure constant.

4.1.2.6 Substrate and Substrate Cleaning

For thin film deposition, several types of substrates are used. Generally, glass, quartz, plastic and ceramic substrates are used for polycrystalline films. However, in the present work, thin films were deposited on glass substrates. The most commonly microscope glass slides having 5 cm long, 2 cm wide and 0.1 cm thickness were used. These were fine smooth high quality microscope glass slides.

The cleaning of substrate has a major influence on the properties of the thin film deposited onto them. Surface contaminations manifest it in pinholes, which can cause open resistor or localized high resistance. The following procedures were used for substrate cleaning. The gross contamination of each of the substrates were first removed by acetone and then washed with distilled water. After washing in distilled water, the

substrates were dipped at first into nitric acid for some time and again washed in distilled water. Taking them out of one by one and then these were washed and thoroughly rinsed with deionized water for several times. Finally, these were dried in hot air and preserved for use. During the whole process the substrates were always held by slide holding forceps.

4.1.3 Working Solution

The working solution was prepared by taking tin (II) chloride dihydrate [$SnCl_2.2H_2O$] as a source material dissolved into ethanol (CH_3CH_2OH) and water (H_2O). Aqueous solutions were prepared by mixing 0.20 M of ($SnCl_2.2H_2O$) and (CH_3CH_2OH) for pure and addition of (1wt%-8wt %) copper nitrate Cu (NO_3)$_2$.$3H_2O$ at different concentrations for copper doped tin oxide thin films. To enhance the solubility of prepared solution, a few drops of HCl were added.

Since the spray system used in the present experiment operates via a partial vacuum path as the mouth of the spray nozzle, the concentration of the solution prepared by the solvent was made in such away that it could he at least be drawn by the nozzle.

4.1.4 Film Deposition Parameters

In the chemical spray deposition technique the structure, composition and other characteristics of the deposited films depend on a number of process variables such as solution flow rate, substrate temperature, deposition time, quality of the substrate material, size of the atomized particles, substrate to spray outlet distance, solution concentration, gas rate (air pressure) etc. are affected on the film properties.

4.1.5 Optimization of the Deposition Process

To obtain the optimum condition of the film deposition process, it is essential to select at first the requirements with respect to which the process should be optimizes. The optimization process is very lengthy because there are a number of process variables. The basic requirement was to get a film of high transparency as well as high electrical conductivity.

For the process of optimization following set of films have been deposited:

(i) The first set of films was deposited at various substrate temperatures, keeping all other deposition parameters constant at an arbitrary level. From the set of films the optimum substrate T_s was selected with respect to the best conducting and transparent film.

(ii) After obtaining the optimum value of T_s, second set of films were deposited by varying the substrate to spray outlet distance, d_s using the optimized T_s and other parameters were kept constant to the arbitrary level as they were in the first set. From this second set of films the optimum distance d_s was selected corresponding to the best film.

(iii) Fixing the distance d_s and substrate temperature T_s, the carrier gas P_a a third set of films were deposited by varying the molar concentration of solution. From this set, optimum molar concentration was selected.

(iv) Keeping T_s, d_s, P_a and molar concentration (0.20 M) as fixed fourth set of films (pure films) were deposited by taking constant spray rate S_r for 5/6 minutes deposition.

(v) The fifth set of films (Cu doped) were deposited keeping T_s, d_s, P_a S_r, molar concentration, deposition time fixed at there optimum values. In this case, the concentration of Cu was varied for Cu doped SnO_2 thin films. Thus in all cases the optimum values of the parameters (T_s, d_s, P_a, S_r and C) were selected for deposition of films that exhibit good conductivity and high transparency.

The resulting optimization is undoubtedly a tentative one because the process variables are in some degree mutually interdependent.

4.1.6 Film Preparation

It has been stated earlier that spray pyrolysis technique for preparing SnO_2 and Cu doped SnO_2 thin film, is an economically attractive method, which consists basically pf spraying solution on a heated glass substrate. The apparatus needed to carry out the chemical spray process consists of a device to atomize the spray solution and a substrate heater. Figure 4.2 shows a typical experimental setup. A considerable amount of (about 50 ml) solution taken in the container 'F' fitted with the spray nozzle 'A'. The clean substrate with a suitable mask was put on the susceptor of the heater 'H'. The distance between the tip of the nozzle and the surface of the glass substrate was kept 30 cm. Before supplying the compressed air the substrate temperature 'T_s' was to be kept at a level slightly higher than

the required substrate temperature because at the onset of spraying a slight fall of temperature is likely. The temperature of substrate was controlled by controlling the heater power using a variance. The substrate temperature was measured by placing a copper constantan thermocouple on the substrate. Deposition rate and time was kept constant for every film such that the thickness of the film may same.

When compressed air is passed through 'P' at constant pressure (1 bar), a fine SnO_2 was produced and was automatically carried to the reactor zone where film was deposited on the heated substrate. We have adjusted a situation such that 5 to 6 minutes of spray produces SnO_2 thin film, thickness of the range 190 nm to 210 nm keeping substrate temperatures ranging from 300°C to 400°C. AR grade $SnCl_2.2H_2O$ taken in the deposition unit was heated and subjected to thermal evaporation. The rate of flow of the working solution can he controlled by a suitable nozzle 'A' and adjusting the airflow rate. The $SnCl_2$ vapors formed were sprayed onto the heated substrate with the help of an air pump; there they transform into tin oxide. The main reaction that leads to the formation of SnO_2 is [64]

$$SnCl_2(g) + O_2(g) \rightarrow SnO_2(s) + Cl_2(g) \uparrow$$
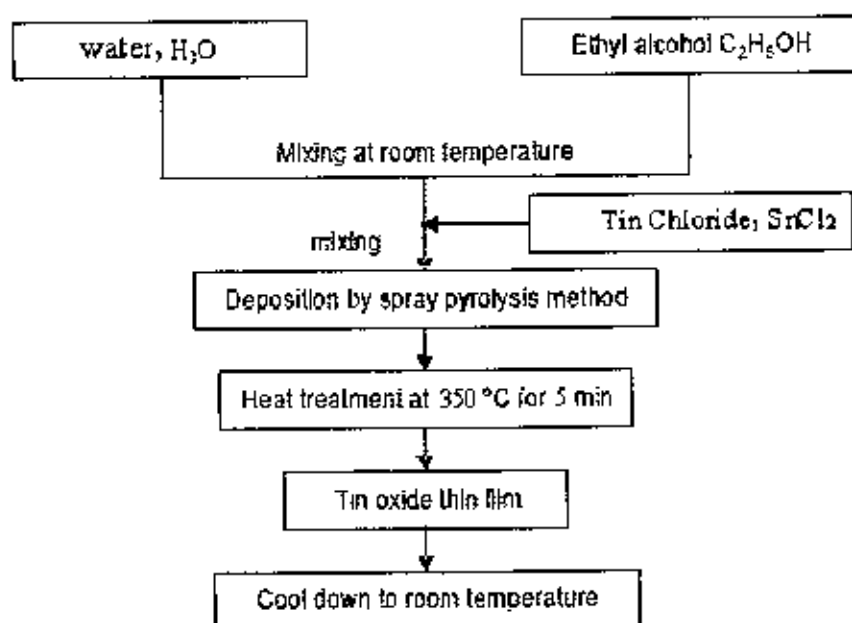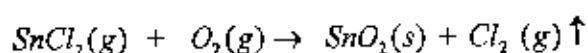
Preparation procedure of a thin film by the spray pyrolysis technique

4.2. Measurement Details

4.2.1 Methods for the Film Thickness Measurement

Film thickness plays an important role on the properties of thin film and those it is one of the most significant film parameter and thickness measurement is a most essential job. Therefore, the thickness should be measured with great care as far as possible to have an accurate value. The thickness may be measured either by monitoring the rate of deposition or after the film is taken out of the deposition chamber. The latter type is appropriate for the spray deposition for the spray deposition technique because it is operated in open atmosphere. In the present work, the film thickness is measured after taking out the film from the chamber. There are many techniques for measuring film thickness, such as Gravimetric Method, Microbalance Technique, Stylus Method, Photometric, Crystal Oscillatory, Color Comparison and Optical Interference etc. Thickness may be directly known by in-site monitoring the rate of deposition or it may be measured after the film is taken out of the deposition chamber. In the present work the later method was used. There are several methods for the measurement of film thickness and in the present work optical interference fringe method was used.

4.2.1.1 Optical Interference Method

The thickness of the film can be measurement accurately by optical interference method and it is one of the best method comparative others process. In this method two reflecting surfaces are brought into close proximity to produce interference fringes. Weiner was the first to use interference fringes for the measurement of film thickness. Latter on using Fizeau fringes, Tolansky developed this method to a remarkable degree and is now accepted as a standard method [44, 45].When two reflecting surfaces are brought into close proximity, interference fringes are produced, the measurement of which makes possible a direct determination of film thickness and surface topography with high accuracy. In this method, two types of fringes are utilized for thickness measurement. The first produces Fizeu fringes of equal thickness, using a monochromatic light source. The second uses a white light source and produces fringes of equal chromatic order. The second method is prepared for thinner films.

The Fizeu fringes method was used in the present work for the measurement of film thickness. For the experimental set up a low power microscope, a monochromatic source of light, a glass plate and an interferometer are required. To make the Fizeau fringes of equal thickness visible in a multiple beam interferometer formed by a thin absorbing film on a glass substrate, generally and auxiliary reflecting coating on the film surface is required. But if the experimental sample is transparent with a very smooth surface no such auxiliary coating is necessary [46].

The film whose thickness is to be measured is required to form a step on a glass substrate and over it another plane glass plate (Fizeau plate) is placed. This illuminated with a parallel monochromatic beam of light a fringe system as shown in figure (2.5) is produced and is viewed with low power microscope. In this method, thickness from 3 nm to 2000 nm can be measured with an accuracy of ± 5nm. The fringe spacing and fringe displacement across the step are measured and used to calculate the film thickness. The displacement 'h' of the fringe system across the film substrate step is then measured to calculate the film thickness 't" using the relation

$$t = \frac{h}{fringes - spacing} \times \frac{\lambda}{2} \quad \text{.........................(4.1)}$$

Where λ is the wavelength of the monochromatic light (sodium light) employed.

If d is the fringe spacing then the film thickness t is given by,

$$t = \frac{h}{d} \times \frac{\lambda}{2} \text{ (nm)} \quad \text{...............................(4.2)}$$

Image plane

Monochromatic source

Microscope

Glass plate

Collimating
Lens

Reference

Film to be measured

Step height (h)

Fringe spacing (d)

h   d
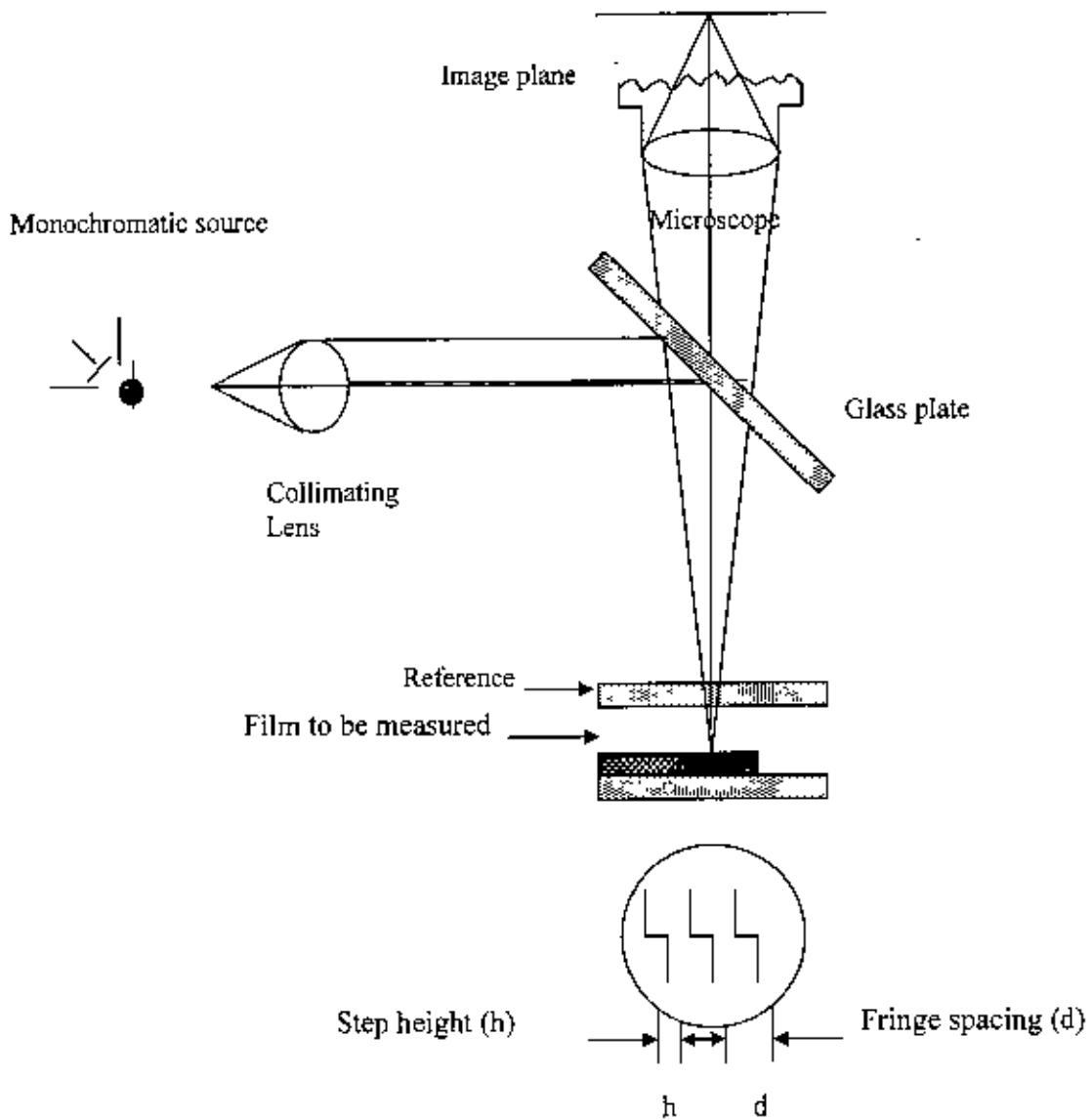
**Figure4.4: Interferometer arrangements for producing Fizeau fringes of equal
thickness**

4.2.2 Surface Morphology and Structural Analysis of Thin Films

4.2.2.1 Study of Scanning Electron Microscopy (SEM) and Energy Dispersive Analysis of X-ray (EDAX)

The scanning electron microscope (SEM) is a type of electron microscope that creates various images (surface morphology) by focusing a high energy beam of electrons onto the surface of a sample and detecting signals from the interaction of the incident electron with the sample's surface. The type of signals gathered in a SEM varies and can include secondary electrons, characteristic x-rays, and back scattered electrons. In a SEM, these signals come not only from the primary beam impinging upon the sample, but from other interactions within the sample near the surface. The SEM is capable of producing high resolution images of a sample surface in its primary use mode, secondary electron imaging. Due to the manner in which this image is created, SEM images have great depth of field yielding a characteristic three-dimensional appearance useful for understanding the surface structure of a sample. This great depth of field and the wide range of magnifications are the most familiar imaging mode for specimens in the SEM. Characteristic x-rays are emitted when the primary beam causes the ejection of inner shell electrons from the sample and are used to tell the elemental composition of the sample. The back-scattered electrons emitted from the sample may be used alone to form an image or in conjunction with the characteristic x-rays as atomic number contrast clues to the elemental composition of the sample.

Scanning Electron Microscopy (SEM) measurement was performed at the Bangladesh Council for Scientific and Industrial Research (BCSIR), Dhaka. S-3400N HITACHI, JAPAN, apparatus is used to carry out the SEM measurement. This apparatus operates in the range of 300 V to 30 KV. It has 5 to 300 thousand times magnification capacity. This apparatus has two imaging system, secondary electron imaging (SE imaging) and back scattered imaging (BS imaging).

EDAX describes the compositional analysis of the thin films. This is done by the scanning electron microscopy (SEM) by focusing the X-ray beam on the full frame or a particular spot of the thin films. The analysis represents the individual weight (%) of the element that is present in the thin films.

4.2.2.2 X-ray Diffraction (XRD) Study

The X-ray diffraction (XRD) provides substantial information on the crystal structure. XRD is one of the oldest and effective tools for the determination of the atomic arrangement in a crystal, X-rays are the electromagnetic waves and its wavelength $\approx$ 0.1nm The wavelength of an X-ray is thus of the same order of magnitude as the lattice constant of crystals

When X-rays are incident on a crystal surface, they are reflected from it. The reflection obeys the following Bragg's law

$$2d \sin\theta = n\lambda \quad \ldots\ldots\ldots\ldots\ldots\ldots\ldots (4.3)$$

Where, d is the distance between crystal planes; θ is the X-ray incident angle; λ is the wavelength of the X-ray and n is a positive integer. Bragg's law also suggests that the diffraction is only possible when $\lambda < 2d$.

Attempts were made to study the structure of the films by X-ray diffraction. X-ray diffractometer system PW3040 X'Pert PRO X-ray Philips Company was used at Magnetic Material Division (MMD) of Atomic Energy Center, Dhaka (AECD). The monochromatic (using Ni filter) CuK_α radiation was used and the accelerating potential was 40 KV constituting a current of 30 mA. The scanning speed was 2θ degree and the measurement was done in the range $20°$ to $60°$, respectively to obtain the X-ray diffraction pattern of the pure and Cu doped SnO_2 thin films. All the data of the samples were analyzed by using computer software "X'PERT HIGHSCORE" from which structural parameters was determined

4.2.3 Optical Property Analysis of Thin Films

The optical behaviors of a semiconductor are investigated in term of the three phenomena namely transmission, reflection and absorption. When a semiconductor is illuminated by light, photon strikes the surface, a fraction of photons are reflected, some of these are absorbed within the semiconductor and the remainder transmitted into the semiconductor and some may be reflected. For optical property studies of pure and copper doped SnO_2 thin films were measured transmittance and absorbance by using a double beam UV spectrophotometer. Measurements were made by placing the sample in the incident beam and another empty glass substrate in the reference beam of the instrument. The optical transmission and reflection spectra of the film with respect to glass substrate were than taken for wavelength range 290 to 1100 nm using UV-1601 PC SHIMADZU VISIBLE SPECTROMETER. The spectral transmittance and absorbance of SnO_2 films were considerer in two wavelength regions, namely, visible and infrared regions. The optical spectra of transmittance, T (%) and absorbance, A (%) have been measured with respect to plain glass substrate were taken using the spectrophotometer.

4.2.3.1 Measurement of Absorption Coefficient and Optical Band Gap

Absorption co-efficient and optical band gap have been calculated using transmittance and absorption spectra taken at room temperature directly. Knowing the film thickness and transmittance at the corresponding wavelength, one can determine absorption coefficient by using equation (4.4.1).

$$\alpha = -\frac{\ln T}{t} \quad \text{............... (4.4.1)}$$

From the optical transmission data were analyzed using the classical relation for near edge of the optical absorption using the relation (for $\alpha > 10^4$ cm^{-1})

$$(\alpha h\upsilon) = B (h\upsilon - E_g)^n \quad \text{............... (4.4.2)}$$

Where B is a constant in the optical frequency range and E_g is the optical band gap, and n is an index related to the density of state curves for the energy. This n is determined by the nature of the optical transmission involved in the absorption process whereas n = 2 for direct transition and for indirect transition n=1/2. Analysis of the data have been made considering both n =1/2 and n = 2.

4.2.4 Electrical Property Analysis of Thin Films

4.2.4.1 Measurements of the Resistivity and Electrical Conductivity

Resistivity and electrical conductivity of SnO_2 thin film was measured by Van-der Pauw's method. Van-der Pauw Method [47] is one of the standard and widely used techniques for the measurement of resistivity of thin film. The Van-der Pauw method is a technique for doing 4-probe resistivity and Hall effect measurements. The advantages of this method include low cost and simplicity. The Van-der Pauw technique can be used on any thin sample of material and the four contacts can be placed anywhere on the perimeter/boundary, provided certain conditions are met:

- The contacts are on the boundary of the sample (or as close to the boundary as possible)
- The contacts are infinitely small (or as close as possible)
- The sample is thin relative to the other dimensions

A brief account of this method is given bellow because in our measurement we have used Van-der Pauw Method.
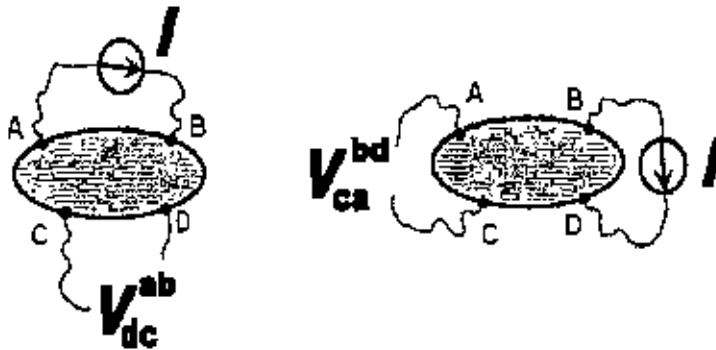
Figure 4.5: Van-der Pauw method for resistivity measurements of a thin film of arbitrary shape

At first we select a region on the sample where four electrical contacts were made at four corners, say A, B, C, and D as shown in figure 4.5. Silver past was used to the contact. The sample should not need to be of the shape as shown in figure. This method is applicable for any arbitrary shape of uniform sheet of material with four contacts applied

to the periphery. Through commutative switches the connections are made between the film and the meter terminals.

If a dc current I_{AB} entering the specimen through the contact A and leaving through the contact, B produces a potential difference V_D-V_C between C and D then the resistance $R_{AB,CD}$ can be expressed as

$$R_{AB,CD} = \frac{V_D - V_C}{I_{AB}} = \frac{V_{CD}}{I_{AB}} \quad \dots\dots\dots\dots \quad (4.5)$$

Similarly,

$$R_{BC,DA} = \frac{V_A - V_D}{I_{BC}} = \frac{V_{DA}}{I_{BC}} \quad \dots\dots\dots\dots \quad (4.6)$$

$$R_{CD,AB} = \frac{V_B - V_A}{I_{CD}} = \frac{V_{AB}}{I_{CD}} \quad \dots\dots\dots\dots\dots \quad (4.7)$$

And

$$R_{DA,BC} = \frac{V_C - V_B}{I_{DA}} = \frac{V_{BC}}{I_{DA}} \quad \dots\dots\dots\dots\dots \quad (4.8)$$

The resistivity of a thin film can be expressed as by the equation

$$\rho = \frac{\pi t}{\ln 2}\left[\frac{R_{AB,CD} + R_{BC,AD}}{2}\right] \times f\left[\frac{R_{AB,CD}}{R_{BC,DA}}\right] \quad \dots\dots\dots\dots \quad (4.9)$$

$$\text{or,} \quad \rho = 4.53t \times \left[\frac{R_{AB,CD} + R_{BC,AD}}{2}\right] \times f\left[\frac{R_{AB,CD}}{R_{BC,DA}}\right] \quad \dots\dots\dots\dots \quad (4.10)$$

Where t is the thickness of the film and the function f can be evaluated from the equation

$$\left[\frac{R_{AB,CD} - R_{BC,DA}}{R_{AB,CD} + R_{BC,DA}}\right] = \frac{f}{\ln 2}\text{arccos}h\frac{\exp(\ln 2 / f)}{2} \quad \dots\dots\dots \quad (4.11)$$

If, $R_{AB,CD}$ and $R_{BC,DA}$ is almost equal, f may approximately equal to unity and then the equation (4.11) takes the form,

$$\rho = 2.265t\left(R_{AB,CD} + R_{BC,DA}\right)ohm - cm \quad \dots\dots\dots\dots \quad (4.12)$$

4.2.4.2 Sheet Resistance

The resistance of a thin film directly proportional to the resistivity ρ and inversely proportional to the thickness t and we can write for a rectangular film of length L and width W. Then the resistance, R of the film is given by,

$$R = \left(\frac{\rho}{t}\right) \times \left(\frac{L}{W}\right) = R_s \left(\frac{L}{W}\right) \quad \text{................} \quad (4.13)$$

Where, $R_s = \frac{\rho}{t}$ is known as the sheet resistance and expressed in ohms per square.

4.2.4.3 Activation energy

The energy requisite to transfer charge from one neutral island to another is known as activation energy and it is denoted by ΔE. This is equivalent to the electrostatic binding energy of the charge to the island. The activation energy, which is related to the electron transport process in the material, can be expressed by a conventional type relation

$$\sigma = \sigma_0 \exp\left(\frac{-\Delta E}{2kT}\right) \quad \text{...............} \quad (4.15)$$

Where k is the Boltzmann constant and T is the absolute temperature.

Equation (4.15) can be written as,

$$\ln \sigma = \ln \sigma_0 + \left(\frac{-\Delta E}{2kT}\right) \quad \text{..............} \quad (4.16)$$

The activation energy ΔE is calculated from the slop of a curve $\ln\sigma$ vs. (1/T). So the activation energy is given by

$$\Delta E = -\frac{\ln \sigma}{1/T} 2k \quad \text{..................} \quad (4.17)$$

The circuit arrangements used for the resistivity and conductivity measurement are shown in Fig. 4.6.
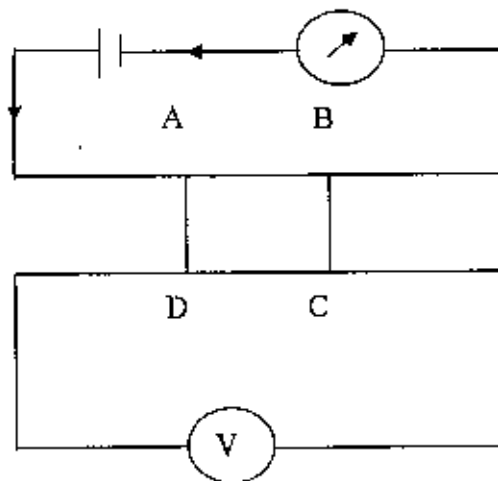
Figure 4.6: Circuit arrangements to measure resistivity

CHAPTER-V

RESULTS AND DISCUSSION

5.1. Introduction

5.2. Deposition of SnO_2 Thin Film

5.3 Thickness Measurement

5.4. Surface Morphology and Structural Investigation

5.4.1 SEM EDX Study

5.4.2 XRD Study

5.5. Optical Properties

5.5.1 Optical Transmission and Absorption Coefficient

5.5.2 Optical Absorbance

5.5.3 Optical Band Gap

5.5.4 Refractive Index

5.6. Electrical Properties

5.6.1 Variation of Resistivity with Temperature

5.6.2 Variation of Sheet Resistance with Temperature

5.6.3 Variation of Conductivity ($\ln\sigma$) with Inverse Temperature

5.6.4 Variation of Activation Energy with Cu Doping

CHAPTER-V

RESULTS AND DISCUSSION

5.1 Introduction

The objective of this study is to synthesis and characterizes of pure and Cu doped SnO_2 thin films by home fabricated spray pyrolysis system. Here films deposited by the reduced of the preparation cost and made it economically feasible. In this chapter the results and discussion of the various experimental studies viz. surface morphology structural, optical and electrical properties of pure and Cu doped SnO_2 thin films have been presented and discussed step by step.

5.2 Deposition of Pure (tin oxide) and Cu Doped SnO_2 Thin Films

To prepare SnO_2 thin film tin chloride ($SnCl_2 2H_2O$) was taken as a source material and copper nitrate [Cu $(NO_3)_2.3H_2O$] was taken for Cu doped Ethanol and water was taken as solvent since tin chloride dissolves well in water and ethanol at room temperature and ethanol may take easy vaporized. 0.2 M concentration of tin chloride solutions were made where 0-8% copper nitrate was dissolved. In the present spray deposited, the deposition time was 5 minutes, substrate temperature was kept 350° C and substrate to spray nozzle distance was 30 cm and flow rate of solution was kept constant as 5ml/min. The colour of the pure tin oxide thin film is white (deep) which turns grays white on copper doping. In looking the film is uniform and homogeneous.

5.3 Thickness Measurement

The thickness of the films was measured by the setup of Fizeau fringes at Department of Physics, BUET, and Dhaka. Thickness of the films was varying with ± 10 nm, but here films were used for measurement only whose films thickness was about 200 nm. Photograph of composted SnO_2 thin film shows uniform deposition and surface consistency of the film slightly changed for Cu doping

5.4 Surface Morphology and Structural Investigation

5.4.1 SEM and EDX Study

Scanning Electron Microscopy (SEM) has been used to characterize the surface morphology and to find out the grain and impurity of pure and Cu doped SnO_2 thin films, respectively. SEM images Fig. 5.1 to5.4 is shown that the surface of the film is uniform and homogeneous. After Cu doping the surface nature of the film may little change. SEM images show that there are no remarkable grains and impurity for the SnO_2 thin films. The films were found uniform and well covered on the glass substrate surface. SEM photograph reveals that sprayed particles (atoms) are absorbed onto the glass substrate into clusters as the primary stage of nucleation. After Cu doping the surface of the films little change and for 5% Cu doping it is shown that surface of the films may vast change. So, the SEM surface studies of both pure and Cu doped SnO_2 and films exhibit a smooth and homogeneous growth in the entire surface.

The EDX images of pure and Cu doped SnO_2 thin films are shown in Fig.5.5 to 5.8.The quantitative analysis of the deposited films carried out by EDX images (Fig. 5.5) shown that there are two strong peaks corresponding to Sn and O were found in the spectrum which confirms the high purity of the SnO_2 thin films. An average atomic percentage of Sn and O were found to be 56.37 and 43.63 respectively. It is significance to mention that the deposited films are stoichiometric. It is cleared from EDX images (Fig. 5.6 to 5.8) that the grains were typically comprised of both Cu and Sn metals. The percent of Sn, O, and Cu present in films for different concentration of Cu are shown in table 5.1. From EDX images it is observed that the height of the peak for Sn decreases and Cu increases with the increases of the Cu doping. From the table 5.1 it is evident that for all the films the amount of Sn and O for pure and Sn, O and Cu for doped films are present at an excellent ratio. There is a shift in the wavelength at which it occurs clearly signifying a crystal field effect. Further evidence is presented in the form of X-ray diffraction patterns shown in figure 5.9. Hence from the EDX, optical absorption spectra and X-ray diffraction patterns, it is clear that the Cu^{+2} ions are acting as dopants in the SnO_2 structure.
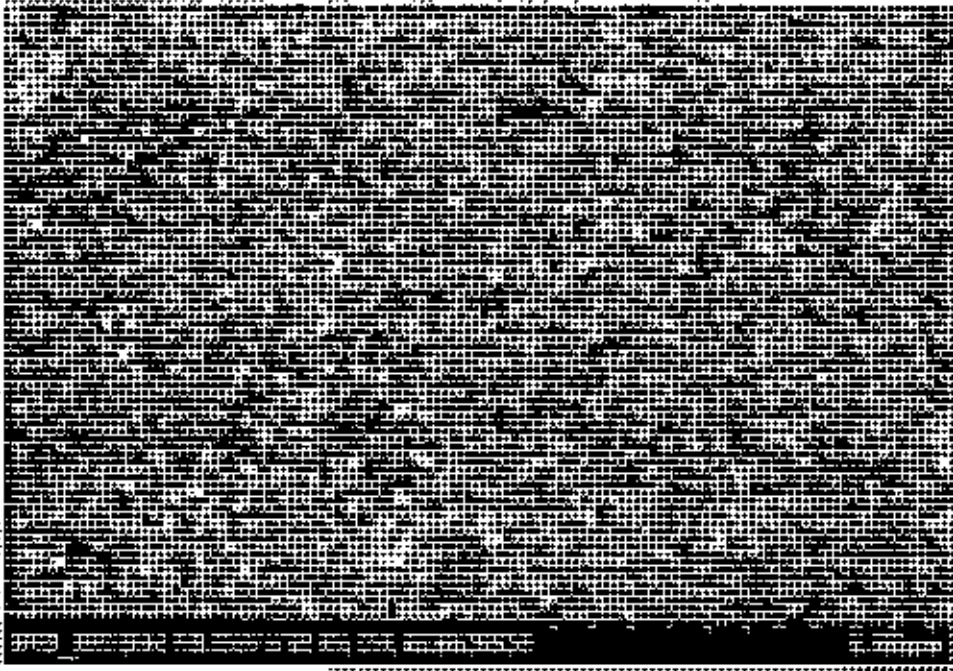
Figure 5.1: SEM image of pure SnO_2 thin film
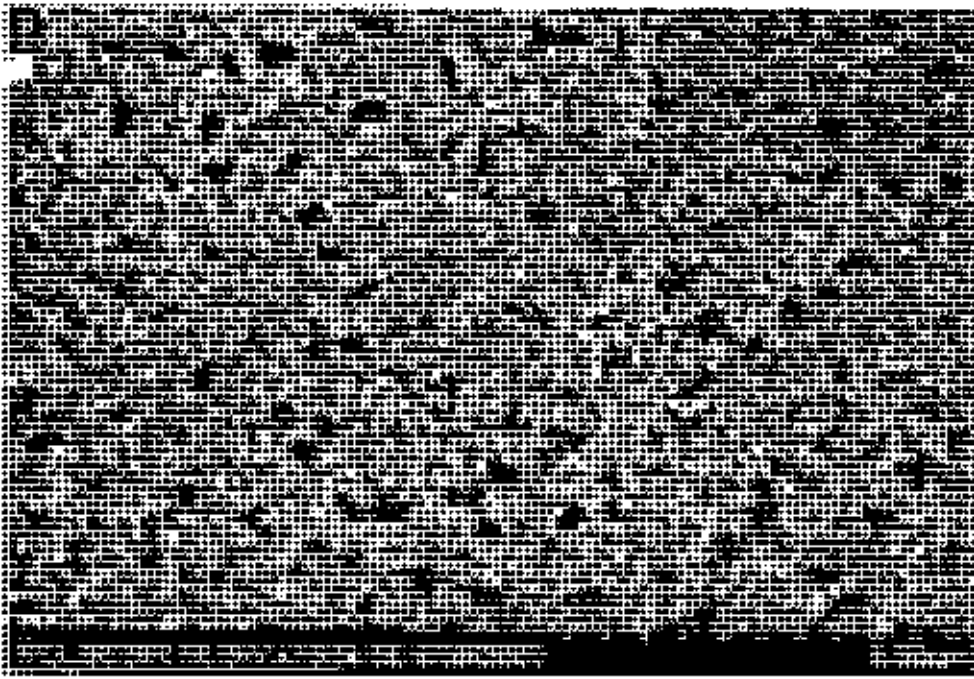
Figure 5.2: SEM image of 2% Cu doped SnO_2 thin film
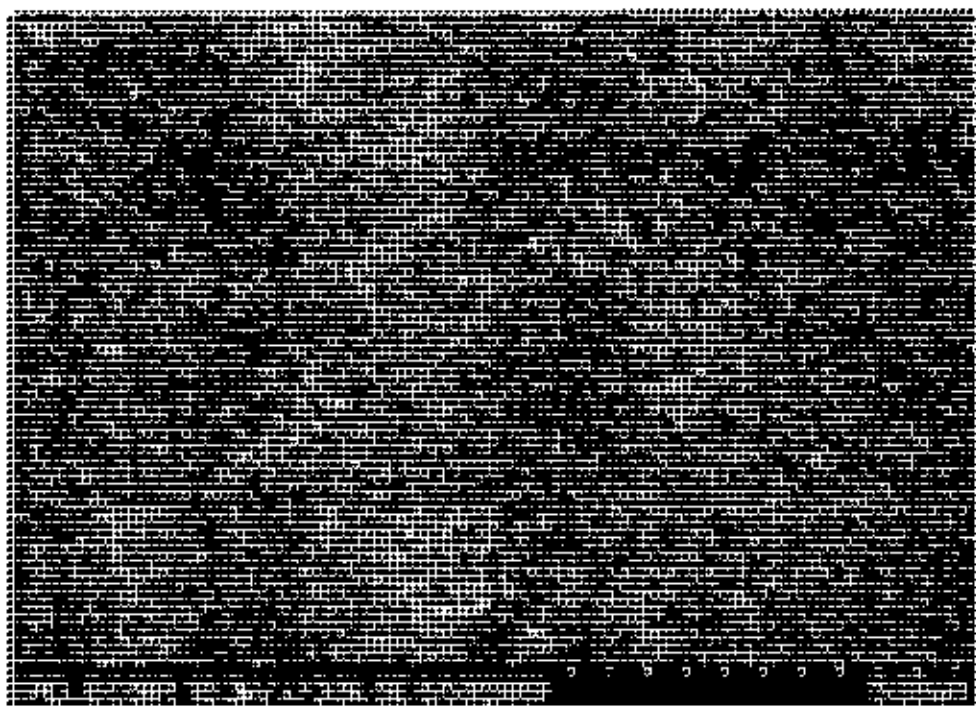
Figure 5.3: SEM image of 4% Cu doped SnO_2 thin film
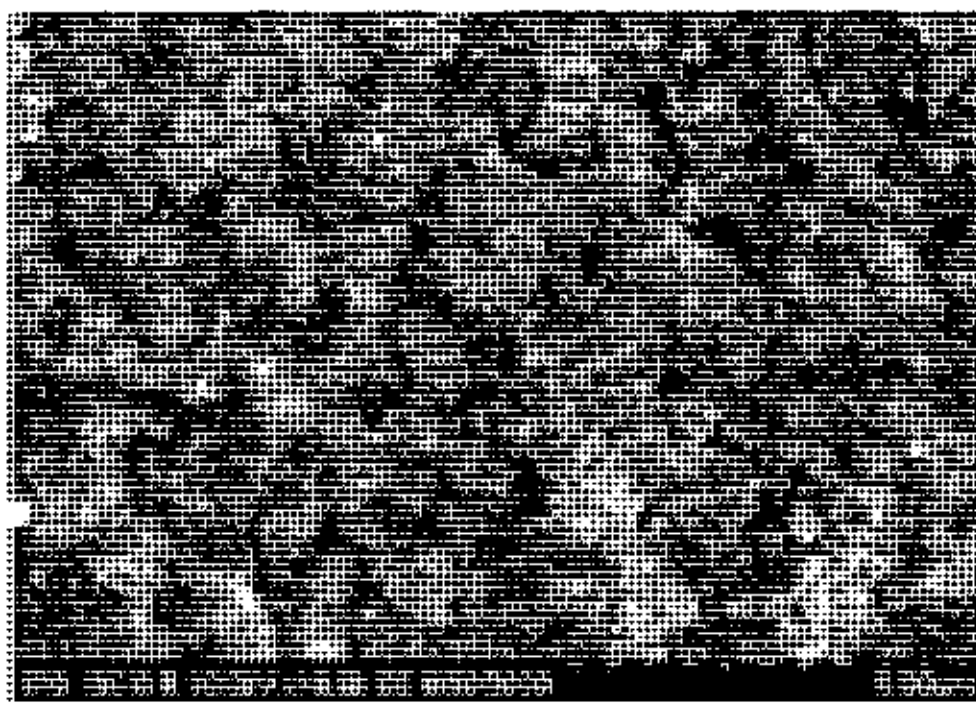
Figure 5.4: SEM image of 5% Cu doped SnO_2 thin films

Table 5.1: Quantitative results of pure and Cu doped SnO_2 thin films from EDX analysis.

Sample	Element	Net counts	Weight %	Atom %
Pure SnO_2 film	O	5879	9.45	43.63
	Sn	69545	90.55	56.37
2% Cu SnO_2 film	O	12185	51.84	88.85
	Sn	8818	48.06	11.10
	Cu	17	0.10	0.04
4% Cu SnO_2 film	O	6931	17.30	60.41
	Sn	37286	81.12	38.19
	Cu	609	1.58	1.39
5% Cu SnO_2 film	O	9517	20.50	63.30
	Sn	33688	69.52	28.94
	Cu	4378	9.98	7.76
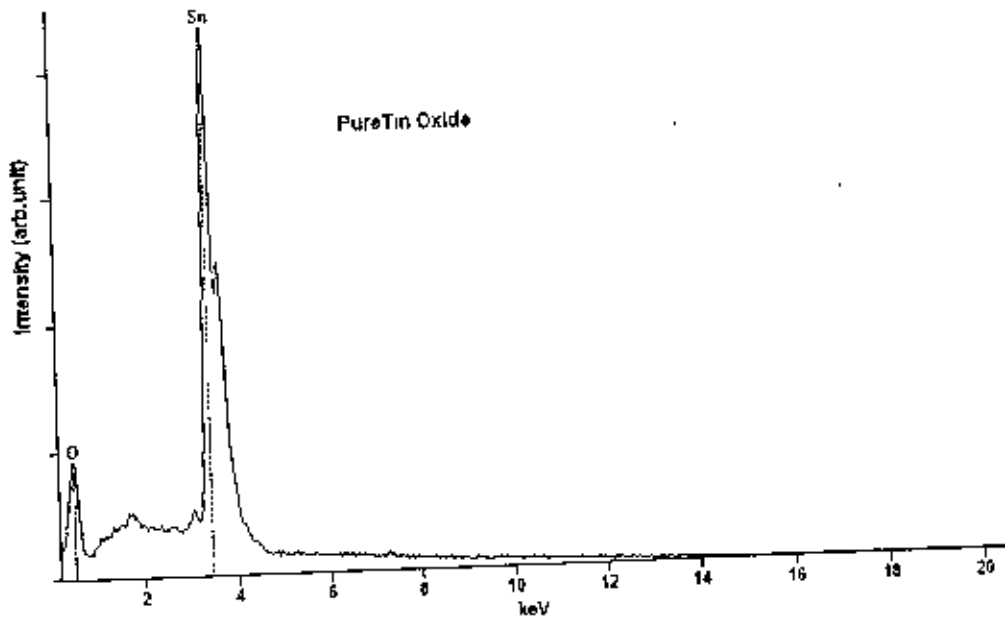
Figure 5.5: EDX spectra of pure SnO₂ thin films
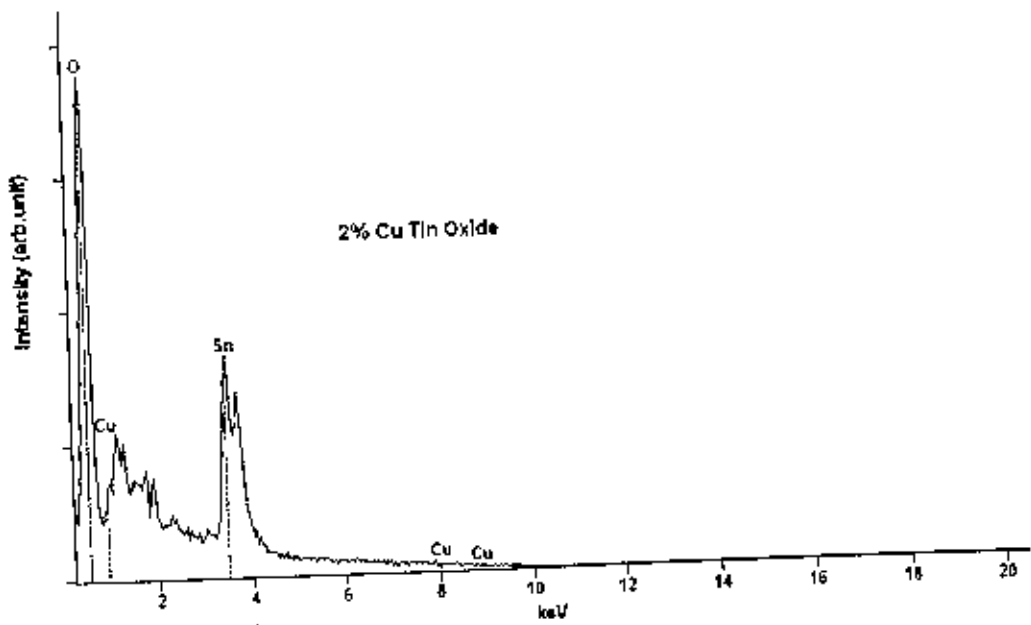
Figure 5.6: EDX spectra of 2% Cu doped SnO₂ thin films
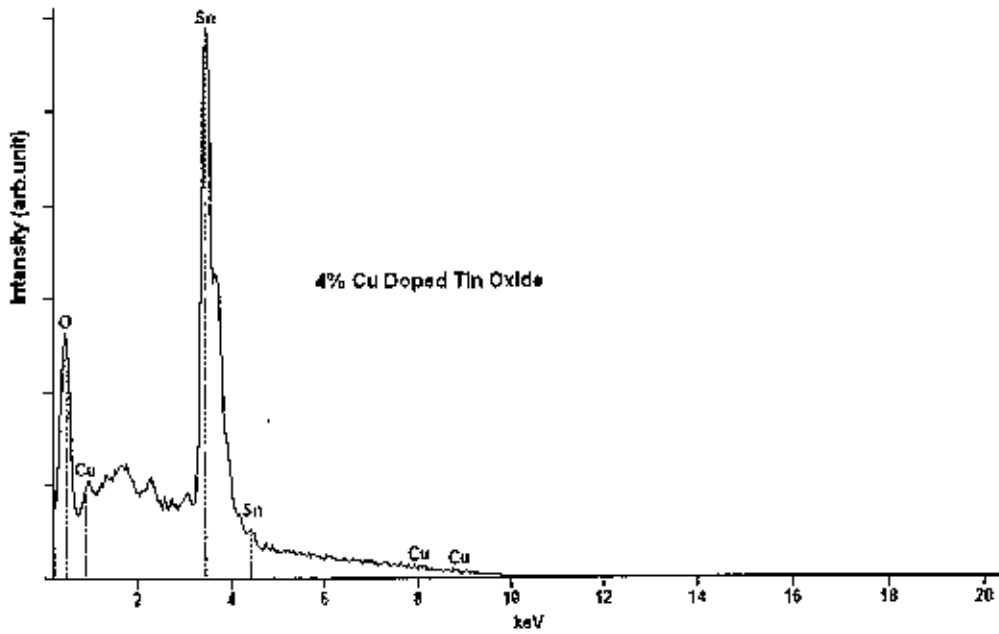
Figure 5.7: EDX spectra of 4% Cu doped SnO$_2$ thin films.
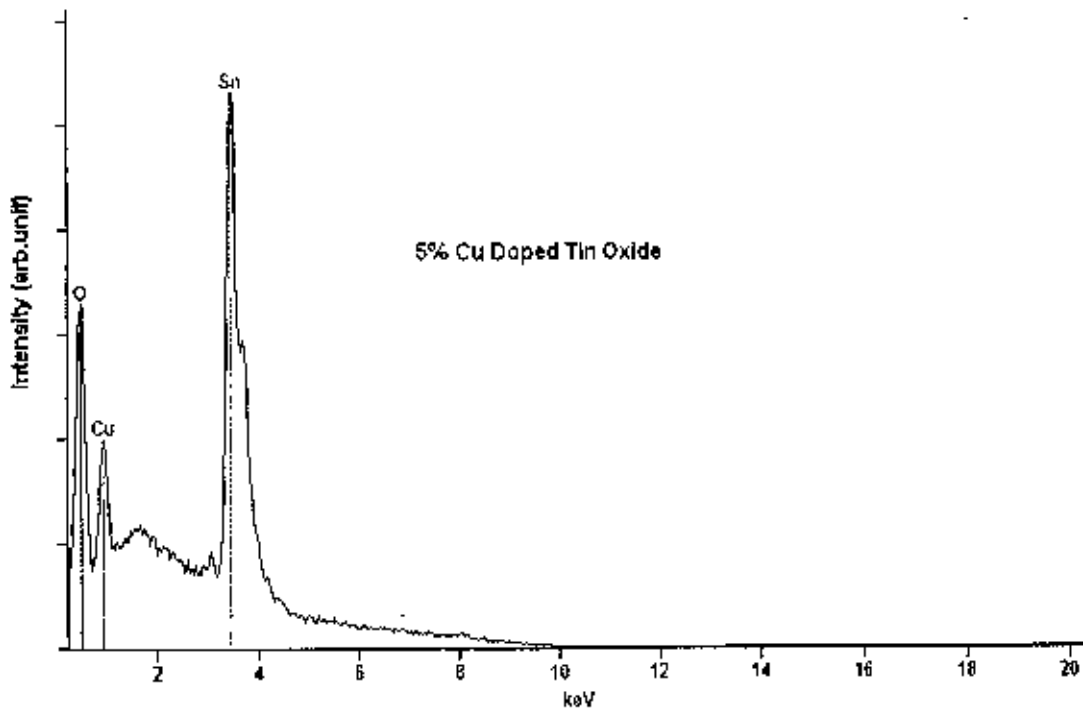
Figure 5.8: EDX spectra of 5% Cu doped SnO$_2$ thin films.

107357

5.4.2 XRD Study

The X-ray diffraction of pure and Cu doped SnO_2 thin film samples has been done using a diffractometer, PHILIPS model "X'Pert PRO XRD System .X-ray diffractograms of all the samples have been recorded using monochromatic CuK_α radiation (λ = 1.54178 Å), scanning speed 2 degree/min, starting from 10° and ending at 60° to ensure the information of the single phase nature of the sintered product. Peak intensities are recorded corresponding to their 2θ values.

Using the data of diffractogram, the d_{hkl} (inter-planar distance) values and their corresponding <hkl> values have been calculated. The d_{hkl} values of pure and Cu doped films and their corresponding <hkl> values from the standard JCPDS Card# 4-0854 [74], and the calculated lattice parameter (a, b, c) values, deviation of 2θ and grain size of these samples are tabulated in table 5.2 to 5.3. The X-ray diffractogram of SnO_2 samples with different concentration of Cu are shown in Fig.3.1 and 3.4, respectively. It is seen from these diffractograms that the pure and Cu doped SnO_2 films respectively, have different peak at d_{hkl} values with its corresponding crystal planes in JCPDS card. Different fundamental peaks were identified as (110), (101), (200), (210), (211), and (220), for pure SnO_2 films which indicate the tetragonal structure of SnO_2. This is tetragonal wurtzite type structure which is formed in the present case during pyrolysis of SnO_2. Grain size of the prepared SnO_2 thin film was determined from the stronger peaks of (110) from each XRD patterns using Scherrer formula [58],

$$D_g = \frac{K\lambda}{\delta\omega\cos\theta}$$

Where D_g is the average grain size, λ is the wavelength of the radiation used as the primary beam of CuK_α (λ= 1.54178 Å), θ is the angle of incidence in degree (Bragg angle) and δω is the full width at half maximum (FWHM) of the peak in radian, which was determined experimentally after correction of instrumental broadening (in the present case it is 0.05°).Thin films, where two strong peaks (110) and (101) are shown in expanded form to understand the variation of FWHM and peak shift of Bragg peaks with temperature. Lattice parameters a and c were determined from the 2θ value. It is seen that the value of lattice parameter a was observed 4 7522 Å for pure SnO_2 and it shifted to 4.7482 Å after 2% Cu doping. Similarly the value of a was observed changed due to

different percentage of Cu dopping is given in table 5.3. Similarly the value of the parameter c was 3.1804 Å for pure SnO_2 films and it shifted to 3.1927 Å for 2% Cu doping. Both the values of a and c change with increasing of Cu doping. Average grain size of SnO_2 thin film have been obtained in the range of 7 244579 Å to 6.06995 Å, which indicates the Angstrom size of SnO_2 grains developed in the film. It was observed that $\Delta 2\theta^\circ$ value is different for Cu doped SnO_2 films than pure SnO_2 thin films. Peak shift was observed very clearly in figure 5.9 to 5.12 and in table 5.2.to 5.3. From this figure it is observed that the peaks in the doped films shift from their standard positions in the presence of the dopant. The shift in the lattice parameter is mainly due to the dopant occupying interstitial positions in the lattice. XRD patterns of SnO_2 films is pound to have a better polycrystalline nature oriented along the (110), (101), and (200), (211) planes at $2\theta = 26.591^\circ$, 33.888°, 37.959 and 51.787° respectively with single phase SnO_2. This is in good agreement with [21, 24, 59, and 60]. The presence of other orientations such as (210), (220) was also detected with another agreements. The (110) surface of SnO_2 is energetically the most stable and the predominant crystal face found in polycrystalline samples. On Cu doped no peaks corresponding to their compounds were detected. The intensity of the peak corresponding to the plane (200) is increased on Cu doping, which shows better atomic arrangement and lower scattering in these planes. On increasing the concentration of Cu the intensity of the SnO_2 peaks were further decreased due to the decrease in the atomic density in these planes. The decrease in peak intensities is basically due to the replacement of Sn^{+4} ions with Cu ions in the lattice of SnO_2 film as in [69]. This process leads to the movement of Sn^{+4} ions in the interstitial sites and also an increase in the amorphous phase and disorder.

Table 5.2: X-ray diffraction data for pure and Cu doped SnO₂ thin films

Sample	hkl	I/I₀ [%]	2θ° (cal)	2θ° (exp)	Δ2θ°
Pure SnO₂ thin film	(110)	100	26.591	26.5262	+0.0648
	(101)	29.76	33.888	33.8882	-0.0002
	(200)	8.86	37.959	37.8692	+0.0898
	(210)	11.68	42.645	42.9309	-0.2859
	(211)	22.72	51.787	51.6729	+0.1141
	(220)	5.77	54.767	54.6531	+0.1139
2% Cu doped SnO₂ thin film	(110)	100	26.591	26.5491	+0.0419
	(101)	22.83	33.888	33.8334	+0.0546
	(200)	17.39	37.959	37.9569	+0.0021
	(211)	21.54	51.787	51.7535	+0.0335
	(220)	4.83	53.767	54.694	-0.927
4% Cu doped SnO₂ thin film	(110)	100	26.591	26.5286	+0.0624
	(101)	20.13	33.888	33.8561	+0.0319
	(200)	30.05	37.959	37.8459	+0.1131
	(211)	19.08	51.787	51.6989	+0.0881
	(220)	7.34	53.767	54.6763	-0.9093
5% Cu doped SnO₂ thin film	(110)	100	26.591	26.4947	+0.0963
	(101)	30.09	33.888	33.7773	+0.1107
	(200)	21.53	37.959	37.8364	+0.1226
	(211)	11.57	42.645	43.2374	-0.5924
	(220)	26.67	51.787	51.7163	+0.0707

Table 5.3: Lattice parameters and grain size for pure and Cu doped SnO₂ thin films

Sample(film)	Lattice parameter, a	Lattice parameter, c	Grain size in Å
Pure SnO₂	4.7522	3.1804	7.244579
2% Cu doped SnO₂	4.7482	3.1927	6.585204
4% Cu doped SnO₂	4.7518	3.1874	7.244096
5% Cu doped SnO₂	4.7578	3.1972	6.06995
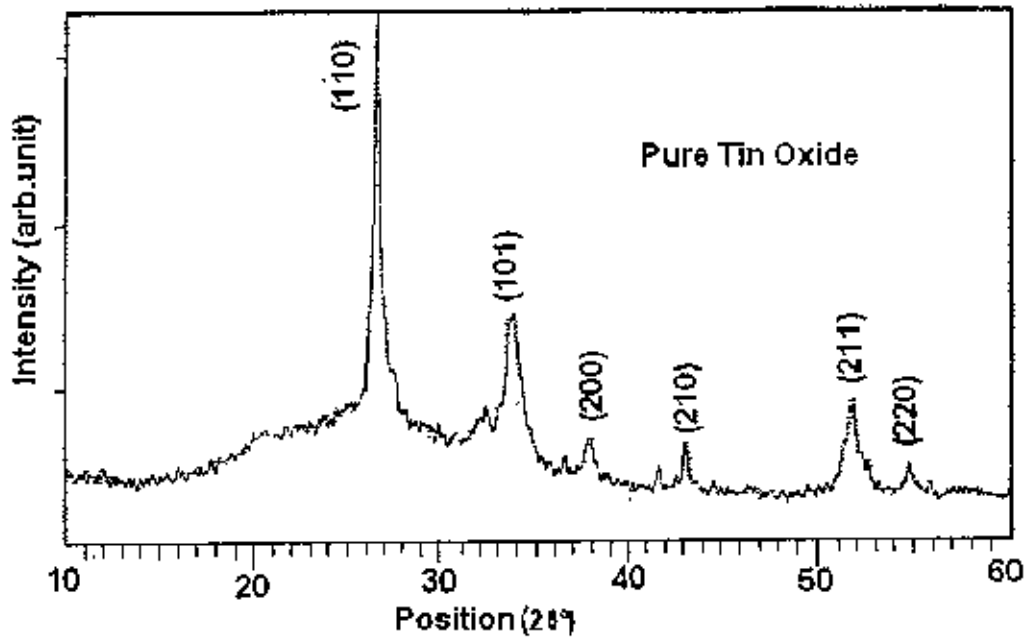
Figure 5.9: XRD spectra for pure SnO₂ thin film
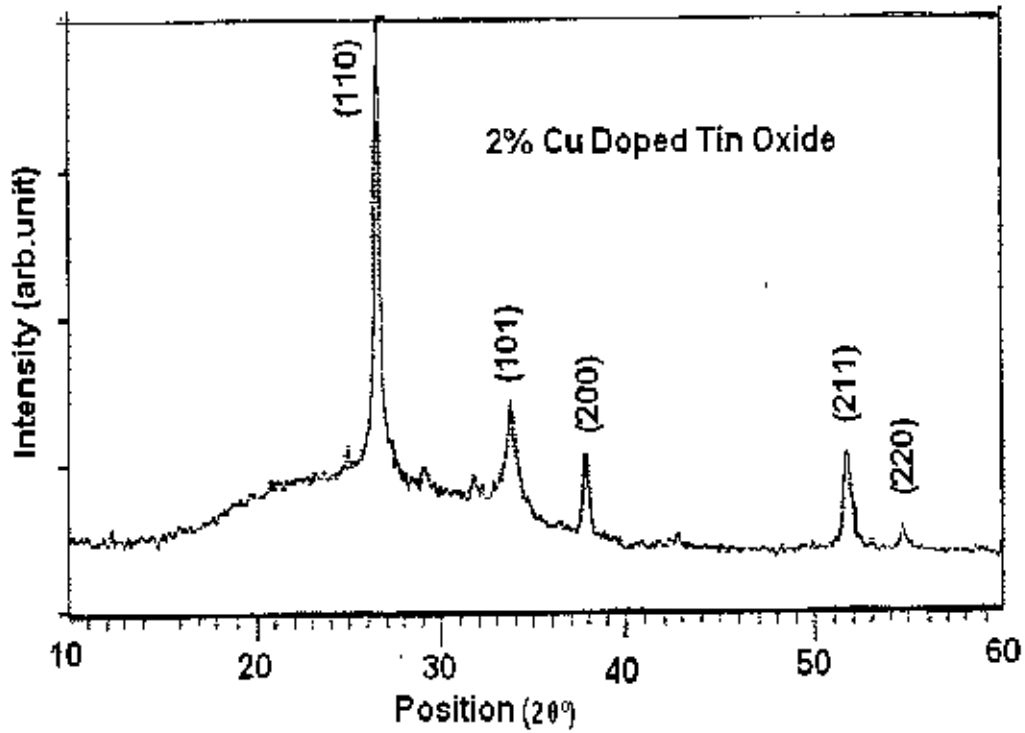
Figure 5.10: XRD spectra for pure 2% Cu doped SnO₂ thin film
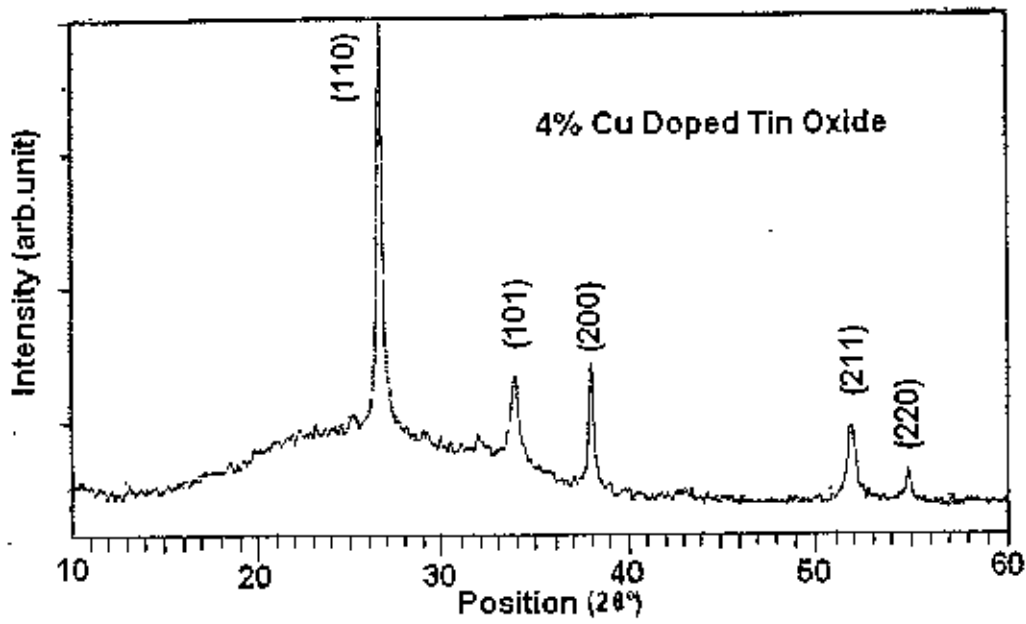
Figure 5.11: XRD spectra for pure 4% Cu doped SnO₂ thin film.
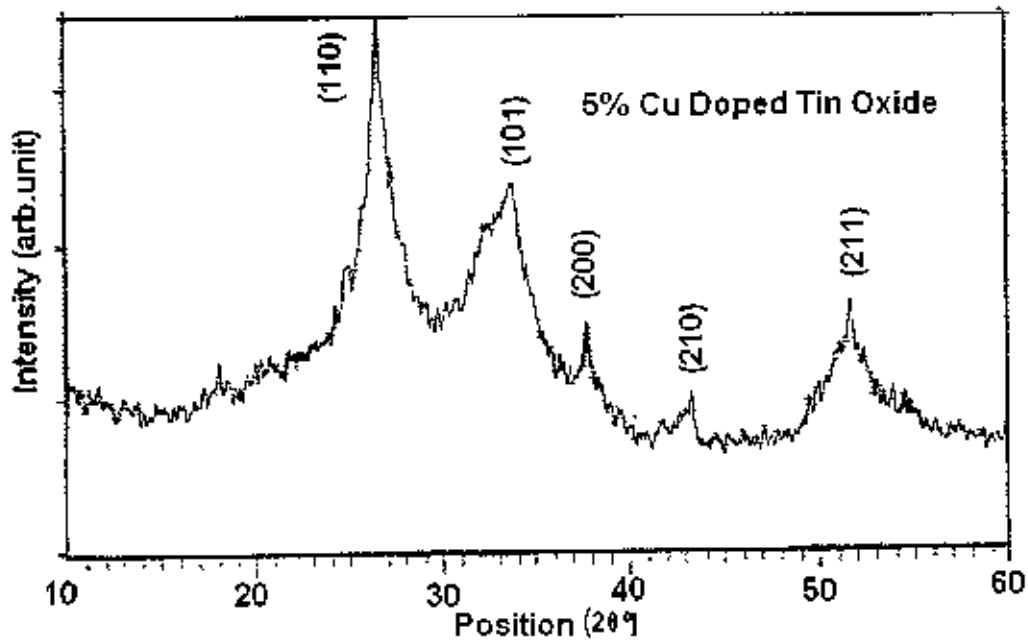
Figure 5.12: XRD spectra for 5% Cu doped SnO₂ thin film

5.5 Optical Properties

5.5.1 Optical Transmission and Absorption Coefficient

Optical properties of pure and Cu doped SnO_2 thin films such as transmittance, absorbance, direct and indirect band gap, refractive index, etc were calculated as deposited films. Transmission spectra were taken within range of 300 nm to 1100 nm for films. Fig.5.13 shows the variation of transmittance with wavelength for pure and Cu doped SnO_2 thin films having thickness 200nm, and its data are shown in table 5.10 to 5.18. It is seen from the graph that the values of transmittance is high in the visible and IR region it is minimum at wavelength ~ 300 nm. Among these transmittance plots it is also seen from the graph that films deposited at 4% Cu doped is the highest in transmittance value. The values of transmittance are decrease after 4% Cu doped films. Films prepared at 350° C exhibit a transmission of > 60% in the visible and IR region, again it is found > 70% in the visible and IR region for Cu doped film, which is found to be greater than that of undoped film. It is found that transmittance decreases with increasing concentration of the dopant, which is due to the increase in the amorphous nature of the doped films as revealed by XRD. The transmittance of the films is also influenced by a number of effects, which include surface roughness and optical inhomogenity in the direction normal to the film surface.

From transmittance spectra, the absorption coefficient and optical band gap were calculated for pure and Cu (1%-8%). The absorption coefficient (α) was calculated from the transmission spectra using the relation

$$\alpha = - \ln T/t \quad \ldots\ldots\ldots\ldots (5.1)$$

Variation of absorption coefficient (α) with photon energy (hυ) for pure and Cu doped SnO_2 thin films is shown in Fig.5.14. This figure shows the distinction of α with photon energy for Cu doping. The absorption coefficient is of the order of 10^6 m^{-1} which may also be suitable for a transparent conducting film. From both the figures it is observed that the absorption coefficient first increases slowly in the low energy region i.e. in the

high wavelength region and then increases sharply near the absorption edge. The value of the absorption coefficient depends on Cu doping. It is decreases as the concentration of Cu increases but it is increases as Cu doping as more than 4%.

Significantly, it was observed that at a dopant concentration of ~ 8 wt% the transmission in the films reached a minimum accompanied by a increase in the optical band gap. At the same value of dopant concentration the resistivity also reached a peak. This behavior appears to be a consequence of valence fluctuation in Sn between the 2^+ and 4^+ states. The transparent conductivity behavior it's into a model that attributes it to the presence of Sn interstitials rather than oxygen vacancies alone in the presence of Sn^{2+}.

5.5.2 Optical Absorbance

Figure 5.15 shows the variation of absorption with wavelength of pure and Cu doped thin films. It is found that the absorption is decreased with higher wavelength slowly. It is also observed that absorption is rapid increase at lower wavelength. For Cu doping absorbance shifted to low intensity but more than 4% Cu doped it shifted to high intensity compare to pure SnO_2 thin films. The absorbance spectrum for pure and Cu doped SnO_2 thin film is shown in Fig.5.15, absorbance spectrum shows low absorbance in the entire wavelength region but it high at wavelength < 350 nm. This reduction of absorbance in Cu doped samples can be explained as due to the removal of defects and disorder in the as-deposited film by Cu doping.

The important optical characteristic of SnO_2 film is that they are transparent in the wavelength ranging from 400 to 1100 nm. At wavelengths shorter than 400 nm, absorption occurs due to the fundamental band gap, and thus light cannot be transmitted due to quantum phenomenon. At longer wavelengths, reflection occurs because of the plasma edge, and light cannot be transmitted due to a classical phenomenon. The corresponding wavelengths for those transmissions are determined by a number of fundamental characteristics as well as by the concentration of free electrons.
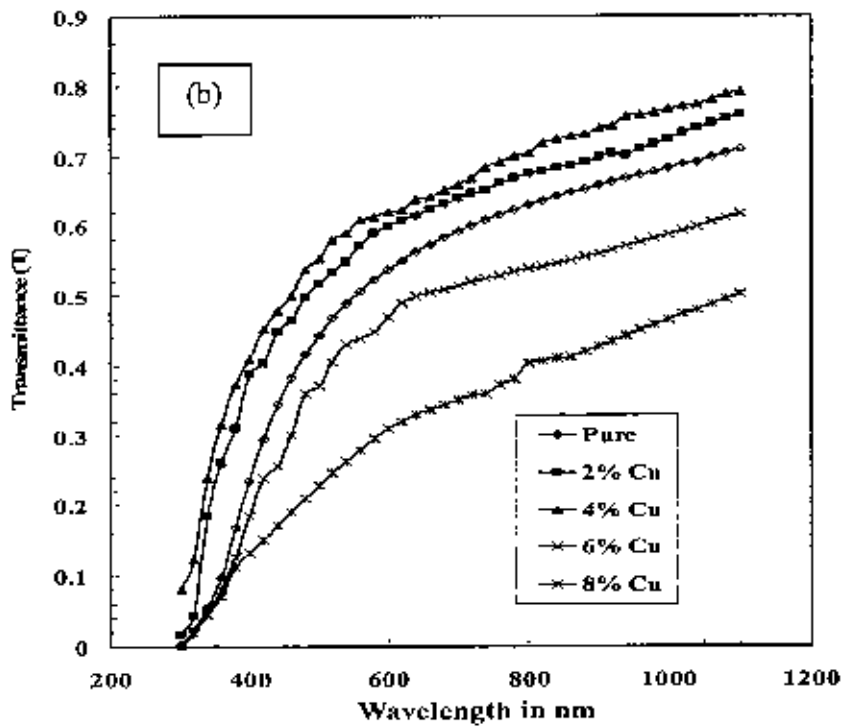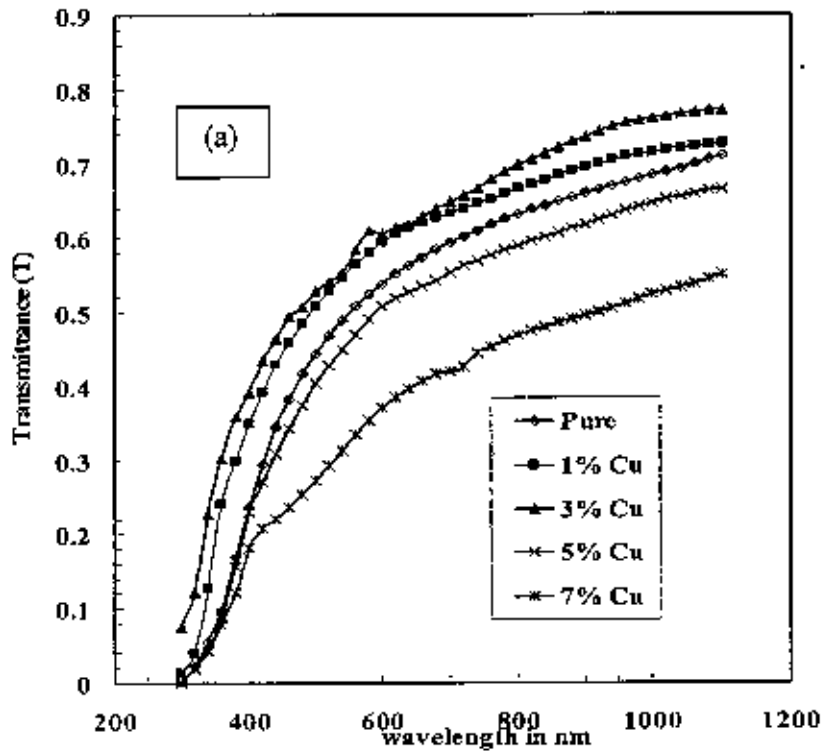
Figure 5.13(a) & (b): Variation of transmittance as a function of wavelength for (a) pure and Cu (1% to 7%) and (b) pure and Cu (2-8%) doped of SnO_2 thin films.
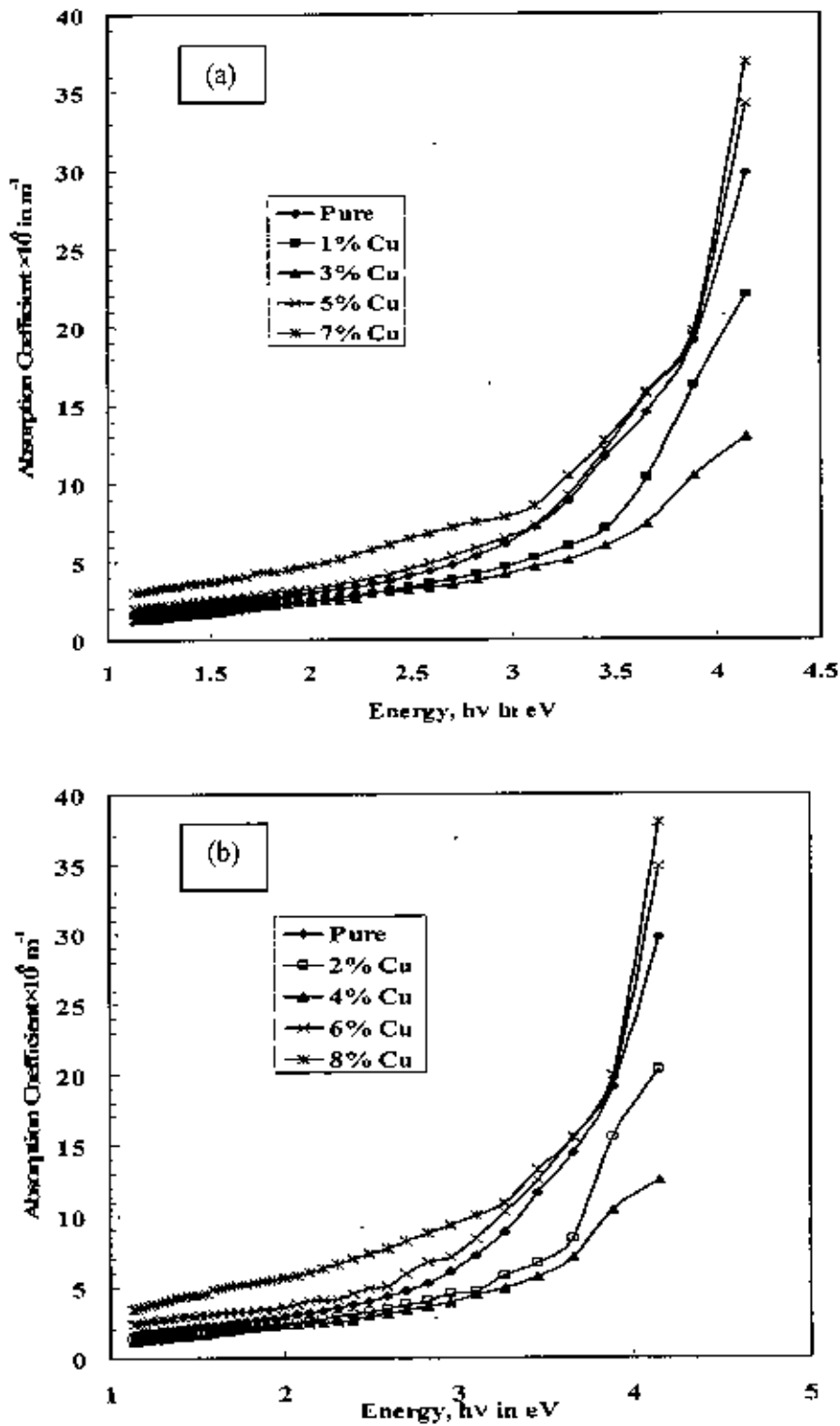
Figure 5.14: Variation of absorption coefficient as a function of photon energy for (a) pure and Cu (1-7%) & (b) pure and Cu (2-8%) doped of SnO₂ thin films.
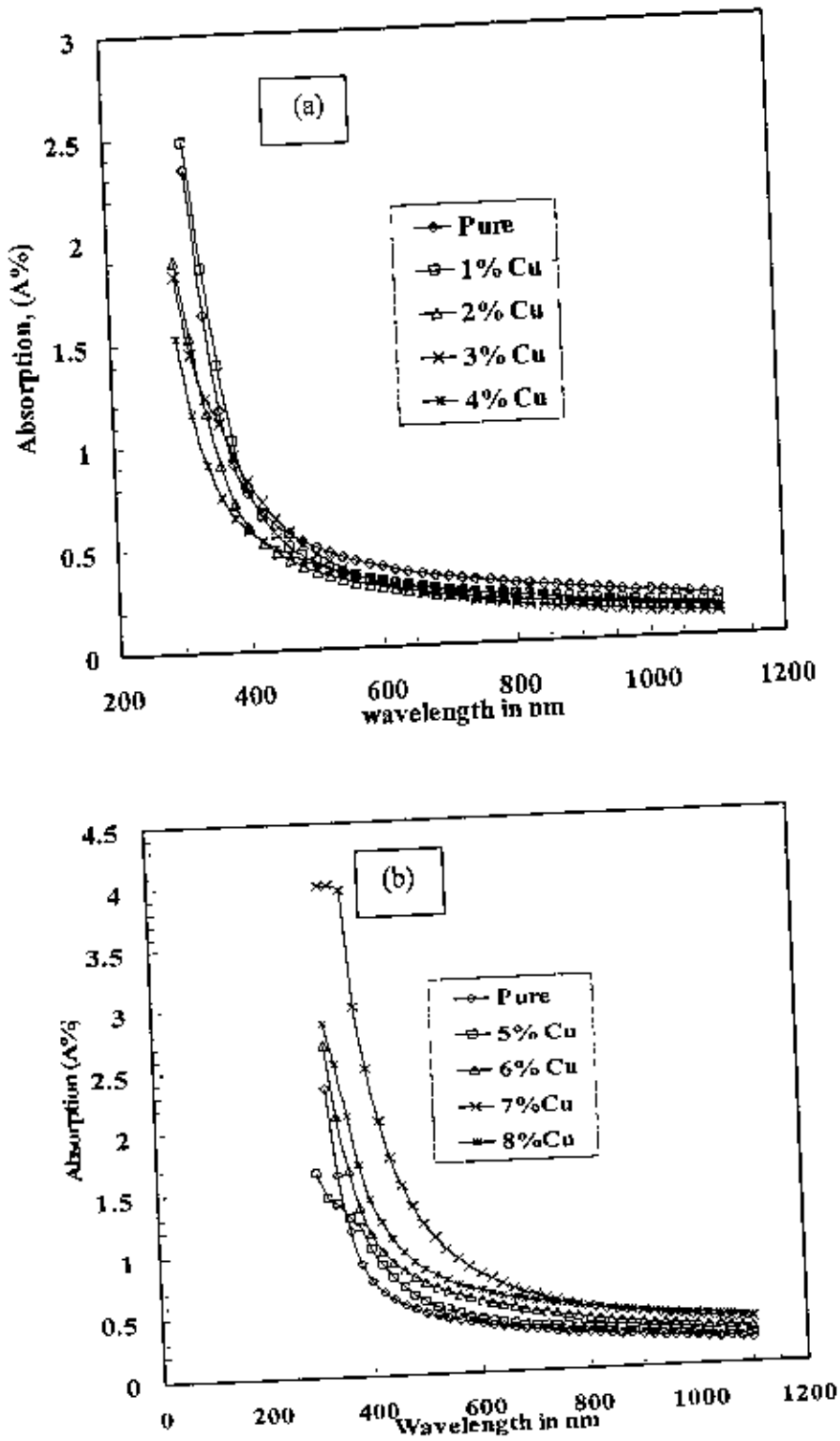
Figure 5.15 Variation of absorption with respect to wavelength for (a) pure and Cu(1-4%) & (b) pure and Cu(5-8%) doped SnO$_2$ thin films.

5.5.3 Optical Band Gap

The optical band gap (E_g) is determined from the plots of $(\alpha h\upsilon)^2$ vs. photon energy ($h\upsilon$) for direct transition and $(\alpha h\upsilon)^{1/2}$ vs. $h\upsilon$ for indirect transition for pure and Cu doped SnO_2 thin films. These statesments are shown in figures 5 16 to 5.17. The direct and indirect band gap energy of the films have been obtained from intercept on the energy axis after extrapolation of the straight line section of $(\alpha h\upsilon)^2$ vs. $h\upsilon$ curve and $(\alpha h\upsilon)^{1/2}$ vs $h\upsilon$ respectively. The variation of optical band gap obtained for direct and indirect transitions for pure and Cu (1%-8%) doped are given in table 5.8. The variation of band gaps both direct and indirect for Cu doped is shown in figure 5.17 The direct band gap of pure SnO_2 thin films obtained 3.75 eV which is an excellent agreement with the reported value of band gap determined by others workers. For 4% Cu doping the direct band gap of the film becomes 3.50 eV. So it is clear that for Cu doping change the direct band gap of the pure SnO_2 thin films. These values are very close to the reported values. Similarly, indirect band gap of the films obtained 1.75 eV for pure and 1.25 eV for 4% Cu doped SnO_2 thin films These values are very close to the reported values. From figures and data table it is seen that in both cases (direct and indirect) the energy gap decreases slightly with increasing Cu doping but not after more than 4% Cu doping. The direct band gap is higher than the indirect band gap energy.
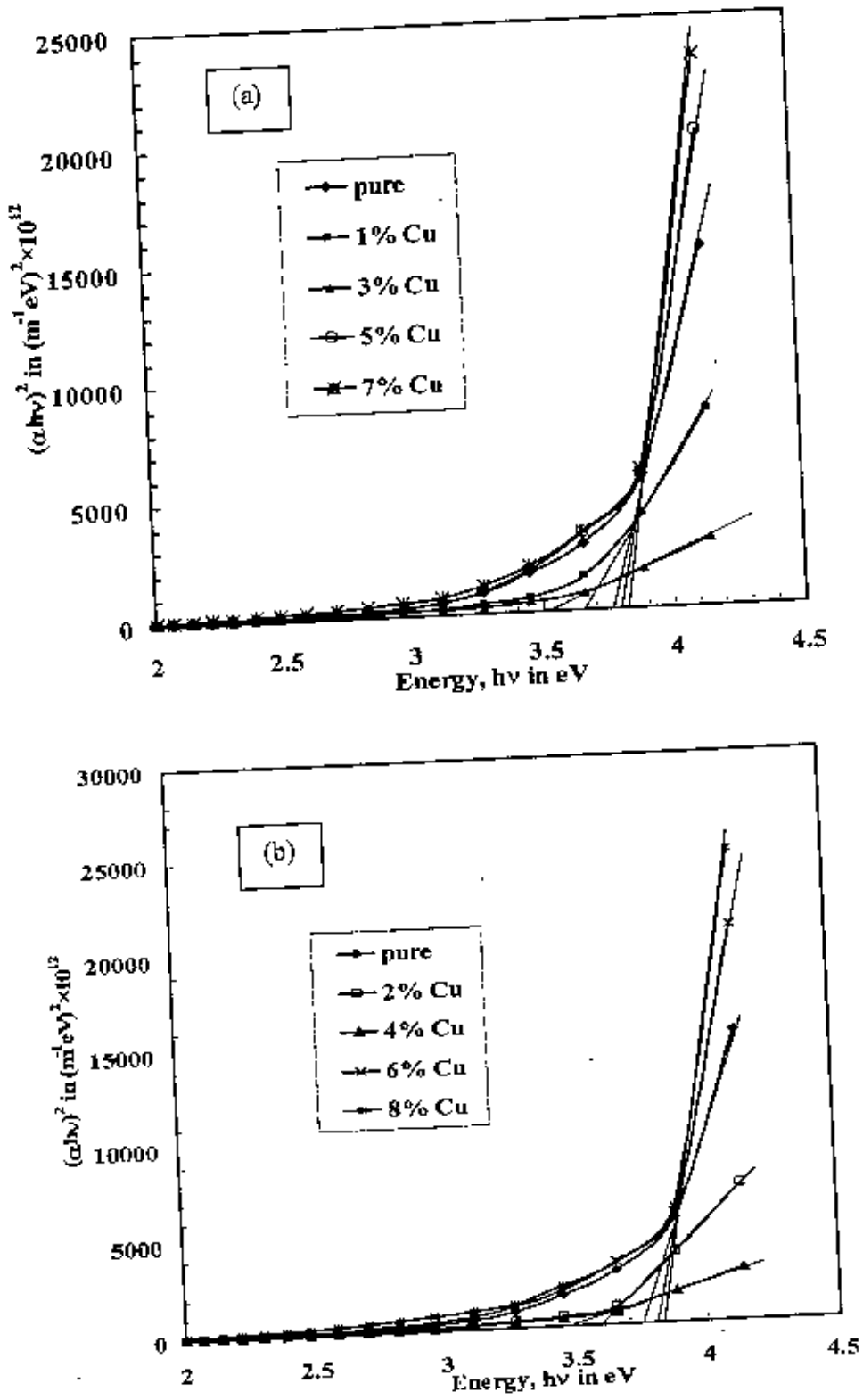
Figure 5.16: Variation of $(\alpha h\nu)^2$ with photon energy for (a) pure and Cu (1-7%) and (b) pure and Cu (2-8%)doped of SnO_2 thin films.
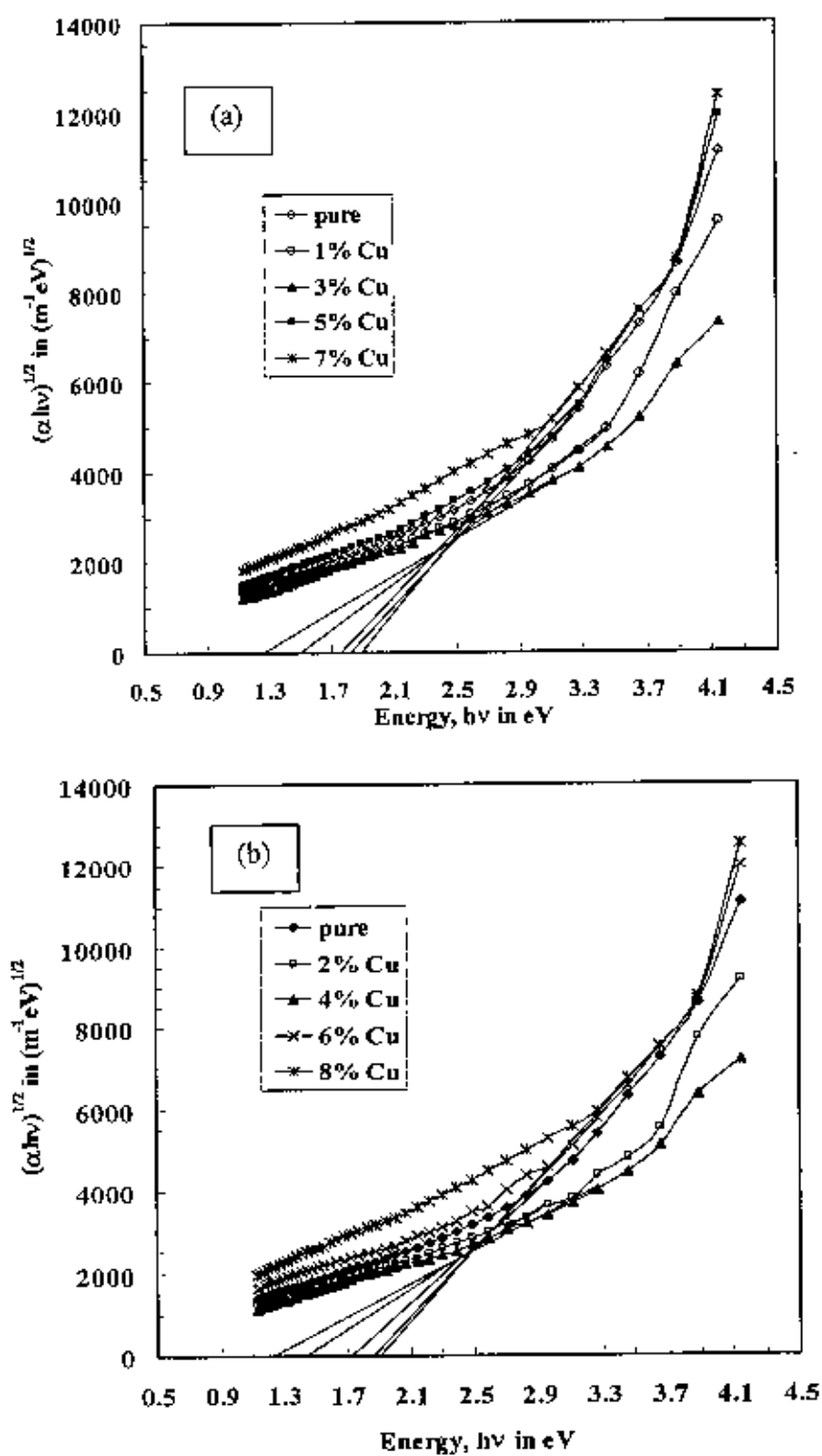
Figure 5.17: Variation of $(\alpha h\nu)^{1/2}$ with photon energy for (a) pure and Cu (1-7%) and (b) pure and Cu (2-8%) doped of SnO_2 thin films

Table: 5.8.Variation of direct and indirect band gap of pure and copper (Cu) doped SnO₂ thin films.

Sample	Direct Band Gap in eV	Indirect Band Gap in eV
Pure SnO₂	3.75	1.75
1% Cu Doped SnO₂	3.66	1.50
2% Cu Doped SnO₂	3.59	1.45
3% Cu Doped SnO₂	3.55	1.30
4% Cu Doped SnO₂	3.5	1.25
5% Cu Doped SnO₂	3.79	1.80
6% Cu Doped SnO₂	3.8	1.88
7% Cu Doped SnO₂	3.83	1.90
8% Cu Doped SnO₂	3.85	1.92
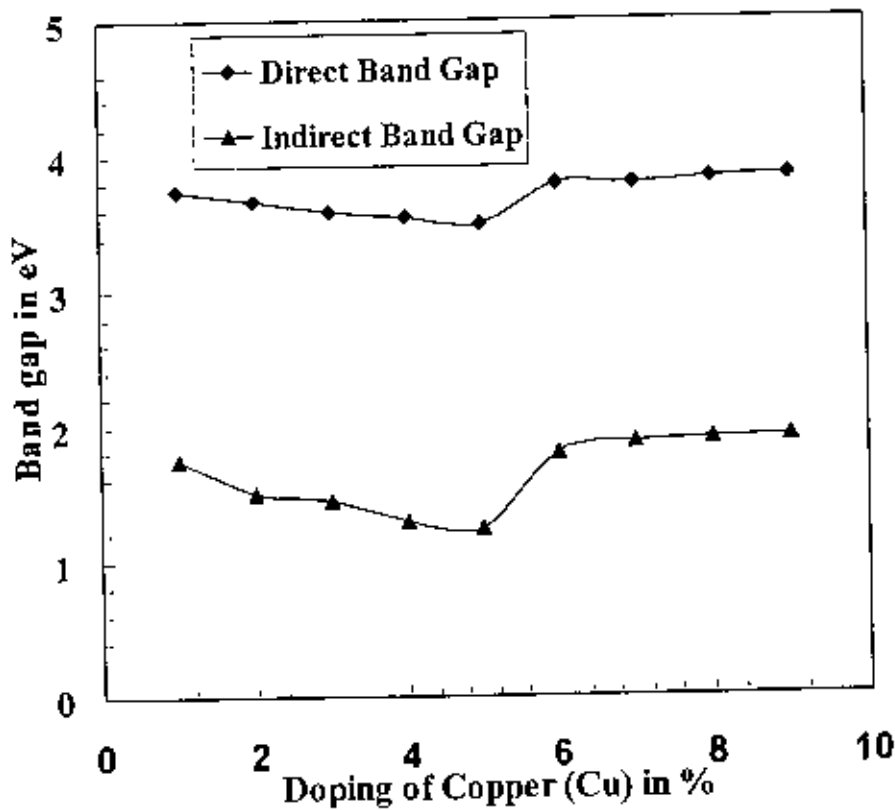
Figure 5.18: Variation of direct and indirect band gap of SnO₂ thin films with Cu doping.

5.5.4 Refractive Index

The refractive index of the films has been calculated from the transmission spectra using the relation as equation (5.2) and considered highest transmission at wavelength 740 nm and lowest transmission at wavelength 380 nm.

$$n^2 = \left(\frac{n_a^2 + n_g^2}{2} + 2n_a n_g T_0\right) + \left\{\left(\frac{n_a^2 + n_g^2}{2} + 2n_a n_g T_0\right)^2 - n_a^2 n_g^2\right\}^{1/2} \quad \dots\dots\dots (5.2)$$

The variations of refractive index d for pure and C doped SnO_2 thin films with Cu doping is shown in table 5.9 and these statesman are graphically shown in Fig. 5.19. The refractive index of pure SnO_2 thin film have been obtained 1.631625 which values is very close to the reported values 1.70 to 1.8 [24, 29] and lowest refractive index become 1.541791for 4% Cu doping. The observed value is low compared to the reported values for similar films [56]. As suggested by Arai [57]. this low value of refractive index may probably due to the smaller density of the films. It is observed that refractive index increases further than Cu doped. At the films shows high index because the impurity in the film increases optical properties.

Table: 5.9 Variation of refractive index of pure and Cu (1%-8%) doped
SnO$_2$ thin films.

Doping of Copper (Cu)	Refractive Index
0%	1.631625
1%	1.559606
2%	1.556328
3%	1.543559
4%	1.541791
5%	1.640421
6%	1.674082
7%	1.673183
8%	1.676674
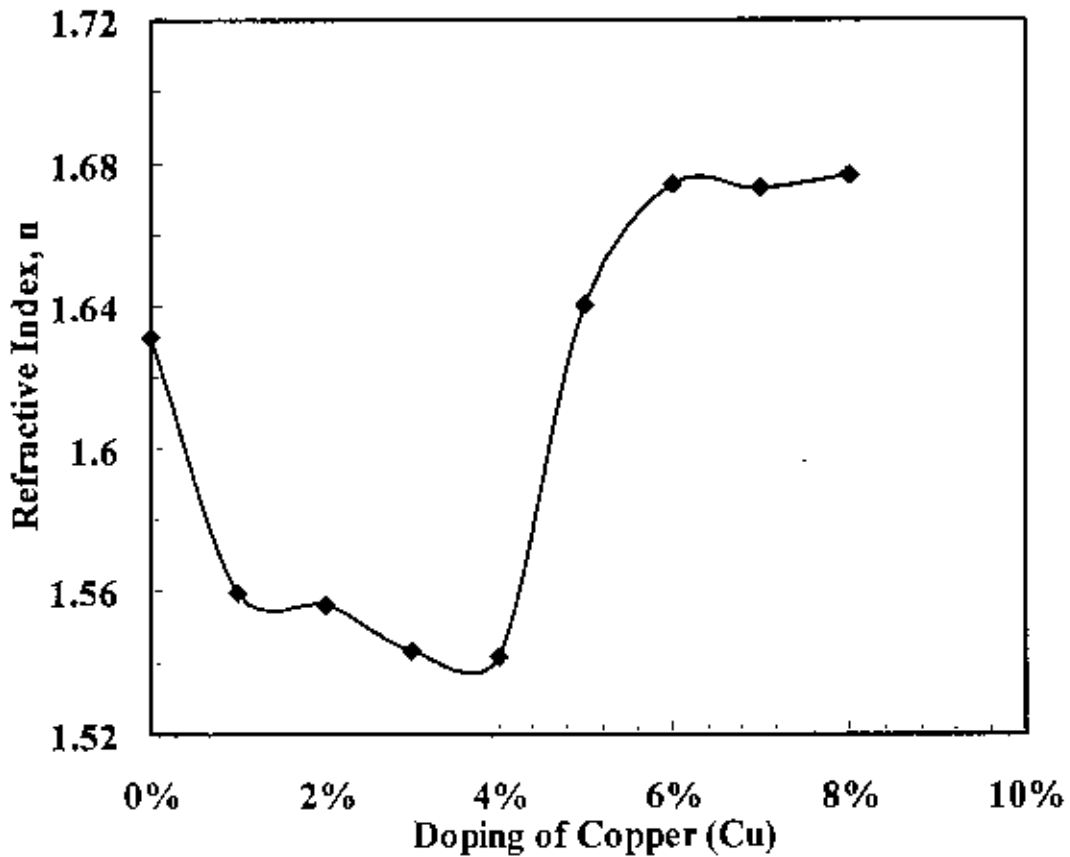
Figure 5.19: Variation of refractive index of pure and Cu doped SnO$_2$ thin films.

5.6 Electrical Properties

Electrical parameters like resistivity, conductivity, resistance, activation energy etc. of the SnO_2 films were measured by the four probe method from the laboratory of Applied Physics Department, Rajshahi University. D.C electrical resistivity measurements were made in air for freshly deposited films from room temperature 305 K to 475 K by Van der Pauw (four prove) method and data were taken by increasing the temperature of the film slowly. On increasing up to a maximum temperature (475 K) and then film cooled down slowly to room temperature. Variation of current and voltage corresponding temperature recorded in data and then calculated electrical parameters these values are given in table (5.25-5.31).

5.6.1 Variation of Resistivity with Temperature

From Fig.5.20 it is observed that the resistivity the as-deposited SnO_2 thin films is decreased (close to linear) with increasing temperature. This behavior indicates the semiconductor nature of the films. It is also observed from figure that resistivity decreases due to increasing temperature from at first which is the nature of a well semiconductor. The reason is that, at high temperature the mechanism of impurities thermal activation becomes the dominant one. It is seen from the graph that the resistivity decreases with copper (Cu) doping up to 4% once more resistivity increases. The decrease of resistivity means increase of conductivity with temperature may due to the increase of carrier mobility or due to increase of carrier concentration. The resistivity and conductivity pure and Cu doped SnO_2 tin oxide at room temperature are given in table 5.23. It is observed that the resistivity (ρ) of pure SnO_2 film at room temperature (32 °C) is 5.1065×10^{-4} ohm-m and corresponding conductivity (σ) is 1.9582×10^3 (ohm-m)$^{-1}$. The values of ρ and σ are good agreement with that obtained from four prove method. The resistivity, ρ of Cu doped SnO_2 thin films is found to be lower than pure SnO_2 thin films. The lowest resistivity of the film is found 1.1395×10^{-4} ohm-m for 4% Cu doped SnO_2 thin films. So it is clear that conductivity of the SnO_2 film increases due to Cu doping for concentration of charge carriers increases and, as a result, film resistivity decreases. Beyond 4% Cu doping for more carrier concentration exists such that scattering occurs and then resistivity increases.
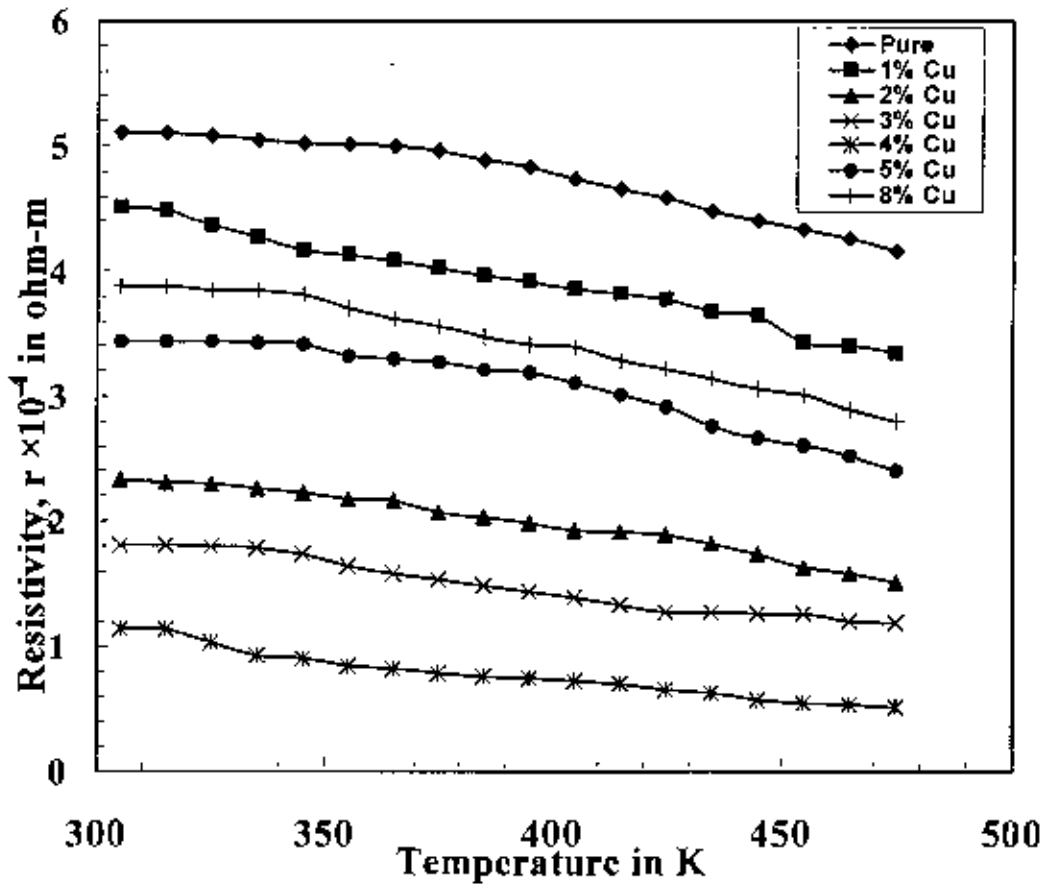
Figure 5.20: Variation of resistivity with respect to temperature for pure and Cu(1%-8%) doped SnO_2 thin films.

Table: 5.23 Resistivity, conductivity and sheet resistance for (0% - 8%) Cu doped SnO$_2$ thin films.

Thickness, t = 200 nm, Room temperature = 305 K

Doping of Copper (Cu)	Resistivity, $\rho \times 10^{-4}$ in ohm-m	Conductivity, $\sigma \times 10^3$ in $(ohm-m)^{-1}$	Sheet Resistance, $R_s \times 10^3$ in ohm/□
0%	5.106545	1.958271	2.553273
1%	4.509502	2.21754	2.254751
2%	2.329714	4.292372	1.164857
3%	1.812	5.518764	0.906
4%	1.139578	8.775177	0.569789
5%	3.44497	2.902783	1.722485
8%	3.882857	2.575423	1.941429
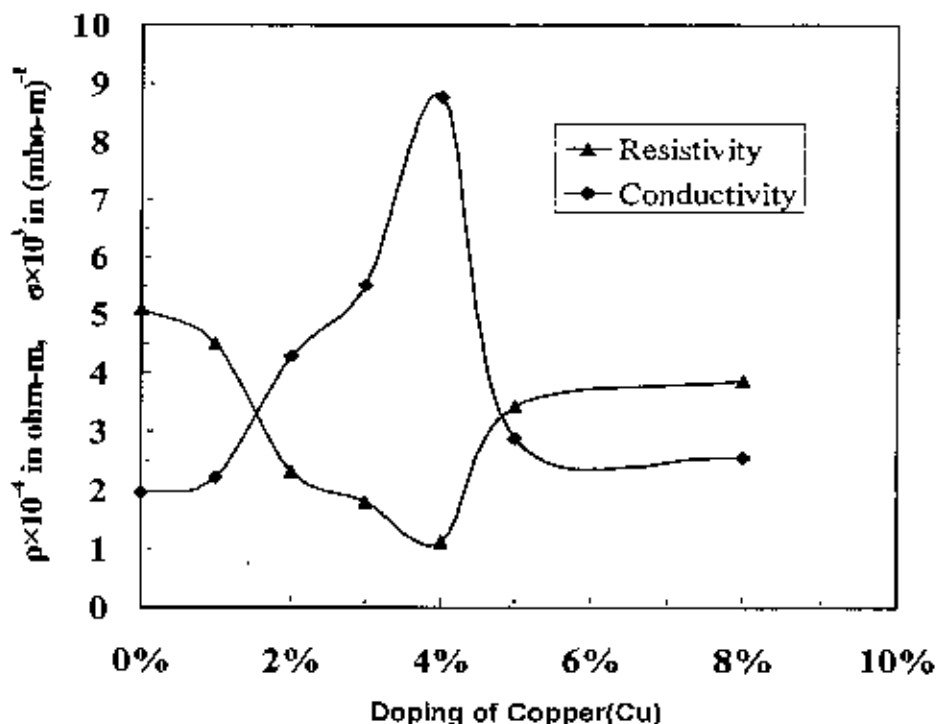
Figure 5.21: Variation of resistivity (ρ) and conductivity (σ) with respect to Cu doped for SnO$_2$ thin films.

5.6.2 Variation of Sheet Resistance with Temperature

Fig.5.22 shows the variation of sheet resistance with temperature for pure and Cu doped SnO_2 thin films. It is seen from Fig.5.22 and Table 5.23 that the sheet resistance of pure and Cu doped SnO_2 thin films is decreased with increasing temperature. On the other hand at room temperature the resistance of the pure SnO_2 thin film is 2.553273×10^3 ohm/sheet and it is reduces to 0.569789×10^3 at 4% Cu doping. A given material might exhibit different values of resistivity depending on how it was synthesized. The decrease in R_s is due to the increase in the crystalline nature as the temperature increases. Again resistivity and sheet resistance of Cu doped (beyond 4%) higher than undoped films due to increase the amorphous nature of the film. On the other hand sheet resistance decreases due to Cu doping in films indicate for increase in carrier concentration. Sn forms an interstitial bond with oxygen and exists either as SnO or SnO_2; accordingly it has a valancy of +2 or +4, respectively. This valence state has a direct bearing on the ultimate conductivity of tin oxide. When Cu incorporated in SnO_2 films increase in carrier concentration might be due to the substitution of Sn^{+4} with dopants at higher oxidation state. This can be attributed as the reason for decreasing R_{sh} with increasing Cu doping. The increase in the value of R_{sh} beyond a certain doping concentration of Cu probably represents a solubility limit of Cu in the SnO_2 lattice. The excess of Cu atoms do not occupy the popper lattice positions to contribute to the free carrier concentration while, at the same time, enhance the disorder of the structure leading to an increase in sheet resistance. This was observed for our films beyond 4% of Cu.
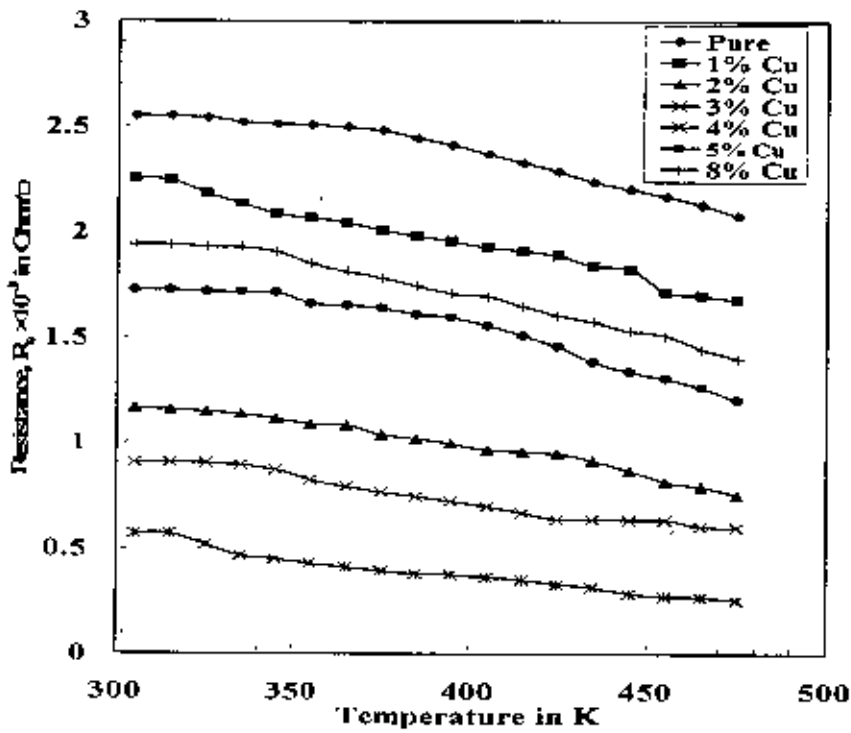
Figure 5.22: Variation of resistance/□ with respect to temperature for pure and Cu(1%-8%) doped SnO$_2$ thin films.
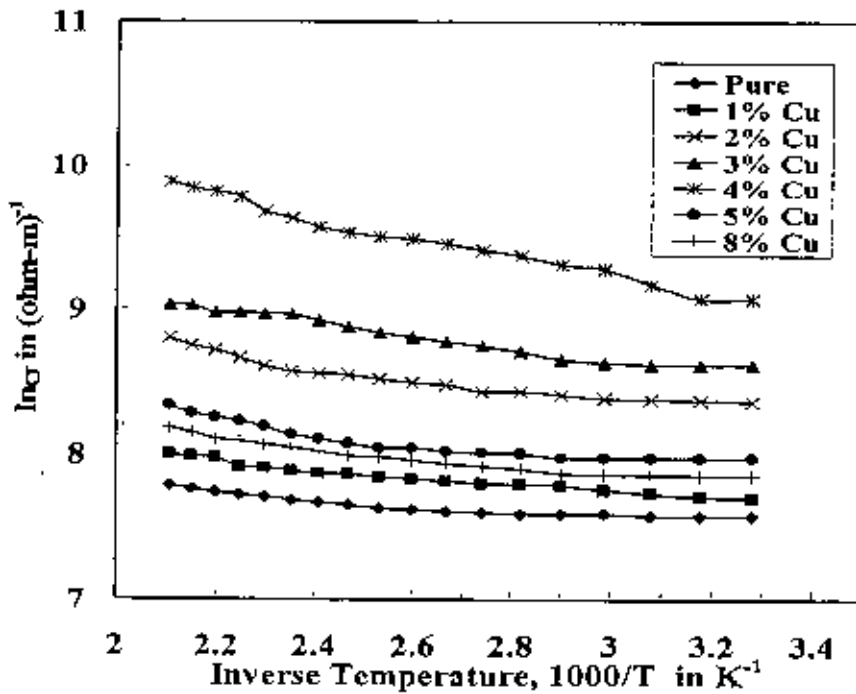
Figure 5.23: Variation of lnσ with respect to inverse temperature for pure and Cu(1%-8%) doped SnO$_2$ thin films.

5.6.3 Variation of Conductivity (lnσ) with Inverse Temperature

From Fig.5.23, it is seen that increasing and decreasing of the logarithm of conductivity (lnσ) of SnO_2 thin films with inverse temperature and their corresponding data are shown in table 5.25 to 5.31. Conductivity of the SnO_2 samples have been calculated from the resistivity measurements and these described in above. The electrical conductivity of tin oxide results primarily from the existence of oxygen vacancies, which act as donors.

It is observed that the conductivity of the samples dependent on dopant concentration and similar oscillatory behavior in resistivity has been observed for temperature getting higher. It is also seen from the graph that the logarithm of conductivity increases when Cu doped in samples but it decreases beyond 4% Cu doping. It may be due to the mean free path of the electron become greater than the mean free path of the conduction electrons and hence surface scattering of conduction electron decreases and conductivity increases. But at certain time means beyond 4% Cu doping logarithm of conductivity of SnO_2 thin films decreases and it is shown in figure 5.23. This is due to the fact that after 5% Cu doping lattice defects and dislocations are involved. From the nature of the conductivity curve of SnO_2 film it may be suggested that more than one types of conduction mechanisms are involved.

5.6.4 Variation of Activation Energy with Cu Doping

The overall conductivity of the SnO_2 samples increases with temperature. The lnσ vs. 1/T graphs as shown in figure 5.23 would be a straight line (close linear) for intrinsic semiconductor. From figure it is shown that lnσ vs. 1/T curve is a linear and it is decreased with inverse temperature for the as-deposited pure and Cu doped SnO_2 films. It is seen from Fig.5.24 and Table 5.24 that the activation energy is found to increase for Cu doping yet again it is decreased beyond 4%. These agrees with the fact that the grain size and activation energy depends on a lot of factors such as deposition condition, annealing temperature, dislocations, minor defects, stacking faults etc [62]. The smaller is the size of the grain, the greater is the activation energy. It is seen that the activation energy for the pure and Cu doped samples are fairly low and is of the order of 0.022 to 0.058 eV. This value of activation energy is well agreed with the other workers. The increase of activation energy with Cu doping above the anomaly temperature can be understood from island structure theory based on tunneling of charged carriers between islands separated by short distance [63]. From the nature of the conductivity curve of SnO_2 film it may be suggested that more than one types of conduction mechanisms are involved. The conductivity is metallic up to temperature 473 K, after which SnO_2 behaves like semiconductor. Activation energy of the samples varies in the semiconductor region 0.022896 to 0.058889 eV. The low value of activation energy may be associated with the localized levels hopping due to excitation of carriers from donor band to the conduction band. The low value of activation energy may be associated with the localized levels hopping due to excitation of carriers from donor band to the conduction band. From the nature of the conductivity curve of SnO_2 film it may be suggested that more than one types of conduction mechanisms are involved. So up to temperature 473 K, SnO_2 behaves like semiconductor. Activation energy of the semiconductor $\Delta E = 0.022896$ eV. The low value of activation energy may be associated with the localized levels hopping due to excitation of carriers from donor band to the conduction band.

Table 5.24: Activation energy for (0% - 8%) Cu doped SnO₂ thin films.

Cu Doping	Activation Energy in eV
0%	0.022896
1%	0.0353
2%	0.039126
3%	0.046189
4%	0.058889
5%	0.052649
8%	0.047056
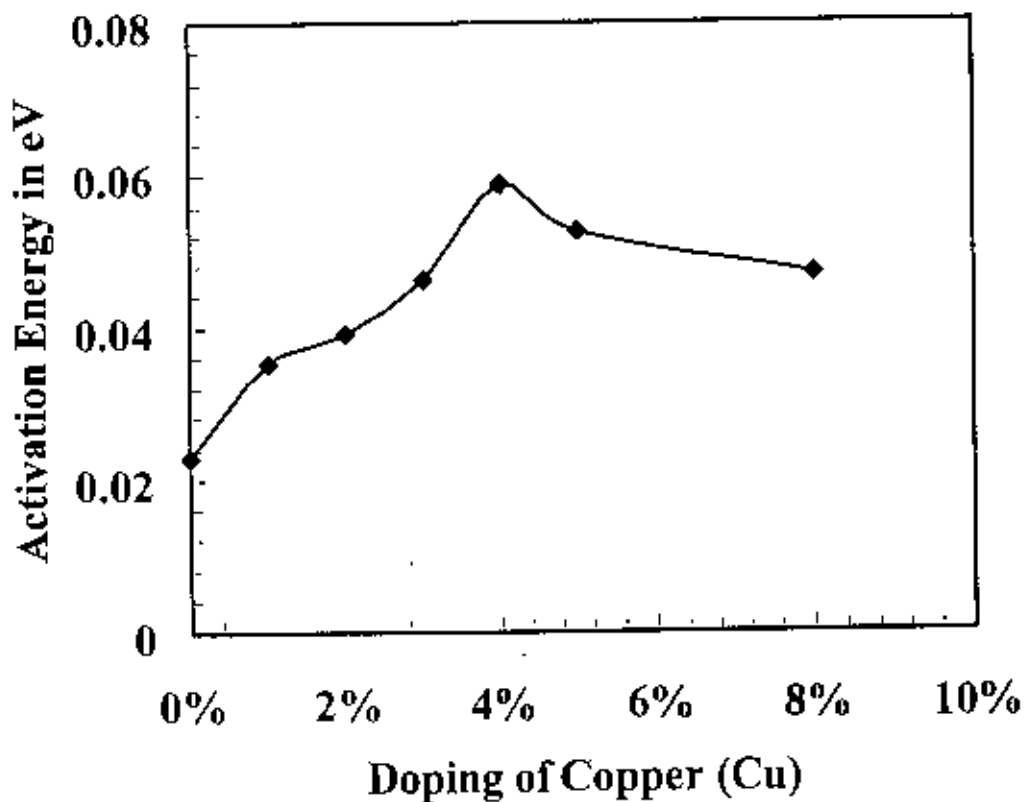
Figure 5.24: Variation of activation energy with Cu doped for SnO₂ thin films.

CHAPTER- VI

CONCLUSIONS AND SUGGESTIONS FOR FUTURE WORK

6.1. Conclusions

6.2. Suggestions for Future Work

CHAPTER- VI

CONCLUSIONS AND SUGGESTIONS FOR FUTURE WORK

6.1 Conclusions

The purpose of this chapter is to summarize the results obtained in this work. As demonstrated, the low-cost spray pyrolysis deposition (SPD) technique, described in this study, can be used to obtain uniform conductive layers of pure and Cu doped SnO_2 thin films with good repeatability. The effects of varying the compositions, thickness, structural, optical and electrical properties were studied of the prepared sample. The results of the present work are summarized and the following noteworthy conclusions as follows:

1 Spray pyrolysis is a suitable and novel technique for the production of quality SnO_2 thin films. The substrate temperature is the most important parameter that should be controlled when spraying. Before spraying, the temperature distribution contributes to the non-uniformity of deposition on the substrate. The structural property, electrical conductivity, and optical transmittance of SnO_2 thin films depend on the concentration of the dopant, which are optimized in the present work.

2. The average thickness of the film is found to be (200 ± 10) nm. But the samples with thickness 200 nm were studied extensively.

3. SEM surface studies of both pure and Cu doped SnO_2 films exhibit a smooth and homogeneous growth in the entire surface. The SEM micrographs of as-deposited film show uniform surface and deposition covers the substrate well. It means that sprayed particles (atoms) are absorbed onto the substrate to form clusters as the primary stage of nucleation. From the EDX, optical absorption spectra and X-ray diffraction patterns, it is clear that the Cu ions are acting as dopants in the SnO_2 structure and in pure SnO_2 films, Sn and O are present. In pure SnO_2 films weight % of Sn and O is found to be 90.55 and 9.45 respectively. On the other hand for 4% Cu doped films, weight % of Sn, O and Cu are found as 69.50, 20.50 and 9.98 respectively.

4. X-ray diffraction studies show that spray deposited thin films are polycrystalline in nature with preferential orientation along the (110), (101) and (211) planes and the films coated are SnO_2 and are found to be n-type semiconductors. Average grain size of the film is found 7.244579 Å, which is agreed well with previous reported value. The decrease of the grain size due to Cu doping is not significant. The shifting in the lattice parameter values is mainly due to the Cu dopant occupying at the interstitial positions in the lattice.

5. The average transmittance of Cu doping SnO_2 films in the visible region is larger than the undoped SnO_2 films. The pure SnO_2 films have good optical transmission and it is about 71% Maximum transmission about 79% is found for 4% Cu doped SnO_2 films but beyond 4% Cu doped, transmission decreases. The absorption coefficient is of the order of 10^6 m^{-1} The direct band gap of pure film is found to be 3.75 eV and it reduces to a minimum energy level of 3.50 eV for 4% Cu doped SnO_2 films and then increases with further increasing of the concentration of the dopants The indirect band gap of pure film is 1 75 eV and it is shifted to 1 25 eV for 4% Cu doped SnO_2 films. The refractive index of the pure films is found for pure film is 1.63 and for 4% Cu doped film is 1.54. The higher doping ratio shows a low refractive index as the incorporated impurity in the film increases the optical transmission properties. The transmittance increases initially with increase in doping concentration and then decreases for higher doping level which is attributed to light absorption.

6. The electrical resistivity of the Cu doped film is lower than that of the pure film. It is found that the conductivity of the films directly depends on temperature and Cu doping. At room temperature, the electrical resistivity and sheet resistance of pure SnO_2 films is found to be 5.1065 $\times 10^{-4}$ Ω-m, and 2.5532 $\times 10^3$ $\Omega/\square$ respectively. Conductivity of pure films is varied in the range of 1 9582 $\times 10^3$ $(ohm-m)^{-1}$ to 2.4065 $\times 10^3$ $(ohm-m)^{-1}$ in the temperature range 305-475 K. For Cu doping the resistivity is reduced and then its range becomes 1.1395$\times 10^{-4}$ Ω-m to 0.5080 $\times 10^{-4}$ Ω-m. On Cu doping, carrier concentration increases and conductivity enhances remarkably. The reduction of conductivity for more than 4% Cu doping in samples is due to the removal of defects and disorder ness in the pure film The electrical resistivity increases with the addition of more than 4% Cu

doping. This is expected as the periodicity of Sn matrix distributed in the film in presence of Cu atoms might enhance the scattering of the conduction electrons. Activation energy varies in the range of 0.02289 to 0.05888 eV for pure and copper doped samples.

7. The quality of these films prepared by spraying depends on various parameters such as spray rate, substrate temperature and the ratio of the various constituents in the solutions. An oxygen vacancy makes tin oxide thin films to possess semiconducting nature. So it is very essential to avoid the complete oxidation of the metal in order to obtain films with good conductivity.

In this research work the results obtained from morphological, structural, optical and electrical studies on SnO_2 thin film deposited by spray pyrolysis method are found to be in good agreement with the results obtained by other techniques. The films show good optical transparency and higher electrical conductivity for 4 wt% Cu doped SnO_2 sample.

6.2 Suggestions for Future Work

This is the first time that SnO_2 thin films have been prepared in our laboratory. We have deposited SnO_2 thin films on glass substrate at 350°C substrate temperature and studied some of their structural, electrical and optical properties. To prepare high quality SnO_2 films and for their details characterization, more studies are necessary. Hence to get better performance from the as deposited pure and Cu doped SnO_2 thin films by spray pyrolysis technique, the following research work may be extended:

1. Study and carry out magnetic properties.

2. Optimization of film growth condition.

3. Measurements of Hall Effect and temperature dependence of Hall Effect.

4. The effect of thickness on pure or doped SnO_2 films.

5. More structural study.

6. Study of photoconductivity properties.

7. Electrochemical study.

APPENDIX

1. Data Tables

    1.1 XRD Data

    1.2 Optical Property Measurement Data

    1.3 Electrical Property Measurement Data

2. References

1. Data Tables

Table 5.4: XRD data (peak least) for pure SnO$_2$ thin films

Position [°2θ]	Height[cts]	FWHM [°2θ]	d-spacing [Å]	Rel. Int. [%]
26.5262	504.33	0.1968	3.36033	100
33.8882	150.07	0.6298	2.64528	29.76
37.8692	44.67	0.3936	2.37585	8.86
42.9309	58.91	0.2165	2.10673	11.68
51.6729	114.6	0.2165	1.769	22.72
54.6531	29.08	0.768	1.67799	5.77

Table 5.5: XRD data (peak least) for 2% Cu doped SnO$_2$ thin films

Position [°2θ]	Height[cts]	FWHM [°2θ]	d-spacing [Å]	Rel. Int. [%]
26.5491	608.79	0.2165	3.35749	100
33.8334	139	0.3149	2.64944	22.83
37.9569	105.89	0.3149	2.37056	17.39
51.7535	131.14	0.2755	1.76643	21.54
54.694	29.43	0.576	1.67683	4.83

Table 5.6: XRD data (peak least) for 4% Cu doped SnO$_2$ thin films

Position [°2θ]	Height[cts]	FWHM [°2θ]	d-spacing [Å]	Rel. Int. [%]
26.5286	610.73	0.1968	3.36003	100
33.8561	122.96	0.2952	2.64703	20.13
37.8459	183.51	0.2165	2.37726	30.05
51.6989	116.51	0.3936	1.76817	19.08
54.6763	44.83	0.288	1.67733	7.34

Table 5.7: XRD data (peak least) for 5% Cu doped SnO$_2$ thin films

Position [°2θ]	Height[cts]	FWHM [°2θ]	d-spacing [Å]	Rel. Int. [%]
26.4947	202.92	0.3936	3.36426	100
29.1448	39.41	0.2362	3.0641	19.42
33.7773	61.06	0.4723	2.65371	30.09
37.8364	43.69	0.3149	2.37784	21.53
43.2374	23.49	0.4723	2.09251	11.57
51.7163	54.12	0.576	1.766552	26.67

Table 5.10: Data for optical measurement for pure SnO_2 thin films
Thickness, t = 200 nm, Substrate temperature, T_s = 350° C, Concentration = 0.2 M

Wavelength in nm	Transmittance, T	Absorption Coefficient in m^{-1}	Energy, hv in eV	$(\alpha hv)^2$ in $(m^{-1}eV)^2$ $\times 10^{12}$	$(\alpha hv)^{1/2}$ in $(m^{-1}eV)^{1/2}$
1100	0 7102	1711043	1 130114	3.739093	1390.566
1080	0 7054	1744951	1.151042	4 034119	1417 22
1060	0.6993	1788377	1.172759	4 398819	1448.218
1040	0.693	1833626	1.195313	4.803797	1480.458
1020	0.689	1862570	1.21875	5.152933	1506.654
1000	0.6836	1901912	1.243125	5.58998	1537.633
980	0.6788	1937144	1.268495	6.038112	1567.564
960	0.6743	1970401	1.294922	6.510229	1597.346
940	0 6694	2006867	1.322473	7.043869	1629.119
920	0.6647	2042097	1.351223	7.613894	1661.123
900	0.6598	2079093	1.38125	8.246929	1694.623
880	0.6545	2119418	1.412642	8.963914	1730.312
860	0.6494	2158532	1 445494	9.735309	1766.393
840	0.6436	2203389	1 479911	10.63294	1805.774
820	0 6379	2247869	1.516006	11.61298	1846.018
800	0.6316	2297495	1.553906	12.74556	1889.469
780	0 625	2350018	1.59375	14.02758	1935.288
760	0 618	2406334	1.635691	15.49224	1983.94
740	0 6105	2467385	1.679899	17.18067	2035.917
720	0.6024	2534168	1.726563	19.14412	2091 746
700	0.5938	2606064	1.775893	21.41921	2151.3
680	0.5846	2684137	1.828125	24.07804	2215.161
660	0.5743	2773017	1.883523	27.28015	2285.397
640	0.5632	2870602	1.942383	31.08964	2361.315
620	0.5514	2976474	2 00504	35.61643	2442.939
600	0 5382	3097625	2.071875	41.18934	2533.356
580	0 5238	3233227	2.143319	48.02263	2632.458
560	0.5073	3393264	2.219866	56 73993	2744.557
540	0.4889	3577987	2.302083	67.84526	2869.987
520	0.4684	3792163	2.390625	82.18583	3010.92
500	0.4442	4057402	2.48625	101.762	3176.116
480	0 4165	4379344	2.589844	128.6368	3367.761
460	0.3831	4797296	2.702446	168.0765	3600.616
440	0.3442	5332662	2.825284	226.9929	3881.531
420	0.2955	6095432	2.959821	325.4918	4247.516
400	0.2361	7217499	3.107813	503.1333	4736.099
380	0 1687	8898166	3.271382	847 3512	5395.303
360	0.0974	11644645	3.453125	1616.876	6341.168
340	0.0549	14511210	3.65625	2815.004	7283.997
320	0 0219	19106343	3.884766	5509 152	8615.316
300	0 00258	29799829	4.14375	15248 06	11112.29

Table 5.11: Data for optical measurement for 1% Cu doped SnO$_2$ thin films
Thickness, t = 200 nm, Substrate temperature, T$_s$ = 350° C, Concentration = 0.2 M

Wavelength in nm	Transmittance, T	Absorption Coefficient, α in m^{-1}	Energy, hv in eV	$(\alpha hv)^2$ in $(m^{-1}eV)^2$ $\times 10^{12}$	$(\alpha hv)^{1/2}$ in $(m^{-1}eV)^{1/2}$
1100	0.7257	1603093	1.130114	3.282174	1345.986
1080	0.7246	1610678	1.151042	3.437156	1361.601
1060	0.7224	1625881	1.172759	3.635763	1380.858
1040	0.7196	1645299	1.195313	3.867698	1402.372
1020	0.7174	1660609	1.21875	4.096036	1422.827
1000	0.7141	1683661	1.243125	4.380655	1446.721
980	0.7117	1700494	1.268495	4.652942	1468.696
960	0.7087	1721615	1.294922	4.970032	1493.103
940	0.7046	1750625	1.322473	5.359943	1521.563
920	0.6996	1786233	1.351223	5.825457	1553.576
900	0.6946	1822096	1.38125	6.33413	1586.433
880	0.6895	1858943	1.412642	6.895986	1620.5
860	0.6838	1900449	1.445494	7.546492	1657.434
840	0.678	1943040	1.479911	8.268648	1695.737
820	0.6718	1988973	1.516006	9.092005	1736.461
800	0.6659	2033079	1.553906	9.980633	1777.418
780	0.6595	2081367	1.59375	11.00367	1821.312
760	0.6528	2132422	1.635691	12.16603	1867.614
740	0.6465	2180910	1.679899	13.42276	1914.082
720	0.6403	2229092	1.726563	14.81224	1961.802
700	0.6339	2279320	1.775893	16.38492	2011.922
680	0.6276	2329261	1.828125	18.1321	2063.536
660	0.6213	2379706	1.883523	20 09039	2117.128
640	0.6143	2436359	1.942383	22 39507	2175 395
620	0.6057	2506852	2.00504	25.26409	2241.95
600	0.5942	2602697	2.071875	29.07865	2322.168
580	0.5808	2716744	2 143319	33 90557	2413.058
560	0.5646	2858189	2 219866	40.25644	2518.888
540	0.547	3016532	2.302083	48.22343	2635.206
520	0.528	3193295	2.390625	58.27751	2762.964
500	0.5081	3385385	2.48625	70.84443	2901.192
480	0.4851	3617001	2.589844	87.74945	3060.632
460	0.4587	3896794	2.702446	110.8993	3245 131
440	0.4292	4229161	2.825284	142.7686	3456.672
420	0.3922	4679917	2.959821	191.8701	3721.79
400	0.3502	5246254	3.107813	265.8326	4037.868
380	0.2997	6024867	3.271382	388.4698	4439.554
360	0.2416	7102359	3 453125	601.492	4952.306
340	0.1266	10333614	3 65625	1427.5	6146.729
320	0.039	16220968	3.884766	3970.847	7938.177
300	0.01225	22011147	4.14375	8319.025	9550.324

Table 5.12: Data for optical measurement for 2% Cu doped SnO₂ thin films
Thickness, t = 200 nm, Substrate temperature, T$_s$ = 350° C, Concentration = 0.2 M

Wavelength in nm	Transmittance, T	Absorption Coefficient, α in m⁻¹	Energy, hv in eV	$(\alpha h v)^2$ in $(m^{-1}eV)^2$ ×10¹²	$(\alpha h v)^{1/2}$ in $(m^{-1}eV)^{1/2}$
1100	0.7598	1373500	1 130114	2.40936	1245.878
1080	0 7548	1406512	1.151042	2.621013	1272.381
1060	0.7478	1453099	1.172759	2 904076	1305 425
1040	0.7408	1500123	1.195313	3.215264	1338.073
1020	0.7336	1548957	1.21875	3.563755	1373.969
1000	0.7251	1607229	1.243125	3.991948	1413.501
980	0 7181	1655732	1.268495	4.411209	1449.237
960	0 7108	1706821	1.294922	4.884983	1486.674
940	0.7025	1765549	1.322473	5.451721	1528.035
920	0 7045	1751335	1.351223	5.600055	1538.325
900	0.6995	1786947	1.38125	6.092116	1571.057
880	0.6929	1834348	1.412642	6.714717	1609.744
860	0.688	1869832	1.445494	7.305299	1644.029
840	0.6842	1897525	1.479911	7.885805	1675.759
820	0.6801	1927577	1.516006	8.539362	1709.45
800	0.6749	1965954	1.553906	9.332462	1747.829
780	0.6702	2000896	1.59375	10.16926	1785.757
760	0 6631	2054147	1.635691	11.28926	1833.017
740	0 6524	2135487	1.679899	12.86945	1894 044
720	0 6481	2168551	1.726563	14.01858	1934.978
700	0.641	2223629	1.775893	15.59402	1987.191
680	0 6323	2291957	1.828125	17.55596	2046.945
660	0 6255	2346020	1.883523	19.52563	2102.09
640	0.6165	2418485	1.942383	22.06766	2167.4
620	0 6104	2468204	2 00504	24.4911	2224.601
600	0 6	2554128	2.071875	28.00351	2300.399
580	0.5912	2628005	2.143319	31.72677	2373.321
560	0 5727	2786966	2 219866	38.27516	2487.306
540	0.55	2989185	2.302083	47.35302	2623.233
520	0.5336	3140544	2.390625	56.368	2740.048
500	0.5181	3287935	2.48625	66.82455	2859.131
480	0 4986	3479756	2.589844	81.21656	3002.003
460	0.4651	3827514	2.702446	106.9911	3216.154
440	0 4493	4000322	2.825284	127.7363	3361.852
420	0 4045	4525518	2.959821	179.4186	3659.88
400	0.3887	4724737	3.107813	215.608	3831.918
380	0.3108	5843028	3.271382	365 3746	4372.045
360	0.2614	6708517	3.453125	536 6334	4813.039
340	0.185	8436997	3 65625	951.585	5554.077
320	0 04401	15616692	3 884766	3680.508	7788.914
300	0.0169	20402208	4.14375	7147 291	9194.653

Table 5.13: Data for optical measurement for 3% Cu doped SnO$_2$ thin films
Thickness, t = 200 nm, Substrate temperature, T$_s$ = 350° C, Concentration = 0.2 M

Wavelength in nm	Transmittance, T	Absorption Coefficient, α in m^{-1}	Energy, hν in eV	$(\alpha h\nu)^2$ in $(m^{-1}eV)^2$ $\times 10^{12}$	$(\alpha h\nu)^{1/2}$ in $(m^{-1}eV)^{1/2}$
1100	0.772	1293854	1.130114	2.138034	1209.215
1080	0.7709	1300983	1.151042	2.242464	1223.718
1060	0.7686	1315923	1.172759	2.381655	1242.281
1040	0.7662	1331560	1.195313	2.533288	1261.598
1020	0.7642	1344629	1.21875	2.685555	1280.143
1000	0.7605	1368896	1.243125	2.895812	1304.496
980	0.7577	1387339	1.268495	3.097009	1326.587
960	0.7544	1409163	1.294922	3.329733	1350.835
940	0.7491	1444414	1.322473	3.64886	1382.1
920	0.7427	1487315	1.351223	4.038872	1417.637
900	0.736	1532626	1.38125	4.481432	1454.971
880	0.7292	1579036	1.412642	4.975634	1493.524
860	0.7214	1632808	1.445494	5.570609	1536.299
840	0.7141	1683661	1.479911	6.208412	1578.502
820	0.7057	1742825	1.516006	6.980871	1625.464
800	0.6975	1801264	1.553906	7.834374	1673.02
780	0.6885	1866200	1.59375	8.846198	1724.603
760	0.6786	1938617	1.635691	10.0551	1780.724
740	0.6666	2027826	1.679899	11.60452	1845.682
720	0.6572	2098834	1.726563	13.1317	1903.62
700	0.6494	2158532	1.775893	14.69436	1957.887
680	0.6398	2232998	1.828125	16.66436	2020.445
660	0.6289	2318915	1.883523	19.07706	2089.911
640	0.6171	2413621	1.942383	21.97899	2165.22
620	0.614	2438802	2.00504	23.91108	2211.311
600	0.6045	2516768	2.071875	27.19027	2283.512
580	0.6092	2478043	2.143319	28.20924	2304.612
560	0.584	2689271	2.219866	35.63878	2443.322
540	0.552	2971036	2.302083	46.77976	2615.258
520	0.5406	3075378	2.390625	54.05302	2711.471
500	0.5277	3196137	2.48625	63.14519	2818.935
480	0.5065	3401155	2.589844	77.58896	2967.905
460	0.4937	3529136	2.702446	90.96007	3088.252
440	0.4637	3842587	2.825284	117.8614	3294.905
420	0.4347	4165496	2.959821	152.0073	3511.285
400	0.3926	4674820	3.107813	211.0763	3811.622
380	0.3594	5116597	3.271382	280.172	4091.252
360	0.3029	5971763	3.453125	425.2357	4541.062
340	0.2281	7389856	3.65625	730.035	5197.996
320	0.1227	10490065	3.884766	1660.68	6383.686
300	0.07503	12949336	4.14375	2879.268	7325.218

Table 5.14: Data for optical measurement for 4% Cu doped SnO₂ thin films
Thickness, t = 200 nm, Substrate temperature, T_s = 350° C, Concentration = 0.2 M

Wavelength in nm	Transmittance, T	Absorption Coefficient, α in m^{-1}	Energy, hv in eV	$(\alpha hv)^2$ in $(m^{-1}eV)^2$ $\times 10^{12}$	$(\alpha hv)^{1/2}$ in $(m^{-1}eV)^{1/2}$
1100	0.792	1165969	1.130114	1.736275	1147.902
1080	0.7877	1193190	1.151042	1.886258	1171.926
1060	0.7813	1233980	1.172759	2.094278	1202.981
1040	0.7748	1275752	1.195313	2.325387	1234.877
1020	0.7709	1300983	1.21875	2.514042	1259.195
1000	0.7678	1321130	1.243125	2.697247	1281.534
980	0.7626	1355108	1.268495	2.954781	1311.086
960	0.7585	1382062	1.294922	3.202893	1337.783
940	0.7568	1393281	1.322473	3.395092	1357.416
920	0.7429	1485969	1.351223	4.031564	1416.995
900	0.7403	1503499	1.38125	4.312715	1441.079
880	0.7325	1556460	1.412642	4.834371	1482.808
860	0.7291	1579722	1.445494	5.214276	1511.118
840	0.7251	1607229	1.479911	5.657522	1542.256
820	0.7185	1652948	1.516006	6.27943	1582.997
800	0.7056	1743534	1.553906	7.340242	1645.992
780	0.7002	1781946	1.59375	8.065469	1685.223
760	0.6919	1841569	1.635691	9.073577	1735.58
740	0.6856	1887305	1.679899	10.05195	1780.584
720	0.6697	2004627	1.726563	11.97931	1860.407
700	0.6617	2064715	1.775893	13.44478	1914.866
680	0.6528	2132422	1.828125	15.19701	1974.42
660	0.6422	2214277	1.883523	17.39425	2042.215
640	0.6394	2236125	1.942383	18.86522	2084.085
620	0.6246	2353219	2.00504	22.26235	2172.165
600	0.6221	2373272	2.071875	24.1781	2217.459
580	0.6142	2437173	2.143319	27.28641	2285.528
560	0.6105	2467385	2.219866	30.00042	2340.356
540	0.591	2629696	2.302083	36.64825	2460.443
520	0.5807	2717605	2.390625	42.20808	2548.877
500	0.5534	2958371	2.48625	54.0997	2712.056
480	0.5381	3098554	2.589844	64.39696	2832.803
460	0.5001	3464736	2.702446	87.67065	3059.945
440	0.4784	3686540	2.825284	108.4831	3227.309
420	0.4521	3969259	2.959821	138.0225	3427.579
400	0.4098	4460430	3.107813	192.1601	3723.195
380	0.3723	4940276	3.271382	261.195	4020.14
360	0.3164	5753740	3.453125	394.7527	4457.397
340	0.2405	7125176	3.65625	678.6767	5104.06
320	0.1232	10469731	3.884766	1654.248	6377.496
300	0.0812	12554200	4.14375	2706.233	7212.591

Table 5.15: Data for optical measurement for 5% Cu doped SnO₂ thin films
Thickness, t = 200 nm, Substrate temperature, T_s = 350° C, Concentration = 0.2 M

Wavelength in nm	Transmittance, T	Absorption Coefficient, α in m^{-1}	Energy, hv in eV	$(\alpha hv)^2$ in $(m^{-1}eV)^2$ ×10^{12}	$(\alpha hv)^{1/2}$ in $(m^{-1}eV)^{1/2}$
1100	0.6644	2044355	1.130114	5.337731	1519.985
1080	0.6626	2057919	1.151042	5.610979	1539.075
1060	0.6592	2083642	1.172759	5.971231	1563.205
1040	0.6556	2111022	1.195313	6.3672	1588.5
1020	0.6517	2140855	1.21875	6.807751	1615.292
1000	0.6462	2183231	1.243125	7.365954	1647.431
980	0.6415	2219730	1.268495	7.928261	1678.01
960	0.6365	2258854	1.294922	8.555858	1710.275
940	0.6305	2306211	1.322473	9.301903	1746.397
920	0.6237	2360429	1.351223	10.17269	1785.907
900	0.6179	2407143	1.38125	11.05474	1823.422
880	0.6125	2451032	1.412642	11.98842	1860.761
860	0.6068	2497780	1.445494	13.0359	1900.139
840	0.6013	2543307	1.479911	14.16669	1940.069
820	0.5953	2593449	1.516006	15.45814	1982.848
800	0.59	2638164	1.553906	16.80556	2024.712
780	0.5831	2696983	1.59375	18.47552	2073.238
760	0.5764	2754767	1.635691	20.30356	2122.722
740	0.5698	2812349	1.679899	22.32054	2173.583
720	0.5623	2878599	1.726563	24.7017	2229.368
700	0.5532	2960178	1.775893	27.63562	2292.806
680	0.5427	3055993	1.828125	31.21163	2363.628
660	0.5354	3123706	1.883523	34.6164	2425.607
640	0.5275	3198032	1.942383	38.58649	2492.349
620	0.5194	3275405	2.00504	43.12968	2562.678
600	0.5073	3393264	2.071875	49.42678	2651.494
580	0.491	3556556	2.143319	58.10759	2760.948
560	0.4711	3763424	2.219866	69.7943	2890.38
540	0.4507	3984767	2.302083	84.14879	3028.74
520	0.4282	4240825	2.390625	102.7835	3184.057
500	0.4038	4534178	2.48625	127.0828	3357.544
480	0.3755	4897484	2.589844	160.8767	3561.421
460	0.3441	5334115	2.702446	207.7967	3796.73
440	0.3096	5862371	2.825284	274.3284	4069.75
420	0.2706	6535568	2.959821	374.1947	4398.194
400	0.2301	7346206	3.107813	521.2378	4778.141
380	0.1569	9260733	3.271382	917.8108	5504.125
360	0.0882	12140742	3.453125	1757.58	6474.836
340	0.044	15617828	3.65625	3260.717	7556.632
320	0.0208	19364011	3.884766	5658.747	8673.214
300	0.00107	34200483	4.14375	20084.06	11904.55

Table 5.16: Data for optical measurement for 6% Cu doped SnO$_2$ thin films
Thickness, t = 200 nm, Substrate temperature, T$_s$ = 350° C, Concentration = 0.2 M

Wavelength in nm	Transmittance, T	Absorption Coefficient, α in m^{-1}	Energy, hν in eV	$(\alpha h\nu)^2$ in $(m^{-1}eV)^2$ ×10^{12}	$(\alpha h\nu)^{1/2}$ in $(m^{-1}eV)^{1/2}$
1100	0.6182	2404716	1.130114	7.385364	1648.515
1080	0.6132	2445321	1.151042	7.922345	1677.697
1060	0.6069	2496956	1.172759	8.575111	1711.236
1040	0.6005	2549963	1.195313	9.290322	1745.853
1020	0.5953	2593449	1.21875	9.990441	1777.854
1000	0.5891	2645797	1.243125	10.81789	1813.575
980	0.5837	2691841	1.268495	11.6594	1847.86
960	0.5784	2737448	1.294922	12.56547	1882.759
940	0.5725	2788713	1.322473	13.60133	1920.416
920	0.5665	2841391	1.351223	14.74063	1959.427
900	0.5613	2887499	1.38125	15.907	1997.087
880	0.5564	2931339	1.412642	17.14732	2034.928
860	0.5515	2975567	1.445494	18.50002	2073.925
840	0.5474	3012877	1.479911	19.8808	2111.585
820	0.5428	3055072	1.516006	21.45086	2152.094
800	0.5391	3089271	1.553906	23.0442	2190.99
780	0.5348	3129312	1.59375	24.87357	2233.236
760	0.5302	3172505	1.635691	26.92818	2277.99
740	0.5259	3213221	1.679899	29.13717	2323.335
720	0.5214	3256189	1.726563	31.60704	2371.079
700	0.5164	3304368	1.775893	34.43581	2422.438
680	0.5106	3360844	1.828125	37.74926	2478.718
660	0.5057	3409058	1.883523	41.22974	2533.977
640	0.4998	3467736	1.942383	45.36927	2595.317
620	0.4908	3558593	2.00504	50.90997	2671.165
600	0.47	3775113	2.071875	61.17683	2796.706
580	0.45	3992538	2.143319	73.2271	2925.283
560	0.4389	4117418	2.219866	83.54175	3023.263
540	0.4306	4212878	2.302083	94.05891	3114.225
520	0.4052	4516873	2.390625	116.6	3286.054
500	0.3718	4946996	2.48625	151.2769	3507.06
480	0.3606	5099930	2.589844	174.4518	3634.284
460	0.3009	6004886	2.702446	263.3441	4028.384
440	0.2573	6787563	2.825284	367.7494	4379.132
420	0.2389	7158551	2.959821	448.9327	4603.046
400	0.1856	8420807	3.107813	684.8841	5115.691
380	0.1278	10286444	3.271382	1132.382	5800.938
360	0.0812	12554200	3.453125	1879.328	6584.165
340	0.0439	15629205	3.65625	3265.469	7559.384
320	0.02031	19483210	3.884766	5728.628	8699.868
300	0.00094	34848153	4.14375	20851.95	12016.74

Table 5.17: Data for optical measurement for 7% Cu doped SnO$_2$ thin films
Thickness, t = 200 nm, Substrate temperature, T$_s$ = 350° C, Concentration = 0.2 M

Wavelength in nm	Transmittance, T	Absorption Coefficient, α in m^{-1}	Energy, hν in eV	$(\alpha h\nu)^2$ in $(m^{-1}eV)^2$ $\times 10^{12}$	$(\alpha h\nu)^{1/2}$ in $(m^{-1}eV)^{1/2}$
1100	0.5496	2992823	1.130114	11.43948	1839.084
1080	0.5441	3043111	1.151042	12.26924	1871.563
1060	0.5385	3094839	1.172759	13.17328	1905.125
1040	0.5325	3150862	1.195313	14.18475	1940.687
1020	0.5282	3191401	1.21875	15.12837	1972.187
1000	0.5234	3237046	1.243125	16.19301	2006.004
980	0.5177	3291797	1.268495	17.43586	2043.435
960	0.5117	3350084	1.294922	18.81908	2082.81
940	0.5056	3410047	1.322473	20.33736	2123.605
920	0.5002	3463736	1.351223	21.90502	2163.395
900	0.4952	3513968	1.38125	23.55809	2203.104
880	0.4902	3564709	1.412642	25.35785	2244.027
860	0.4856	3611850	1.445494	27.25789	2284.931
840	0.4805	3664640	1.479911	29.41262	2328.807
820	0.4753	3719045	1.516006	31.78812	2374.467
800	0.4694	3781500	1.553906	34.52851	2424.066
780	0.4619	3862034	1.59375	37.88547	2480.951
760	0.4537	3951595	1.635691	41.77797	2542.359
740	0.4459	4038303	1.679899	46.02183	2604.6
720	0.4269	4256027	1.726563	53.99747	2710.774
700	0.4204	4332743	1.775893	59.20514	2773.894
680	0.4174	4368551	1.828125	63.78032	2825.997
660	0.4072	4492254	1.883523	71.59297	2908.825
640	0.3969	4620355	1.942383	80.5416	2995.747
620	0.385	4772560	2.00504	91.5691	3093.408
600	0.3713	4953725	2.071875	105.3394	3203.669
580	0.355	5178187	2.143319	123.1769	3331.442
560	0.3348	5471110	2.219866	147.5042	3484.986
540	0.3141	5790219	2.302083	177.6774	3650.968
520	0.2927	6143035	2.390625	215.6696	3832.192
500	0.2734	6484097	2.48625	259.8894	4015.107
480	0.2545	6842272	2.589844	314.0131	4209.562
460	0.2371	7196366	2.702446	378.2165	4409.965
440	0.2218	7529896	2.825284	452.5871	4612.385
420	0.2084	7841480	2.959821	538.6753	4817.611
400	0.1815	8532498	3.107813	703.1727	5149.505
380	0.123	10477855	3.271382	1174.917	5854.661
360	0.079	12691537	3.453125	1920.671	6620.08
340	0.0426	15779505	3.65625	3328.576	7595.645
320	0.0193	19738251	3.884766	5879.589	8756.625
300	0.00063	36848954	4.14375	23315.11	12356.89

Table 5.18: Data for optical measurement for 8% Cu doped SnO₂ thin films
Thickness, t = 200 nm, Substrate temperature, T_s = 350° C, Concentration = 0.2 M

Wavelength in nm	Transmittance, T	Absorption Coefficient, α in m^{-1}	Energy, hv in eV	$(\alpha hv)^2$ in $(m^{-1}eV)^2$ ×10^{12}	$(\alpha hv)^{1/2}$ in $(m^{-1}eV)^{1/2}$
1100	0.5028	3437814	1.130114	15.09416	1971.071
1080	0.4957	3508922	1.151042	16.31284	2009.705
1060	0.4883	3584127	1.172759	17.66788	2050.2
1040	0.4807	3662560	1.195313	19.16604	2092.344
1020	0.4741	3731685	1.21875	20.68422	2132.602
1000	0.4668	3809272	1.243125	22.42402	2176.098
980	0.4594	3889170	1.268495	24.33836	2221.124
960	0.4517	3973685	1.294922	26.47732	2268.394
940	0.4436	4064160	1.322473	28.88787	2318.349
920	0.4358	4152859	1.351223	31.48824	2368.847
900	0.4281	4241992	1.38125	34.33083	2420.589
880	0.4204	4332743	1.412642	37.46193	2473.988
860	0.4125	4427595	1.445494	40.96081	2529.835
840	0.4115	4439731	1.479911	43.17023	2563.28
820	0.4065	4500857	1.516006	46.55778	2612.15
800	0.4035	4537894	1.553906	49.72311	2655.459
780	0.381	4824780	1.59375	59.12829	2772.993
760	0.3734	4925525	1.635691	64.90939	2838.421
740	0.3602	5105479	1.679899	73.55957	2928.598
720	0.3589	5123557	1.726563	78.25423	2974.246
700	0.3516	5226306	1.775893	86.14362	3046.532
680	0.3445	5328306	1.828125	94.88337	3121.027
660	0.3376	5429468	1.883523	104.5818	3197.894
640	0.3303	5538770	1.942383	115.7434	3280.002
620	0.3214	5675344	2.00504	129.4883	3373.321
600	0.3103	5851079	2.071875	146.9599	3481.767
580	0.2963	6081914	2.143319	169.9238	3610.468
560	0.2803	6359474	2.219866	199.2948	3757.284
540	0.2639	6660925	2.302083	235.1317	3915.866
520	0.2468	6995885	2.390625	279.7102	4089.564
500	0.2294	7361440	2.48625	334.9772	4278.128
480	0.2103	7796101	2.589844	407.6637	4493.404
460	0.1903	8295768	2.702446	502.6053	4734.856
440	0.1711	8827535	2.825284	622.0183	4994.026
420	0.1514	9439150	2.959821	780.5429	5285.66
400	0.1333	10075765	3.107813	980.5409	5595.855
380	0.1136	10875359	3.271382	1265.755	5964.683
360	0.07016	13284885	3.453125	2104.458	6773.062
340	0.0447	15538909	3.65625	3227.846	7537.515
320	0.01863	19914910	3.884766	5985.306	8795.724
300	0.0005	38004512	4.14375	24800.33	12549.15

Table 5.21: Data for optical absorption varies with wavelength for pure and Cu (1%-7%) doped SnO₂ thin films.

Wavelength in nm	Pure	1% Cu	3% Cu	5% Cu	7%Cu
1100	0.2	0.1528	0.1123	0.2395	0.3583
1080	0.2052	0.1565	0.115	0.2441	0.3636
1060	0.2104	0.1605	0.1182	0.2487	0.3696
1040	0.2162	0.1648	0.1215	0.2573	0.3768
1020	0.2211	0 1686	0.1248	0 2592	0.3834
1000	0.2268	0.1732	0.1294	0.2653	0.3925
980	0.2319	0.1777	0.1339	0.2722	0.4019
960	0.2372	0 1825	0.139	0.2791	0.4116
940	0.2427	0.1875	0.1448	0.2861	0.4213
920	0.2485	0 1927	0.1506	0.2932	0.4304
900	0.2543	0.1979	0.1565	0.2993	0.4393
880	0.2601	0.2031	0.1624	0.3047	0.4486
860	0.2664	0.2085	0.1683	0.3099	0.4596
840	0.2726	0.2141	0.1741	0.3152	0.4718
820	0 2798	0.2203	0.181	0.3217	0.4866
800	0.287	0.2266	0.1873	0.3273	0.4997
780	0 2938	0.2329	0.1951	0.333	0.5212
760	0.3021	0.2401	0 2035	0.34	0.5359
740	0.3108	0.2474	0.2129	0.3468	0.5543
720	0.3199	0.2551	0.2225	0.354	0.5706
700	0.3297	0.2634	0.233	0 3619	0.5878
680	0.34	0.2723	0.2443	0.3706	0.6101
660	0.3514	0.282	0.2572	0.3804	0.63301
640	0.3638	0.2925	0.272	0 3917	0.6538
620	0.3768	0.304	0.2887	0.4056	0.67543
600	0.3914	0.3176	0.3079	0.4236	0.70025
580	0.4076	0.3331	0.3302	0.4468	0.72595
560	0.4257	0.3513	0.3567	0.475	0.7579
540	0.4459	0.3717	0.3884	0.5083	0.7923
520	0.4684	0.3956	0.4252	0.54	0.83156
500	0.4945	0.4236	0.4666	0.5895	0.87008
480	0.5255	0.458	0.5157	0.6423	0.90821
460	0.5636	0.5031	0.5741	0.7084	0.9575
440	0.6095	0.563	0.6429	0.7888	1.02001
420	0 6725	0.6515	0.7273	0.8937	1.08696
400	0.7661	0.7343	0.8285	1.0291	1.1484
380	0.9111	0.8221	0.9513	1.1982	1.2803
360	1.1731	1.10927	1.1149	1.5854	1.6265
340	1.6383	1.4639	1.2301	2.0952	2.1499
320	2.3463	2.1819	1.4478	2.8447	2.9899
300			1.8307		

Table 5.22: Data for optical absorption varies with wavelength for pure and Cu (2%-8%) doped SnO$_2$ thin films.

Wavelength in nm	Pure	2% Cu	4% Cu	6% Cu	8%Cu
1100	0.2	0.1362	0.1407	0.29	0.3759
1080	0.2052	0.1399	0.145	0.297	0.3834
1060	0.2104	0.1436	0.1494	0.304	0.391
1040	0.2162	0.1476	0.1543	0.3115	0.3993
1020	0.2211	0.1514	0.1587	0.318	0.4059
1000	0.2268	0.1561	0.1646	0.3252	0.4136
980	0.2319	0.1603	0.1698	0.3319	0.4208
960	0.2372	0.1646	0.1754	0.3389	0.4285
940	0.2427	0.1691	0.1813	0.3462	0.4365
920	0.2485	0.174	0.1875	0.3535	0.4447
900	0.2543	0.1787	0.1937	0.3612	0.4529
880	0.2601	0.1833	0.2001	0.3694	0.4617
860	0.2664	0.1887	0.207	0.3781	0.4709
840	0.2726	0.1937	0.2137	0.387	0.4802
820	0.2798	0.2	0.2203	0.3982	0.4911
800	0.287	0.2057	0.2273	0.4097	0.5011
780	0.2938	0.2118	0.2344	0.4225	0.5121
760	0.3021	0.2184	0.2424	0.4355	0.5244
740	0.3108	0.2255	0.2493	0.4506	0.5374
720	0.3199	0.2327	0.2577	0.4653	0.551
700	0.3297	0.2405	0.2666	0.4811	0.5654
680	0.34	0.2488	0.2748	0.4976	0.5811
660	0.3514	0.2578	0.2833	0.516	0.5981
640	0.3638	0.2676	0.2931	0.536	0.6172
620	0.3768	0.2782	0.3041	0.5569	0.6378
600	0.3914	0.29	0.3167	0.579	0.6613
580	0.4076	0.3033	0.3309	0.6036	0.6882
560	0.4257	0.3184	0.3472	0.6306	0.7192
540	0.4459	0.3356	0.3654	0.6627	0.7556
520	0.4684	0.3549	0.3861	0.6996	0.7976
500	0.4945	0.3771	0.4087	0.7421	0.8485
480	0.5255	0.4042	0.434	0.7906	0.9142
460	0.5636	0.4363	0.462	0.8478	1.0011
440	0.6095	0.4755	0.4935	0.9152	1.1077
420	0.6725	0.5282	0.5326	1.0076	1.2428
400	0.7661	0.605	0.5834	1.1516	1.436
380	0.9111	0.7212	0.651	1.3621	1.7153
360	1.1731	0.9076	0.7529	1.6705	1.9176
340	1.6383	1.16	0.9091	2.1107	2.2424
320	2.3463	1.5348	1.1584	2.6963	3.4727
300		1.8981	1.5277		

Table 5.25: Data of electrical measurement for pure SnO₂ thin films.

Thickness, t = 200 nm, Molar Concentration = 0.2M

T in °C	T in K	1000/T in K⁻¹	Resistivity, ρ× 10⁻⁴ in ohm-m	Conductivity, σ×10³ in (ohm-m)⁻¹	ln σ	Resistance, Rₛ×10³ in ohm/
32	305	3.278689	5.10654545	1.958271	7.579817	2.553273
42	315	3.174603	5.10654545	1.958271	7.579817	2.553273
52	325	3.076923	5.08631579	1.96606	7.583787	2.543158
62	335	2.985075	5.04182125	1.98341	7.592573	2.520911
72	345	2.898551	5.02512235	1.990001	7.595891	2.512561
82	355	2.816901	5.01740506	1.993062	7.597427	2.508703
92	365	2.739726	5.00245399	1.999019	7.600412	2.501227
102	375	2.666667	4.96264045	2.015056	7.608402	2.48132
112	385	2.597403	4.89068826	2.044702	7.623007	2.445344
122	395	2.531646	4.82893401	2.07085	7.635715	2.414467
132	405	2.469136	4.73941606	2.109965	7.654426	2.369708
142	415	2.409639	4.65942857	2.146186	7.671448	2.329714
152	425	2.352941	4.57870968	2.184021	7.688923	2.289355
162	435	2.298851	4.47407407	2.235099	7.712041	2.237037
172	445	2.247191	4.4053211	2.269982	7.727527	2.202661
182	455	2.197802	4.33564356	2.306463	7.74347	2.167822
192	465	2.150538	4.26018809	2.347314	7.761027	2.130094
202	475	2.105263	4.15533835	2.406543	7.785947	2.077669

Table 5.26: Data for electrical measurement for 1% Cu doped SnO₂ thin films.

Thickness, t = 200 nm, Molar Concentration = 0.2M

T in °C	T in K	1000/T ln K^{-1}	Resistivity, $\rho \times 10^{-4}$ in ohm-m	Conductivity, $\sigma \times 10^{3}$ in (ohm-m)$^{-1}$	ln σ	Resistance, $R_s \times 10^{3}$ in ohm/
32	305	3.278689	4.509502	2.21753963	7.704154	2.254751
42	315	3.174603	4.489189	2.22757375	7.708668	2.244595
52	325	3.076923	4.366265	2.29028698	7.736432	2.183133
62	335	2.985075	4.270707	2.34153264	7.758561	2.135354
72	345	2.898551	4.168712	2.39882266	7.782733	2.084356
82	355	2.816901	4.130699	2.42089772	7.791894	2.06535
92	365	2.739726	4.08338	2.44895143	7.803415	2.04169
102	375	2.666667	4.02141	2.48669004	7.818708	2.010705
112	385	2.597403	3.959383	2.52564602	7.834252	1.979692
122	395	2.531646	3.912273	2.55605902	7.846222	1.956136
132	405	2.469136	3.855319	2.59381898	7.860887	1.92766
142	415	2.409639	3.820482	2.61747083	7.869964	1.910241
152	425	2.352941	3.775	2.64900662	7.88194	1.8875
162	435	2.298851	3.677491	2.71924543	7.90811	1.838745
172	445	2.247191	3.643007	2.74498512	7.917531	1.821503
182	455	2.197802	3.431818	2.91390728	7.97725	1.715909
192	465	2.150538	3.399134	2.94192562	7.98682	1.699567
202	475	2.105263	3.350959	2.98422042	8.001094	1.675479

Table 5.27: Data for electrical measurement for 2% Cu doped SnO₂ thin films.

Thickness, t = 200 nm, Molar Concentration = 0.2M

T in °C	T in K	1000/T in K^{-1}	Resistivity, $\rho \times 10^{-4}$ in ohm-m	Conductivity, $\sigma \times 10^3$ in (ohm-m)$^{-1}$	ln σ	Resistance, $R_s \times 10^3$ in ohm/
32	305	3.278689	2.329714	4.292372	8.364595	1.164857
42	315	3.174603	2.311862	4.325518	8.372287	1.155931
52	325	3.076923	2.2952	4.356919	8.37952	1.1476
62	335	2.985075	2.265	4.415011	8.392766	1.1325
72	345	2.898551	2.223818	4.496771	8.411115	1.111909
82	355	2.816901	2.1744	4.59897	8.433588	1.0872
92	365	2.739726	2.164333	4.62036	8.438228	1.082167
102	375	2.666667	2.074263	4.820989	8.480734	1.037132
112	385	2.597403	2.0385	4.905568	8.498126	1.01925
122	395	2.531646	1.991915	5.020295	8.521244	0.995957
132	405	2.469136	1.931473	5.177397	8.552058	0.965736
142	415	2.409639	1.914351	5.223701	8.560961	0.957176
152	425	2.352941	1.895855	5.274665	8.57067	0.947928
162	435	2.298851	1.825522	5.477884	8.608474	0.912761
172	445	2.247191	1.733217	5.769617	8.660361	0.866609
182	455	2.197802	1.631383	6.12977	8.720912	0.815691
192	465	2.150538	1.583435	6.315385	8.750744	0.791717
202	475	2.105263	1.51	6.622517	8.798231	0.755

Table 5.28: Data for electrical measurement for 3% Cu doped SnO$_2$ thin films.

Thickness, t = 200 nm, Molar Concentration = 0.2M

T in °C	T in K	1000/T in K^{-1}	Resistivity, $\rho \times 10^{-4}$ in ohm-m	Conductivity, $\sigma \times 10^3$ in (ohm-m)$^{-1}$	ln σ	Resistanc, $R_s \times 10^3$ in ohm/
32	305	3.278689	1.812	5518.764	8.615909	0.906
42	315	3.174603	1.812	5518.764	8.615909	0.906
52	325	3.076923	1.802595	5547.557	8.621113	0.901298
62	335	2.985075	1.781026	5614.742	8.633151	0.890513
72	345	2.898551	1.743454	5735.741	8.654472	0.871727
82	355	2.816901	1.646076	6075.055	8.711946	0.823038
92	365	2.739726	1.588207	6296.408	8.747735	0.794104
102	375	2.666667	1.538067	6501.668	8.779814	0.769033
112	385	2.597403	1.49236	6700.797	8.809982	0.74618
122	395	2.531646	1.445215	6919.388	8.842083	0.722607
132	405	2.469136	1.392399	7181.851	8.879312	0.696199
142	415	2.409639	1.335713	7486.639	8.920875	0.667856
152	425	2.352941	1.277692	7826.61	8.965285	0.638846
162	435	2.298851	1.273429	7852.814	8.968627	0 636714
172	445	2.247191	1.2651	7904.515	8.975189	0.63255
182	455	2.197802	1.263098	7917.041	8.976773	0.631549
192	465	2.150538	1.205565	8294.869	9.023392	0.602782
202	475	2.105263	1.194337	8372.846	9.032749	0.597168

Table: 5.29 Data for electrical measurement for 4% Cu doped SnO₂ thin films.

Thickness, t = 200 nm, Molar Concentration = 0.2M

T in °C	T in K	1000/T in K^{-1}	Resistivity, $\rho \times 10^{-4}$ in ohm-m	Conductivity, $\sigma \times 10^3$ in (ohm-m)$^{-1}$	ln σ	Resistance, $R_s \times 10^3$ in ohm/
32	305	3.278689	1.139578	8775.1772	9.079682	0.569789
42	315	3.174603	1.139578	8775.1772	9.079682	0.569789
52	325	3.076923	1.033606	9674.8699	9.177287	0.516803
62	335	2.985075	0.930486	10747.066	9.282388	0.465243
72	345	2.898551	0.900078	11110.143	9.315614	0.450039
82	355	2.816901	0.849727	11768.49	9.373181	0.424863
92	365	2.739726	0.819198	12207.067	9.40977	0.409599
102	375	2.666667	0.781034	12803.532	9.457476	0.390517
112	385	2.597403	0.760033	13157.318	9.484733	0.380017
122	395	2.531646	0.748435	13361.218	9.500112	0.374217
132	405	2.469136	0.7248	13796.909	9.5322	0.3624
142	415	2.409639	0.69762	14334.451	9.570421	0.34881
152	425	2.352941	0.655771	15249.216	9.632283	0.327886
162	435	2.298851	0.625964	15975.369	9.678803	0.312982
172	445	2.247191	0.56625	17660.044	9.77906	0.283125
182	455	2.197802	0.547224	18274.052	9.813237	0.273612
192	465	2.150538	0.533146	18756.583	9.8393	0.266573
202	475	2.105263	0.508007	19684.763	9.8876	0.254004

Table 5.30 Data: for electrical measurement for 5% Cu doped SnO₂ thin films.

Thickness, t = 200 nm, Molar Concentration = 0.2M

T in °C	T in K	1000/T in K⁻¹	Resistivity, ρ× 10⁻⁴ in ohm-m	Conductivity, σ×10³ in (ohm-m)⁻¹	ln σ	Resistance, Rₐ×10³ in ohm/
32	305	3.278689	3.44497	2.902783	7.973425	1.722485
42	315	3.174603	3.44497	2.902783	7.973425	1.722485
52	325	3.076923	3.434687	2.911474	7.976415	1.717343
62	335	2.985075	3.431006	2.914597	7.977487	1.715503
72	345	2.898551	3.420885	2.92322	7.980441	1.710442
82	355	2.816901	3.321114	3.011038	8.01004	1.660557
92	365	2.739726	3.301525	3.028903	8.015956	1.650763
102	375	2.666667	3.276493	3.052044	8.023567	1.638247
112	385	2.597403	3.21328	3.112085	8.043048	1.60664
122	395	2.531646	3.192571	3.132271	8.049514	1.596286
132	405	2.469136	3.111913	3.213457	8.075103	1.555957
142	415	2.409639	3.013837	3.31803	8.107126	1.506918
152	425	2.352941	2.913412	3.432402	8.141016	1.456706
162	435	2.298851	2.767418	3.613476	8.192426	1.383709
172	445	2.247191	2.670316	3.744875	8.228144	1.335158
182	455	2.197802	2.608655	3.833393	8.251506	1.304328
192	465	2.150538	2.5217	3.965579	8.285407	1.26085
202	475	2.105263	2.406563	4.155305	8.332141	1.203281

Table 5.31 Data: for electrical measurement for 8% Cu doped SnO₂ thin films. Thickness, t = 200 nm, Molar Concentration = 0.2M

T in °C	T in K	1000/T in K⁻¹	Resistivity, $\rho \times 10^{-4}$ in ohm-m	Conductivity, $\sigma \times 10^3$ in (ohm)⁻¹	ln σ	Resistance, $R_s \times 10^3$ in ohm/
32	305	3.278689	3.882857	2.575423	7.853769	1.941429
42	315	3.174603	3.882857	2.575423	7.853769	1.941429
52	325	3.076923	3.8505	2.597065	7.862137	1.92525
62	335	2.985075	3.8505	2.597065	7.862137	1.92525
72	345	2.898551	3.810529	2.624307	7.872572	1.905265
82	355	2.816901	3.701657	2.701493	7.90156	1.850829
92	365	2.739726	3.624	2.759382	7.922762	1.812
102	375	2.666667	3.559286	2.809552	7.94078	1.779643
112	385	2.597403	3.481736	2.872131	7.962809	1.740868
122	395	2.531646	3.412658	2.930267	7.982849	1.706329
132	405	2.469136	3.391266	2.948751	7.989137	1.695633
142	415	2.409639	3.29079	3.038784	8.019213	1.645395
152	425	2.352941	3.210646	3.114638	8.043868	1.605323
162	435	2.298851	3.142267	3.182416	8.065396	1.571134
172	445	2.247191	3.05818	3.269919	8.092521	1.52909
182	455	2.197802	3.016497	3.315104	8.106244	1.508248
192	465	2.150538	2.887996	3.462609	8.149778	1.443998
202	475	2.105263	2.800855	3.570339	8.180416	1.400427

2. References

[1] Kumar A, Chung Y. W, Moore J.J and Smugeresky J.E, in "Surface Engineering Science and Technology 1", The Minerals, Metals & Materials Society, Warrendale, 1999.

[2] Gloker D.A and Shah S.I, in "Hand Book of Thin Film Process Technology", Instute of Physics Publishing, Bristol and Philadelphia, 1998.

[3] Patil P.S, Mater. Chem. Phys. 59, 185, 1999.

[4] Haacke G, Annu. Rev. mater. Sci. 7, 73, 1977.

[5] Thangaraju B, Thin Solid Films 402, 71, 2002.

[6] Chopra K.L and Das S.R, in "thin Film Solar Cells" New Age Int. (P) Ltd. Publishers, New Delhi, 1983.

[7] Vossen J.L, Phys. Thin Films 9, 1, 1997

[8] Chopra K.L, Major S, Pandya D.K, Thin Solid Films 102, 1, 1983.

[9] Elangovan E, Singh P. M, Dharmaprakash M. S, Ramamurthi K, J. Optoelectron. Adv. Mater. 6(1), 197, 2004.

[10] Thangaraju B, " Structural and electrical studies on highly conducting spray deposited fluorine and antimony doped SnO_2 thin films from precursor", Thin Solid Films 402(1-2), pp.71-78, 2002.

[11] Riad A. S, Mahmud S.A, Ibrahim A, "Structural and DC electrical investigations of ZnO thin films prepared by spray pyrolysis technique", Physica B 296(4), pp 319-325, 2001.

[12] Chopra K. L, " Thin Film Phenomena", McGraw-Hill Book Company, New York, 1995.

[13] Elangovan E, Singh M. P, Dharmaprakash M. S, Ramamurthi K, Optoelectron J, Adv. Mater. 6(1),197 (2004).

[14] A. Bouteville, J. Optoelectron. Dv. Matter. 7(2), 599, 2005.

[15] V. Cracium, D. Cracium, X.Wang, T. J Anderson, R.K. Singh, J. Optoelectron. Adv. Mater. 5(2), 401, 2003.

[16] Agashe Chitra, R, B. Marathe, G.M Takwale and G.V Bhide, "Structural properties of SnO_2:F films deposited by spray pyrolysis technique", Thin Solid Films, 164, p261-264, 1988.

[17] A. Antonaia, P. Menna, M.L Addonzio and M. Crocchilo, " Transparent properties of polycrystalline tin oxide films", Solar energy Mater. Solar Cells, 28, p167-173.

[18] E. A Rakhshani, y. makdisi and A.H Ramazaniyan, "Electronic and optical properties of flurine-doped tin oxide films", J. Applied Phys., 83, 1049-1057, 1998.

[19] Mohammad T.M, "Performance and characteristics of L-PbS/SnO_2: F selective coating system for photothermal energy conversion", Solar Energy Mater, 20, 297-305, 1990.

[20] Papadopoulos K., Avaritsiotis J. N., Sensors and Actuators B: Chemical 28(3), 201 1995.

[21] Joseph J, Mathew V, Mathew J, Abraham K. E., "Studies on physical properties and carrier conversion of SnO_2:Nd thin films", Turk J. Phys, 32 , p1-10, 2008.

[22] Korotcenkov G, Brinzari V, Boris I Boris, (Cu, Fe, Co, or Ni)-doped tin dioxide films deposited by spray pyrolysis: doping influence on film morphology, J Mater Sci, 43, p2761–2770, 2008.

[23] Thangaraju B, Kaliannan P, "Polycrystalline Lead Tin Chalcogenide Thin Film Grown by Spray Pyrolysis", Cryst. Res. Technol, 35,1 71–75, 2000.

[24] Jachon J, Varghes M, and Abraham K.E, "Studies on Cu, Fe, and Mn Doped SnO_2 Sem Conducting Transparent Films Prepared by a Vapor Deposition Technique", Chinise Journal of Physics, Vol. 45, No.1, p84-97, 2007.

[25] Hong N H, Sakai J, Prellier W, Hassini A, "Transparent Cr-doped SnO_2 thin films ferromagnetism beyond room temperature with a giant magnetic moment", J. Phys.: Condens. Matter,17, p1697–1702, 2005.

[26] KorotcenkovG., Macsanov V., Tolstoy V., Brinzari V., Schwank J. and Faglia G, "Structural and gas response characterization of nano-size SnO_2 films deposited by SILD method", Sensors and Actuators B: Chemical, Vol. 96, 3, p602-609, 2003.

[27] Anuar K, Ho S N, Tan W T, Atan M S, Kuang D, Jelas H M, Saravanan N, "Effects of Solution Concentration on the Properties of Cu_4SnS_4 Thin Films", Issn 1392–1320 materials science (medziagotyra), Vol.14, No.2, 2008.

[28] Elangovan E., Ramamurthi K, "Studies on optical properties of polycrystalline SnO_2:Sb thin films prepared using $SnCl_2$ precursor", Cryst. Res. Technol. 38, No. 9, p779 – 784, 2003.

[29] Elangovan E., Ramamurthi K., " Optoelectronic properties of spray deposited SnO_2:F thin films for window materials in solar cells ", Journal of Optoelectronics and Advanced Materials Vol. 5, No. 1, p. 45 – 54, 2003.

[30] Papadopoulos N. D., Tsakiridis P. E., Hristoforou E., "Structural and electrical properties of undoped SnO_2 films developed by a low cost CVD technique with two different methods : comparative study", Journal of Optoelectronics and Advanced Materials Vol. 7, No. 5,2005, p2693 – 2706.

[31] Nocun M, Pajak Z, "The influence of glass surface preparation on electrical and optical properties of SnO_2 thin films obtained by spray pyrolysis technique", Optica Applicata, Vol. XXXVIII, No. 1, 2008.

[32] Hirunlabh J, Suthateeranet S, Kirtikara K and Pynn R D, "Development of a Spray Pyrolysis Coating Process for Tin Oxide Film Heat Mirrors", Thammasat Int. J. Sc. Tech., Vol.3, No.2,1998.

[33] Anuradha S and K. Rajanna, "A novel method for the improvement in thermoelectric property of tin oxide thin films and its application in gas sensing", International journal on smart sensing and intelligent systems,Vol. 1, No. 2, 2008.

[34] Anuar K, Ho S N, Tan W T, Atan M S, Kuang D, Jelas H M, Saravanan N, "Effects of Solution Concentration on the Properties of Cu_4SnS_4 Thin Films", Issn 1392–1320 materials science (medziagotyra). Vol.14, No.2, 2008.

[35] Assia S, Ratiba O, Mahdi M E, and Kadi M, "Optical reflectance of pure and doped tin oxide: from thin films to poly-crystalline silicon/thin film device", Proceedings of world academy of science, engineering and technology", Vol.34, p2070-3740, 2008.

[36] Kim H., Auyeung R.C.Y. and Pique A, "Transparent conducting F-doped SnO_2 thin films grown by pulsed laser deposition", Thin Solid Films, Vol. 516, Issue 15, p5052-5056, 2008.

[37] Lampkin, Curt M., "Aerodynamics of nozzles used in spray pyrolysis", Prog. Crystal Growth Chaact. 1, p 406–416, 1979.

[38] Pashley, D. W., et al. , Phil. Mag., 10, 127, 1964.

[39] Jeson R. B, Wang A , Metz W A, Endleman N. L, Matthew V. M, Lane A. M, Kannewurf C. R, and Marks T. J, "Transparent conducting CdO thin film growth

using a highly volatile, thermally and airstable cadmium precursor", Chem. Vap. Deposition,Vol. 7, p239-242, 2001.

[40] Altiokka B, Aksay S, "Optical properties of CuInS$_2$ films produced by spray pyrolysis method", Journal of Arts and Sciince, 31, p27-34, 2005.

[41] M.G. Ambia, M.N Islam and M.O Hakim, J. Meter Sci. 28, p2659, 1993.

[42] G.A Basset, J. W. Menter and D.W Pashley, "Structure and Properties of Thin Films", 1959.

[43] Blodgett. W. Berry and Pelar M. Hall Merry, T. Haris, Thin Film Technology, D. Vaqn Nostrand co. Inc, 329, 527, 1968.

[44] Wiener, O. Wied, Journal of Electronic materials, 31, p53, 1887.

[45] S. Tolansky " Multifle Beam Interferometry of Surface and Films", Oxford University Press,1948.

[46] J. G. Gottling and W.S. Nikol, J. Opt. Soc. Am., 56, p1227, 1966.

[47] Vander-Pauw, Philips Res. Rept., 13, p1, 1958.

[48] D.L. Smith, in "Thin Film Deposition", McGraw Hill Book Company, New York, 1995.

[49] Suematsu H, Saikusa T, Suzuki T, Jiang W and Yatsui K, "Preparation of TiFe thin films by pulsed ion beam evaporation", Mat. Res. Soc. Symp.Proc.Vol. 697,2002.

[50] Rinaldi F, "Basics of Molecular Beam Epitaxy (MBE)", Annual Report 2002, Optoelectronics Department, University of Ulm.

[51] Xi J., Liu T., Iafelice V., Nugent M., Si K., Cueto J. d, Ghosh M., and Kampus F., "Major improvement in material and device stability of a-Si:H and establishment of high stabilized efficiency of single junction a-si solar cells", Proceedings 23rd IEEE PV Specialists Conf. p.821, 1993.

[52] Samarasekara P." A Pulsed RF Sputtering Method for Obtaining Higher Deposition Rates", Chinese Journal of Physics, Vol. 41, No. 1, p70-74, 2003

[53] Suwanboon S., "The properties of nanostructured ZnO thin Film via sol-gel coating", Naresuan University Journal 16(2), p173-180,2008.

[54] Papadopoulos N. D., Tsakiridis P. E., Hristoforou E., "Structural and electrical properties of undoped SnO$_2$ films developed by a low cost CVD technique with

two different methods: comparative study", Journal of Optoelectronics and Advanced Materials Vol. 7, No. 5, p. 2693 – 2706, 2005.

[55] Podder J, Ramalingom S and Kalkura S. N, " An investigation on the lattice distortion in urea and KCL doped KDP single crystal by X-ray diffraction studies", Cryst. Res. Technol.,36.6 p551-558, 2001.

[56] Haacke G, J appl.Phys. 47, 4086, 1976.

[57] Arai.T, J.phys. Soc. Jpn. 15, 916,1960.

[58] X.C Yang, Matter. Sci. Eng. B93, 249, 2002.

[59] Shamala K.S., Murthy L.C.S., and Rao K.N., Bull Mater. Sci. Vol. 27, No. 3, 295, 2001.

[60] M.M Bagheri-Mohaghery and M. Shokooh-Saremi, J. Phus. D: Appl. Phys. 37, 1248, 2004.

[61] Hirunlabh J, Suthateeranet S, Kirtikara K and Pynn R D, "Development of a Spray Pyrolysis Coating Process for Tin Oxide Film Heat Mirrors", Thammasat Int. J. Sc. Tech., Vol.3, No.2, 1998.

[62] L.I Maissel and R. Glang, "Hand book of Thin Film Technology" McGraw-Hill Book company-New York 1970.

[63] Neugebauer CA, Physics of Thin Films (ed. Hass G. Thun, R.E., Academic Press, New York);1970.

[64] H. Yanagi, H. Kawazoe, A. Kudo, M. Yasukowa, and H. Honoso, J. Electro ceram, 4, 427, 2000.

[65] Shamala K S , Murthy L C S and Rao N, "Studies on tin oxide films prepared by electron beam evaporation and spray pyrolysis methods", Bull.matter.sci.,Vol. 27, No.3, p295-301, 2004.

[66] Brahma R, Krishna M G and Bhatnagar A K, "Optical, structural and electrical properties of Mn doped tin oxide thin films", Bull. Mater. Sci., Vol. 29, No. 3, p317–322, 2006.

[67] Shadia J. I and Riyad N. A-Bitar, "Effect of Processing on the Electrical Properties of Spray Deposited SnO_2:F Thin Films", American Journal of Applied Sciences 5 (6): 672-677, 2008.

[68] Leon-Brito eliza, Melendez A, Ramos I, Pinto N J, Jorge J, Aviles S, "Electrical

Properties of Electrospun Sb–Doped Tin Oxide Nanofibers", IOP Publishing Journal of Physics: Conference Series 61, p683–687, 2007.

[69] Bagheri-Mohagheri M.M. and Shokooh-Saremi M., Sci. Tecnol. 19, 764 (2004).

[70] Korotcenkov G , Sens Actuators B 107:209, 2005.

[71] Moseley PT, Tofield BC (eds) Solid state gas sensors. Adam Hilgen, Bristol, 1987

[72] Korotcenkov G, Mater Sci Eng B 139:1, 2007.

[73] Ivanovskaya M, Bogdanov P, Faglia G, Nelli P, Sberveglieri G, Taroni A, Sens Actuators B 77:268, 2001.

[74] Madou MJ, Morrison SR, Chemical sensing with solid state devices, Academic Press, Inc., San Diego, 1989.

[75] McAleer JF, Moseley PT, Norris JOW, Williams DE, Tofield BC, J Chem Soc Faraday Trans 1 84:441, 1988.

[76] Yamazoe N, Miura N In: Yamauchi N (ed), Chemical sensors technology, vol 4. Kodansha, Tokyo, pp 20–41, 1992.

[77] Qi P, Wang JF, Su WB, Chen HC, Zang GZ, Wang CM, Ming BQ, Mater Chem Phys 92:578, 2005.

[78] Rodriguez-Torres CE, Fabiana Cabrera A, Sanchez FH, Phys B: Condens Mater 389:176, 2007.

[79] Kanazawa E, Sakai G, Shimanoe K, Kanmura Y, Teraoka Y, Miura N, Yamazoe N, Sens Actuators B 77:72, 2001.

[80] Skala T, Veltruska K, Moroseac M, Matolinova I, Korotcenkov G, Matolin V, Appl. Surf Sci 205:196,2003.

[81] Wang W, Xu C, Wang X, Liu Y, Zhan Y, Zheng C, Song F, Wang G, J Mater Chem 12:1922, 2002.

[82] Korotcenkov G, Boris I, Brinzari V, Luchkovsky Y, Karkotsky G, Golovanov V, Cornet A, Rossinyol E, Rodriguez J, Cirera A, Sens Actuators B 103:13, 2004.

[83] Panchapakesan B, De Voe DL, Widmaier MR, Cavicchi R, Semancik S, Nanotechnology 12:336, 2001.

[84] Kawamura F, Yasui I, Sunagawa I, J Cryst Growth 233:517, 2001.